Mathematical Modelling of Unsteady Contact Melting

Thesis Presented for the Degree of

DOCTOR OF PHILOSOPHY

in the Department of

Mathematics and Applied Mathematics

UNIVERSITY OF CAPE TOWN

By

Gift Muchatibaya

Supervisors: Prof T. G. Myers, Dr S. L. Mitchell

November 7, 2008

Abstract

The work in this thesis deals with the heat transfer and fluid flow problem encountered in the analysis of an unsteady contact melting process.

Chapters 2 and 3 deal with only the heat transfer problem without fluid flow. In Chapter 2 the pre-melting problem is treated. The focus is to obtain the best approximate analytical solution to be used in the melting phase where there are no known exact solutions. The approximate solutions are constructed using the heat balance integral method. The semi-analytical solutions obtained using quadratic, cubic and exponential approximations are compared with well known exact solutions. In Chapter 3, the focus is on the melting phase. An asymptotic series solution describing the temperature in the melt region is obtained. In the solid region a modified version of the heat balance integral method is introduced, the thermal boundary layers are approximated by a cubic polynomial. Our approximation proves to be significantly more accurate compared to the quadratic approximation that is commonly used. We present an example relevant to heating an ice layer from below, which occurs with de-icing systems. The semi-analytical method employed has the advantage over numerical solutions in that the dependence of solution on the ambient conditions may be provided explicitly.

Chapters 4 and 5 deal with the coupling of the heat transfer problem with squeezing and fluid flow. The fluid flow problem is described by the Navier-Stokes equations which are reduced to a more tractable form using lubrication theory. The heat flow in the fluid is assumed to be dominated by conduction across the thin film. In the solid layer, the solution developed in Chapter 3 is used. Chapter 4 deals with an isothermal phase change material, whereas Chapter 5 focuses on the non-isothermal case. Results show that the quasi-steady state of previous models is never attained. The film height has an initial and final rapid increase, for intermediate times the height slowly increases. The previously observed initial infinity velocity of the melt is shown to be an artefact of neglecting the temperature variation of the solid, mass variation of the solid or assuming perfect thermal contact.

DECLARATION

Thesis Title: Mathematical Modelling of Unsteady Contact Melting

I hereby grant the University of Cape Town permission to reproduce the above thesis in whole or in part, for the purpose of research.

I hereby declare that:

- the above thesis is my own work and design, apart from the normal guidance from my supervisor,
- neither the substance nor any part of the above thesis has been submitted in the past, or is being, or is to be submitted for another degree or qualification at this or any other University or Institution of higher learning.

Signature:.....

Date:.....

In loving memory of my father, David, and my sister Chipo.

Acknowledgements

I wish to express my sincere gratitude to Professor Timothy Gerald Myers, my supervisor, mentor, and a kind friend. I thank him for his generosity of spirit, his gentleness and for having the vision that sustained me when I did not believe I could complete this work. With his enthusiasm, inspiration and willingness to discuss and thoroughly critique my work, persistently raising questions and encouraging me to demonstrate the significance of my findings, he made me a better researcher. Special thanks goes to Dr. Sarah Mitchell my co-supervisor for her skilful assistance with the computational work as well as proof reading various drafts of this thesis making numerous helpful comments.

I am deeply indebted to Cannon Collins Educational Trust for Southern Africa (CCETSA) whose funding made my doctoral studies possible. I acknowledge and express my appreciation to the University of Cape Town for their invaluable financial assistance through the JW Jagger Centenary Gift Scholarship and the Research Associateship award. I would like to thank the Mathematics and Applied Mathematics Department (UCT) for their financial assistance through the tutorship and part time lectureship positions they offered me throughout the duration of my studies. Special thanks goes to the African Institute for Mathematical Sciences (AIMS) for the role it played in the development of both my mathematical and computational skills leading to my doctoral studies.

I acknowledge the love, moral and emotional support of my dear wife Martha and children: Nyasha, Hilbert, Blessing, Tanaka and Tapiwa, my love and gratitude to them. My heartfelt thanks to my mum Patricia, and my brothers Isaac, Maxwell and their families who have been preparing the celebrations long before I completed. Thank you all for believing in me. Its been indeed a long, winding road. I owe special thanks to Chessman Wekwete and Douglas Magomo whose friendship and encouragement from the beginning to the end is deeply appreciated. Cheers.

Cape Town, South Africa — Gift Muchatibaya

November 7, 2008

Contents

List of Figures

List of Tables

NOMENCLATURE

c	specific heat capacity, J/(kg K)	t	time, s
g	acceleration due to gravity, m/s^2	t_m	time to end of melting, s
h	position of the melt front, m	(u, w)	melt velocity components, m/s
h_m	thickness of the melted solid, m		
h_q	quasi-steady melt height, m		*Greek Symbols*
h_{ij}	heat transfer coefficient, W/m^2	ρ	density, kg/m^3
$H(t)$	instantaneous solid thickness, m	θ	block temperature, K
$\mathcal{H}_l$	liquid thickness scale, m	δ	heat penetration depth, m
k_i	thermal conductivity, W/mK	η	liquid dynamic viscosity, Ns/m^2
L_m	latent heat of melting, J/kg	ϵ	aspect ratio, $\mathcal{H}_l/L$
L	solid length scale, m	κ_i	thermal diffusivity, m^2/s
$M(t)$	instantaneous solid mass, kg	τ	time scale, s
p	liquid pressure, N/m^2		
q	heat flux from substrate, W/m^2		
Pe	Peclet number, UL/κ_l		*Subscripts*
Re	Reynolds number, $\rho_l UL/\eta$	l	liquid
St	Stefan number, $c\Delta T/L_m$	s	solid
T	liquid temperature, K	sl	liquid-solid
T_m	melting temperature, K	ss	solid-solid
T_s	substrate temperature, K	0	initial value

Chapter 1

Introduction and literature review

1.1 Motivation and Research goals

This work is motivated by our interest in developing a mathematical model for an unsteady contact melting process involving a finite thickness phase change material.

The solid-liquid phase change heat transfer is associated with many interesting natural and industrial applications. Perhaps the most obvious example is the melting of ice in a warm environment, examples in the study of in-flight aircraft and power cable de-icing may be found in [21, 40, 50, 53, 66, 78]. Applications in the mining industry are described in [72] where melting of ice blocks or ice particles occur during their transportation for underground refrigeration in mines. Contact melting is a phenomenon of combined solid-liquid phase change heat transfer and fluid flow which occurs when a solid melts while being in close contact with a heat source. The liquid generated at the melting front is squeezed out from under the solid by the pressure maintained in the film by the weight of the free solid, ensuring that the melting solid is always close to the heat source (see Figure 1.1). High heat fluxes associated with close contact heat transfer make it attractive for many industrial applications, for example, process metallurgy and geology [28, 32, 44], latent heat energy storage, and the burial of heat-generating bodies [2, 37, 38, 58]. The high heat fluxes across

the liquid layer separating the melting solid from the heat source, result in the melting times that are considerably reduced compared to those observed for other heat transfer modes [4, 48, 73].

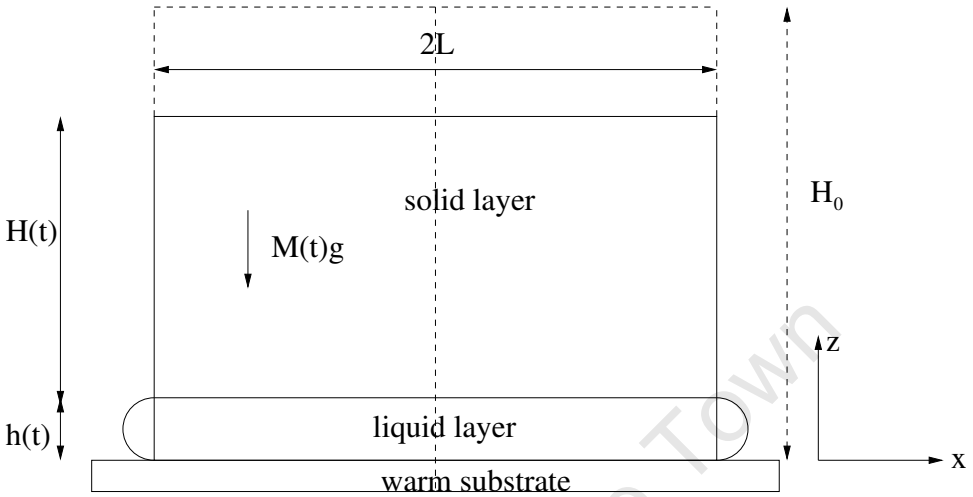

Figure 1.1: *Schematic for solid-substrate contact melting .*

The two most familiar examples of contact melting are the Leidenfrost effect (or rewetting process) and ice skating. The Leidenfrost effect occurs when a liquid comes into contact with a substrate which is at a temperature significantly above the boiling point. An insulating vapour layer forms which allows the liquid to float above the solid and results in much slower evaporation of the drop than if it remained in contact with the surface [8, 11]. Much of the classical work in the field of contact melting was carried out by Bejan and co-workers [3, 4] in relation to sliding on ice and snow.

The process of contact melting is one in which the obvious heat transfer across the melt to the melting interface is intimately coupled with the fluid mechanics of the melt, where the fluid flow is driven by the weight of the melt. The associated heat transfer problem requires modelling the temperature variations in both the melt and the block. The Stefan condition then determines the melting rate in terms of the heat fluxes at the interface. The film thickness and the pressure generated inside the melt to support the melting solid is determined by modelling the fluid flow problem.

In the past mathematical models of contact melting have generally relied on the following assumptions:

1. The temperature of the solid remains at the melting temperature, T_m, throughout the melting process.

2. The melting process is in a quasi-steady state, that is, if the position of the melt front is denoted $h(t)$ then $h_t = 0$. Hence the normal force exerted on the phase change material is balanced by the pressure generated inside the liquid film.

3. Heat transfer in the liquid is dominated by conduction across the film.

4. The lubrication approximation holds in the liquid layer, so the flow is primarily parallel to the solid surface and driven by pressure gradient. The pressure variation across the film is negligible.

5. The amount of melted fluid is small compared to that of the initial solid.

6. There is perfect thermal contact between the liquid and substrate or there is a constant heat flux,

see [4, 27, 37, 85] for example. In this work, we will refer to such models as *steady contact melting* models.

Bareiss *et al* [2] carried out an investigation to determine the melting rates and heat fluxes both experimentally and analyticaly for the heat transfer process during melting of an unfixed solid inside a horizontal tube. Their results show that the quasi-steady state assumption fails in the final stages of the process. In addition, it is shown that the heat transfer in the melt is maximum at the beginning and decreases monotonically to zero at the end of the melting process. This behaviour is attributed to the melting gap, whose thickness and hence heat resistance increases with increasing melting rate. The loss in accuracy of the theoretical model can be attributed to applying certain of the above constraints (which we will investigate). In [47], Moallemi *et al* investigated the same problem both analytically and

numerically. The solid velocity, the melt thickness, melting rates and the solid thickness were found to be significantly below the measured values. These differences were again attributed to the simplifications listed above in constructing the analytical model.

There exist investigations where certain of the restrictions listed above are relaxed. Litsek & Bejan [5] attempt to remove assumption 1 by incorporating a convection term in the solid heat equation. Their expression for the temperature gradient in the solid, at the melting front, is then constant. This result is far from realistic. Groulx & Lacroix [27] assume that the solid is at a constant temperature θ_0 which is below the melt temperature, $\theta_0 < T_m$. Their final expression for the melting rate differs from previous results with the change $L_m \rightarrow L_m + c_s(T_m - \theta_0)$. Assumption 2 is removed by Yoo [84] who shows that in the case of perfect thermal contact the initial velocity of the block is infinite. For both perfect thermal contact and constant flux the melt thickness initially increases rapidly before reaching a constant height. Groulx & Lacroix [27] also attempt to remove assumption 3. They include the vertical convection term in the liquid. The vertical velocity, $w(z)$, required for this may be obtained through the lubrication analysis, however to permit an analytical solution they take w to be a constant equal to the melting rate. Since $w = 0$ at the substrate $z = 0$, except for at the melting interface their choice of w is too high. Perhaps a better constant approximation would be the average value of w across the film. Yoo *et al* [85] retain the full expression for $w(z)$ and so obtain a result in terms of an exponential integral, that must be evaluated numerically. All researchers agree that assumption 4, namely the lubrication approximation is appropriate. Similarly all retain a constant mass for the solid and either assume perfect thermal contact or constant heat flux.

In reality the temperature in the solid is unlikely to be at the melt temperature and rather than being constant it will decrease away from the melt front. Yoo [84] has already noted that initially the melt height is far from constant. For sufficiently small times the mass of melt must be much less than the mass of the solid, but as the melting progresses the melted mass must at some stage be greater than that of the solid. Consequently the solid mass $M(t)$ must be a decreasing function of time (and this has an effect on the quasi-steady height).

Finally, perfect thermal contact is an unlikely scenario. Newton cooling is more realistic. In light of these points, we will study contact melting without invoking assumptions 1, 2, 5, 6. This forms the basis of what we term the *unsteady contact melting model*. Consequently in this thesis we focus on the following:

- the transient behaviour of the film thickness until the final stage of melting,
- modelling of the temperature profile in a melting finite block with Newton cooling conditions,
- modelling of the variable mass of the solid as well as incorporating the effects of solid-liquid density change.

The analytical and semi-analytical solutions produced will not only serve as a reference to validate numerical simulations, but will also be convenient for estimating the limitations involved in the steady analysis. Further the analytical solutions will explicitly show the dependence of the solution on the parametric values as opposed to the numerical solutions.

1.2 Problem description

A schematic representation of the melting of a solid block is depicted in Figure 1.1. Initially a cold block is placed on a substrate whose temperature is above its melting point. The temperature of the surrounding medium (air) is assumed to be above that of the block's melting temperature. The block initially heats up on all sides and subsequently melting begins (usually at the bottom where heat transfer is most rapid). To understand this process we consider a simple version of this, where the sides are insulated so only the top and bottom heat up. The thermal problem is then one-dimensional. At the bottom fluid is squeezed out due to the weight of the solid. We will discuss this flow in §1.4. At the top the fluid flow will be slower and so, to simplify our analysis and to be consistent with previous contact melting models in the literature, we will neglect the flow here. Our problem therefore involves solving

for the flow of the lower liquid layer and temperature in the solid and the two liquid layers. As we will show later, the fluid flow and heat problems are uncoupled except in the definition of the domains which are defined through the Stefan condition. We will therefore initially focus on the one-dimensional thermal problem and later include fluid flow.

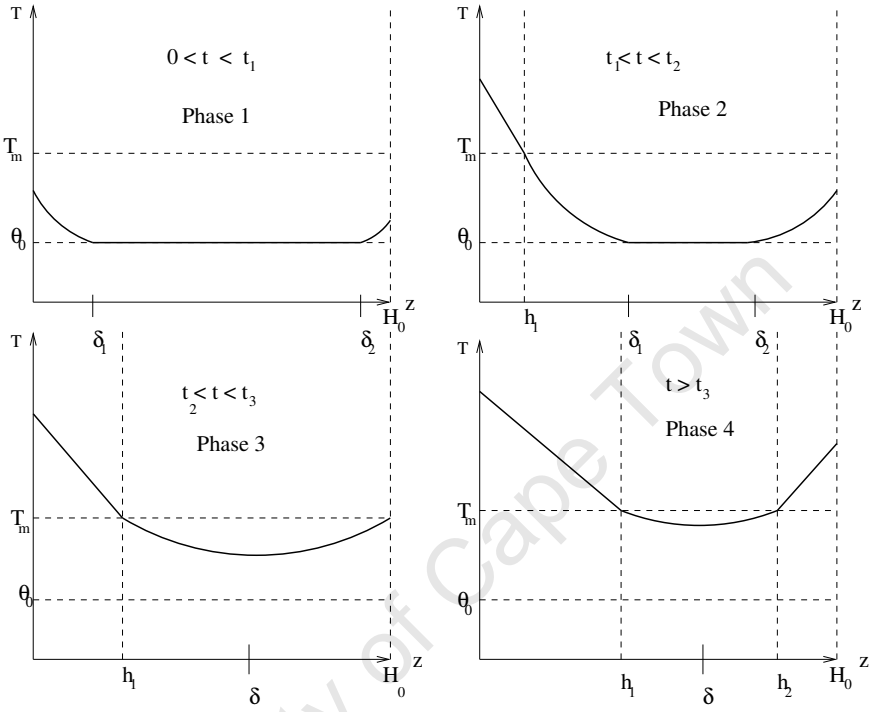

Figure 1.2: *Schematic of the 4 phases of melting when a block is placed on a surface above the melting temperature.*

In Figure 1.2 we depict the four phases that occur from the instant the block is brought in contact with the warm substrate in a warm environment until melting is complete. Phase 1 is a pre-melting stage where the temperature at the top and bottom of the block rises to the melting temperature. To model this stage, we introduce two thermal boundary layers of thickness δ_1 and δ_2 emanating from the bottom and top of the block respectively, between which the temperature is close to the initial θ_0. Phase 1 admits well-known exact solutions, these are given in [18, 20]. In Chapter 2 the solutions are determined subject to the constant flux and Newton cooling boundary conditions. Approximate solutions are also determined using the heat balance integral method; the accuracy of these solutions is determined by

comparing them to the exact solutions. The reason for studying the approximate solutions is to determine the best method which will then be used during the subsequent melting phases where no known exact solutions exist. Phase 2 occurs when the bottom surface starts to melt and ends when the two boundary layers from the top and bottom meet. Phase 3 starts at the end of Phase 2 and will continue until the top layer starts to melt. Phase 4 will start the moment the top layer starts to melt and ends when the two interfaces h_1 and h_2 merge signalling the end of the melting process. We however note that, it is possible that the top may start to melt before the boundary layers meet, but this is a simple variation of the scenario discussed and may be modelled with similar techniques. Chapter 3 deals with modelling the temperature variations in all the phases, the mathematical analysis involves solving the heat equation in the liquid layer and solid layers and then coupling them on the moving interfaces using the Stefan conditions.

Analytical investigations of melting problems have generally been treated when the domains are either semi-infinite [29, 57] or thin [52, 53], however, only a few investigations have focused on the melting of finite slabs [19, 25]. The presence of two moving boundaries, coupled with three partial differential equations, makes the numerical solution problematic. In most of the previous investigations, analytical approximations for the solutions of the melting problems such as the pseudo-state approximation [29], perturbation series solution [29, 43, 63], and the heat balance integral method [22] have been found. In the melt region, especially if the melt region is thin, the pseudo-steady state approximation or regular perturbation techniques have often been applied [45, 53]. The pseudo-steady state approximation involves the assumption that the rate of movement of the boundary is very much slower than the rate of heat conduction [29]. This leads to solving the heat equation without a time derivative. This approximation emerges as the leading order term in the regular perturbation solution for a small Stefan number. Mitchell *et al* [45] showed that a second order regular perturbation approximation in the melt region is more accurate than the heat balance integral method, although the latter is much simpler to implement. In Chapters 3 and 4 we will make use of the regular perturbation technique in the melt region. In the solid phase, where the domain

is not necessarily thin, the heat balance integral method will be applied.

Moving on to the two-dimensional problem, we must analyse the fluid flow between the melting solid and the warm substrate. Since the melt layer remains thin (due to the weight of the solid) the Navier-Stokes equations describing the flow may be reduced using lubrication theory [17, 67]. Using this approach, the melt inertia and the pressure variations in the transverse direction are negligible. Since the development of this approach by Reynolds in 1886 to describe the motion of oil in films bearings, it has become the norm in modelling fluid lubricated bearings and related devices involving thin films. This approach has been widely used in all investigations related to contact melting problems.

Although in recent studies it is standard to investigate the contact melting of a sliding three-dimensional block, we will focus on the base problem, namely the two-dimensional block that is not sliding. The appropriate extension to three dimensions is simple, leading to a standard Couette term in the lubrication approximation for the horizontal velocity and the introduction of a function of the base area which is found by solving Poisson's equation for the pressure. This extension is discussed in more detail in Chapter 3 and also in [55].

Before proceeding with the objectives and aspirations of this study, we will give an overview of concepts that are at the centre of subsequent chapters. We will begin by reviewing existing research into Stefan problems and highlight some of the main findings of these investigations in §1.3. A review of some squeeze film models and lubrication theory is given in §1.4.

1.3 The Stefan Problem

The thermal problem associated with the contact melting process requires solving the transient heat equation in an unknown region, the extent of which has to be determined as part of the solution. Problems of this nature are a form of moving boundary value problem or more specifically Stefan problems; following the four papers he published in 1889. The thermal energy balance at the moving solid/melt interface makes the problem non-linear

and so exact analytical solutions are difficult to obtain, except only for a limited number of specific cases which are well documented in the literature [18, 62, 77]. The only known exact solutions for the melting problems are those of Neumann which only exist in semi-infinite domains with prescribed constant boundary conditions and initial temperature distribution. These are expressible in terms of a single variable $z/t^{1/2}$. No exact solutions have yet been found for the melting problem with arbitrary initial and boundary conditions as well as finite domains. The steady contact melting models discussed in §1.1 do not involve moving boundaries since the film thickness is assumed to be constant, that is, fixed in space. In this case, the thermal problem is simply the standard heat conduction problem with fixed boundaries. In this section we review some of the methods that have been used extensively in the literature in addressing the Stefan problem

The fact that the Neumann solution is the only explicit closed form solution highlights the importance of approximate analytical methods and numerical methods. A variety of approximate analytical solution techniques in the literature have been applied to provide useful solutions to the problems, mostly in semi-infinite domains, with one space variable subject to various types of boundary conditions. The available approximate analytical solution techniques which we are going to discuss in the subsequent chapters are the heat balance integral method [22, 49, 56, 82] and the regular perturbation method [16, 29, 45, 56, 63]. In §1.3.1 and §1.3.2 we discuss these two methods in detail. We focus on these method because of their applicability to the contact melting processes we will study in Chapters 4 and 5.

Other important methods which we do not discuss in the subsequent chapters are those due to Landau [41], Biot [9], Boyle [12] and Tao. A review of these methods is given in Hill [29]. Landau [41] proposed an idealised melting problem and solved for the case of a semi-infinite melting solid with constant properties and with its face heated at a constant rate. The results of Landau were obtained by using numerical integration to solve the heat equation. Biot's variational technique is based on the concept of irreversible thermodynamics and has been applied to numerous problems. Concepts of thermal potential, dissipation function and generalised thermal force are introduced which lead to ordinary differential equations

of the Lagrangian type for the thermal flow field. The method though applicable to a wide variety of heat flow problems including inhomogeneous and nonlinear problems depends on an assumed form for the temperature. Cubic and quadratic temperature profiles have frequently been used and comparison with the exact Neumann solution made. Boyle [12] applied the embedding technique by introducing a fictitious phase occupying the region where the material has been removed, the problem is then solved by using the finite element method. An unknown heat input is applied at the boundary of the extended body, whose magnitude is then determined in such a way as to satisfy the actual boundary conditions on the moving liquid-solid interface. In this way the original partial differential equation is replaced by an integro-differential boundary value problem which may be solved either numerically or in series form. The principle advantage of this method is that it allows an explicit expression for the temperature in terms of the fictitious heat input. Tao [75, 76] obtained numerical solutions for the freezing of a saturated liquid in a cylinder or sphere by the finite difference method.

In Chapters 2 and 3 we will focus on the application of the HBI method and the perturbation method to problems with a constant flux and Newton cooling boundary conditions. In the next two sections we outline briefly the HBI and perturbation methods which we will be using in this work.

1.3.1 Heat balance integral (HBI) method

The HBI method developed by Goodman [22] is the most commonly used method for solving melting problems. The method is an adaptation of the Karman-Pohlhausen integral method for analysing boundary layers in fluid mechanics [64, 71]. The technique is simple and yet it gives reasonable accuracy. Though the method is applicable to a wide variety of diffusion type equations, it has mostly been employed for one-dimensional Stefan problems in a semi-infinite domain, see [23, 82] for example. The main focus has been on semi-infinite problems because of the existence of the exact Neumann solution which can then be used to determine

the accuracy of the HBI approximations. Few investigations have yet been reported on the application of the HBI method to finite domains [25, 56]. This method has not been applied to contact melting problems as far as we know. Since there are no known exact solutions in the case of finite domains, we will provide a criteria for checking the accuracy of the method in Chapter 2.

The HBI method involves choosing a polynomial (or exponential) function to approximate the temperature over an unknown region, δ, known as the penetration depth. Using this approximation the heat equation and the Stefan condition reduce to a single ordinary differential equation for δ whose solution can frequently be expressed in closed analytical form. However, there is never a unique procedure to follow, and the ultimate criterion for determining whether or not a particular procedure is successful involves an assessment of its accuracy and simplicity. This accuracy is particularly sensitive to the form of the profile selected and the boundary conditions used, for example Goodman in [22] treats the semi-infinite slab subject to fixed temperature conditions using a quadratic profile. However, even for this simple case, Wood [82] highlights six variations to the same quadratic HBI solution, all with varying degrees of accuracy.

Goodman and Shea [25] considered a finite slab melting from the top and bottom (see Figure 1.2). Their approach involved approximating the temperature in the water layer and the ice boundary layer by a quadratic polynomial when the other boundary is either isothermal or insulated. A single quadratic approximation is used throughout the ice layer. In Chapter 3, which consists of the results we published in Myers *et al* [56], a modified version of this approach is employed. By using an asymptotic solution in the water layer, the temperature is described by a power series in odd powers of the co-ordinate. To first order this leads to a cubic profile, a form which is in agreement with the small distance or large time expansion of the exact solution of the classical problem of melting an infinite block. Once melting starts the temperature in the solid layer typically has two boundary layers joined by a region of constant temperature as illustrated in Figure 1.2. A single quadratic provides a poor approximation to this profile, hence use is made of two cubics at either side even after the

two boundaries meet. This approach yields more accurate solutions as will be shown in Chapter 3.

The HBI method has also been used with an exponential formulation, see [49], and numerically as discussed in [14, 15]. In trying to alleviate the sensitivity of the HBI method to the form of the selected profile, Nobel [59] suggested the combination of spatial subdivision and low-order piecewise approximations as a refinement of the HBI method. Bell [6, 7] demonstrated the effectiveness of the approach using piecewise linear approximations and sub-divisions for problems in plane and radial geometry. Bell introduced temperature sub-division and the modification was successfully applied to the two-phase solidification problem of estimating the boundary layer. Numerical models for one-dimensional Stefan problems have been applied using level set and moving grid methods in [35], a fixed grid enthalpy formulation in [81], and explicit variable time-step methods [86]. However in this work, we do not apply numerical methods and will focus solely on semi-analytical solutions.

1.3.2 Perturbation Method

The perturbation method has been successfully applied to Stefan problems, see [31, 43, 56, 63] for example. Though the perturbation method normally works, the amount of algebraic work involved makes it difficult to calculate many terms in the solution expansion. In most investigations [53, 52], for example, it is only the zeroth order solution that is obtained explicitly, which corresponds to the quasi-steady state solution of the problem. The quasi-steady solution involves the assumption that the rate of movement of the interface is very much slower than the rate of heat conduction. The quasi-steady solution is then obtained simply by neglecting the time partial derivative in the heat equation [29]. Myers *et al* [56] present the solution up to first order correction terms. Recently Caldwell and Kwan [16] applied the method to Stefan problems with time-dependent boundary conditions. In [46], the boundary immobilisation method is used to obtain the perturbation series method to second order and so improve on the accuracy of the results.

The perturbation method will also come in useful when dealing with the fluid flow in subsequent chapters. Lubrication theory will be used to simplify the Navier-Stokes equations. This approximation may be viewed as the leading order perturbation series in powers of the aspect ratio, ϵ^2 or the reduced Reynolds number $\epsilon^2 Re$ whichever is the smallest. This method is discussed in Chapter 3 and 4 when we deal with the temperature in the liquid layer and fluid flow respectively.

1.4 The Squeeze Flow Problem

The Stefan condition provides a model for the melting rate of the solid layer in terms of the heat fluxes across the interface. However, to determine the temperature gradient in the melt region requires knowledge of the melt thickness. The pressure generated inside the melt to support the descending melting solid plays a significant role on the thickness of the film. Consequently, in addition to the heat transfer mechanism across the film, the fluid mechanics must also be studied. This requires modelling the flow in a squeeze film [1, 33, 60, 61]. The study of squeeze film flows is important in a number of branches of engineering. It is encountered when modelling such flows as; the flow between rotating cylinders (journal bearings) and the flow in a slowly diverging channel, for example. It is a particular application of lubrication theory. Such flows are modelled by making use of the Navier-Stokes and continuity equations. For incompressible fluids, they may be written:

$$\nabla \cdot \mathbf{u} = 0, \tag{1.1}$$

$$\rho_l \left[\frac{\partial \mathbf{u}}{\partial t} + (\mathbf{u} \cdot \nabla)\mathbf{u} \right] = -\nabla p + \eta \nabla^2 \mathbf{u}, \tag{1.2}$$

where the notation is defined in the Nomenclature section. Equation (1.1) represents mass conservation. It states that the mass fluxes entering a control volume exactly balances the outgoing mass fluxes when there are no sources or sinks. Equation (1.2) represents momentum conservation, which corresponds to a Newton's second law for a Newtonian incompressible fluid. The liquid film flowing between the warm substrate and the melting

solid layer is very thin, a full resolution of the complete set of the above equations is not necessary, it may be simplified using the lubrication approximation leading to Reynolds equation for the lubricating flow [2, 17, 84]. The lubrication approximation is based on an asymptotic simplification of the Navier-Stokes equations. This reduces the usual model of the flow to a system of equations that is usually solvable. This simplification is valid provided [17, 60]:

(i) the film is thin. This is measured by the aspect ratio of the flow, ϵ, and requires, $\epsilon^2 \ll 1$.

(ii) the flow regime is laminar, and the reduced Reynolds number of the flow is small, that is $\epsilon^2 Re \ll 1$. The contact melting models studied in the literature makes use of this simplification when studying the fluid flow. It is important to note that it is not necessary for the Reynolds number to be small but only that the reduced Reynolds number $\epsilon^2 Re$ be small. In our analysis the lubrication approximations is assumed to hold throughout the whole melting process. We retain these assumptions and discuss their validity in the case of unsteady contact melting in Chapter 4.

Putting the Navier-Stokes equations into non-dimensional form by using appropriate scales and applying the above assumptions, equations (1.1−1.2) reduce to a simple set of solvable equations [1, 3, 17]:

$$\nabla \cdot \mathbf{u} = 0, \qquad \eta \frac{\partial^2 v}{\partial z^2} = \frac{\partial p}{\partial x} + \mathcal{O}(\epsilon^2, \epsilon^2 Re), \qquad 0 = \frac{\partial p}{\partial z} + \mathcal{O}(\epsilon^4, \epsilon^4 Re). \tag{1.3}$$

The approximation shows that the transverse flow dominates over the longitudinal flow and the pressure in the film is uniform in the crosswise direction. When solving these equations the pressure will be balanced by the weight of the solid. This then provides the coupling of the varying solid mass to the melt thickness.

1.5 Summary and thesis outline

In this chapter, we have outlined the limitations of the existing contact melting models found in the literature. In addition, the basic components required for modelling the thermal

problem and the fluid flow problems which are at the core of unsteady contact melting have been discussed. Key focus areas which have been excluded in the previous areas and which thereby form the core of the current study include: the modelling of the temperature profile in the finite slab; the inclusion of a cooling condition at the solid-substrate interface; modelling of the varying mass; and neglecting the quasi-steady assumption for the film height. These differences to previous models form the main contributions of the thesis to the literature. The present study uses water and ice as liquid and solid because of the availability of the data but the analysis is valid for other melting solids.

The work in this thesis is organised as follows: In Chapter 2 a review of the mathematical methods associated with the heat conduction in a finite slab prior to melting is presented. The first sections deal with the exact solutions obtained using separation of variables and Laplace transform solutions, which are to be used in assessing the accuracy of the approximate solutions to be developed in the following sections. The remaining sections deal with the HBI approximate solutions derived from the exponential, cubic and the quadratic profiles. The purpose is to find the best method for the melting problem considered in the subsequent chapters which has no known solutions. In Chapter 3 we study the melting block undergoing three different melting phases. The asymptotic series expansion method is used to describe the temperature profile in the liquid phase. In the solid phase the thermal boundary layers are approximated using a cubic profile (a profile selected from the results of Chapter 2). In Chapter 4 the unsteady contact melting problem is analysed with an isothermal phase change material. The model couples the perturbation method for heat flow in the melt that is developed in Chapter 3 with a model for the fluid flow. Chapter 5 extends the results of Chapter 4 to cover non-isothermal cases. The temperature variation in the solid layer is determined by making use of the results obtained in Chapter 3, using the HBI method. Chapter 6 contains the conclusions and possible extensions of the results obtained in this work.

Chapter 2

Exact and approximate solutions: Pre-melting stage

2.1 Introduction

When a phase change material is brought in contact with the warm substrate, initially, the solid heats up until melting begins at one of the ends, as described in Chapter 1, §3.2. Melting is then accompanied by fluid flow due to the squeezing of the melt by the weight of the solid. The pre-melting stage is a familiar and elementary example of a linear boundary value problem and readily yields its solution to any of the methods available for treating such problems [18, 20]. However, once melting commences, the linearity of the problem disappears and all the classical solutions are no longer applicable except in the special case where the Neumann solution exists. The main difficulty of these problems is that the position of the moving boundary is not known a priori. Furthermore, the temperature gradient across the interface is not continuous, due to the release of latent heat, and the thermal properties of the melt and the solid phases are not the same. The purpose of this chapter is to develop approximate analytical techniques that may be used to describe the melting process. Our choice will be based on an analysis of the pre-melting stage since we can use known solutions

for comparison. Consequently, we begin our mathematical analysis by examining the pre-melting stage. We remark that the solutions obtained during this phase will then be used as an initial solution for the melting phase considered in Chapter 3.

Though there are several approximate methods available, as discussed in Chapter 1, §1.3.1, in this work we mainly make use of the heat balance integral (HBI) method because it provides sufficient accuracy for practical purposes and also because of its applicability to the melting problems to be discussed in subsequent chapters. We consider the standard quadratic, cubic and exponential approximating functions in the use of this method. We then investigate their relative merit against the available exact solutions.

This chapter is organised as follows: In §2.2, the mathematical model is introduced, where the governing equations and the associated boundary conditions are discussed. In §2.3, the analytical solutions are presented for both the finite and the semi-infinite case. In §2.4, the HBI method of solution is discussed and the solutions are derived based on three types of approximating functions. A comparison with the corresponding classical solution in each case is carried out to ascertain the degree of accuracy of the approximation used, and the results are discussed in §2.5.

2.2 Mathematical formulation and problem description

In this section we describe the governing equations of one dimensional conduction for a finite block of solid material placed on a warm substrate. The treatment of the problem is restricted to one-dimension because, in this case, the techniques for both the exact and approximate solutions have been fully developed. This is always the case when we consider contact melting with the lateral sides insulated and $T = T_m$ at the interface, the heat flow will be one-dimensional. The thermal properties of the solid material are assumed constant. The body is initially at a constant temperature θ_0, which is below the melting temperature

θ_m. Depending on the heat transfer between the block and the surface, melting may occur immediately or there may be an initial transient when the bottom of the block, $z = 0$, heats up to the melting temperature. In either case there will be a growing boundary layer, where heat has diffused into the block, raising its temperature above θ_0. At the top, depending on the boundary conditions and the ambient temperature, there will be an exchange of energy between the ambient gas and the block. This will result in a secondary layer with heat diffusing into (or out) of the block if the ambient gas temperature T_a is greater (or less) than θ_0. In this work, we assume that $T_a > \theta_m$. In the case of non-immediate melting, the end of this phase arises when melting begins at $z = 0$; we denote the time this occurs by $t = t_1$.

In Figure 2.1 we show the movement of the thermal boundary layers that occur when a block is placed on a warm substrate (or when a surface heat flux Q_0 is introduced at the bottom surface) in a warm environment. The figure shows the transition from the initial unheated stage to the stage when melting starts at the bottom, this is denoted as Phase 1 of a four phase process that is undergone by a block before it melts completely. The subsequent phases will be discussed in chapter 3. During this phase, the heat penetrates the slab and raises it above the initial temperature, θ_0, in the regions $(0, \delta_1)$ and (δ_2, H_0), where δ_1 and δ_2 are the *heat penetration* depths from each end, where $\delta_1(0) = 0$ and $\delta_2(0) = H_0$. Since the speed of propagation of the heat wave is infinite, the distances δ_1, δ_2 are a fictitious measure denoting the position where the temperature change is negligible.

For $0 < t < t_1$ we solve the heat equation

$$\frac{\partial \theta_1}{\partial t} = \kappa_s \frac{\partial^2 \theta_1}{\partial z^2}, \qquad \frac{\partial \theta_2}{\partial t} = \kappa_s \frac{\partial^2 \theta_2}{\partial z^2}, \tag{2.1}$$

in the boundary layers $z \in [0, \delta_1]$, $z \in [\delta_2, H_0]$ respectively, where $\kappa_s = k/\rho_s c_s$ is the thermal diffusivity of the material. In between we set $\theta = \theta_0$ for $\delta_1(t) < z < \delta_2(t)$. We note that since this phase occurs for a short time we never allow t to be large enough so that $\delta_1 = \delta_2$ (although this could be dealt with using the method discussed in the next chapter). At the edges of the boundary layers $z = \delta_1, \delta_2$ we impose the continuity conditions

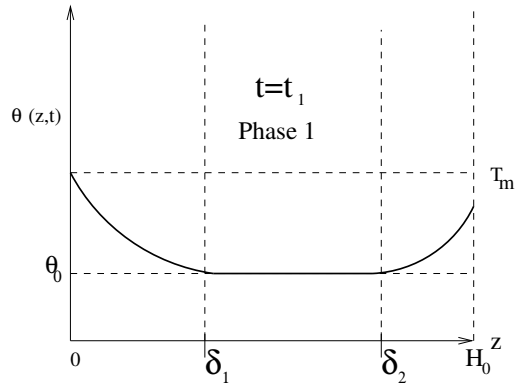

Figure 2.1: *Schematic of the first phase prior to melting when a solid layer is placed on a surface above the melting temperature*

$$\theta = \theta_0, \qquad \frac{\partial \theta_1}{\partial z}(\delta_1(t), t) = 0, \qquad \frac{\partial \theta_2}{\partial z}(\delta_2(t), t) = 0. \tag{2.2}$$

In the past mathematical models of contact melting have generally relied on the assumption that there is perfect thermal contact between the liquid and substrate [4, 27, 37]. This results in immediate melting and so there is no Phase 1. Obviously this is not physically realistic and so we impose a Newtonian cooling condition at $z = 0, H_0$,

$$\frac{\partial \theta_1}{\partial z}(0, t) = -\alpha_1 + \alpha_2(\theta_1 - \theta_s), \qquad \frac{\partial \theta_2}{\partial z}(H_0, t) = -\alpha_3 + \alpha_4(T_a - \theta_2), \tag{2.3}$$

which leads to a pre-melting stage, where $\theta_s > T_m,\ T_a > T_m$ and $\alpha_2 = h_{ss}/k_s,\ \alpha_4 = h_{sa}/k_s$.

In addition to the cooling boundary conditions stated above, we also consider a constant heat flux boundary condition and a fixed temperature condition

$$\frac{\partial \theta_1}{\partial z}(0, t) = -\alpha_1, \qquad \theta_2(H_0, t) = \theta_0, \tag{2.4}$$

on the edges $z = 0$ and $z = H_0$ respectively. This is to allow us to check the dependence of the accuracy of the approximate solutions on different boundary conditions and only need consider one boundary layer. However, in the subsequent chapters, we resort to the more appropriate conditions (2.3) for the contact models.

2.3 Exact solutions

In this section we briefly discuss the methods for solving the linear heat conduction problem in both the finite and the semi-infinite domain. For sufficiently small times, heat applied at one end of the solid will proceed only a relatively short distance into the solid, so that each end of the solid layer can be regarded as the end of a semi-infinite layer while the central part remains at a constant temperature. We therefore treat the corresponding semi-infinite case for each of the boundary conditions stated above. Methods producing analytical solutions to these problems are well known and are given in [18, 19, 41], for example. The separation of variables technique may be used for the finite domain case. In the semi-infinite case, integral transforms or similarity of variables are often used. The similarity of variables approach is only possible when the initial and boundary conditions take special forms; and usually fails when the constant heat flux or the Newton cooling condition is used. In this chapter, use will therefore be made of the integral transform method. For computational purposes, the physical parameter values used are those of water and ice because these are easy to determine; they are given in Table 2.1.

k_l	0.57	$\mathrm{W\,m^{-1}\ K^{-1}}$	k_s	2.18	$\mathrm{W\,m^{-1}\ K^{-1}}$	α_1	26236.73	$\mathrm{W\,m^{-2}}$
ρ_l	1000	$\mathrm{kg\,m^{-3}}$	T_s	288-298	K	α_2	350	$\mathrm{m^{-1}}$
ρ_s	917	$\mathrm{kg\,m^{-3}}$	η	0.001	$\mathrm{N\,s\,m^{-2}}$	α_4	10	$\mathrm{m^{-1}}$
L_m	3.34×10^5	$\mathrm{J\,kg^{-1}}$	κ_l	1.35×10^{-7}	$\mathrm{m^2\ s^{-1}}$	α_6	1500	$\mathrm{m^{-1}}$
T_m	273	K	κ_s	1.16×10^{-6}	$\mathrm{m^2\ s^{-1}}$	α_8	200	$\mathrm{m^{-1}}$
h_{sl}	855	$\mathrm{W/m^2}$	h_{ss}	763	$\mathrm{W/m^2}$	H_0	0.05	m
θ_0	258	K	ν	1×10^{-6}	$\mathrm{m^2/s}$	T_a	298	K

Table 2.1: Parameter values for ice and water.

We also impose the α_i values from Table 2.1 in the boundary conditions. The two values $\alpha_2,\ \alpha_4$ were chosen based on some simple experiments. Ice sheets formed in a freezer at $-20°C$ were placed on a large piece of metal (W400 steel) in a warm room, at $31°C$. The

time taken for the bottom and top surfaces to start melting was measured. Melting at the bottom occurred almost immediately, hence we choose α_2 to give initial melting around 1.87 s. The parameter α_4 was chosen to match the time when the top of the block started to melt, and $\alpha_6,\ \alpha_8$ are typical values taken from published literature. The parameters $\alpha_2,\ \alpha_4,\ \alpha_6,\ \alpha_8$ correspond to heat transfer coefficients between the solid and substrate, ice and air, water and substrate and water and air of 763, 21.8, 855, 114 Wm^{-2} respectively. Any α_i not quoted in Table 2.1 is set to zero. The prescribed heat flux α_1 was deduced using equation (2.27) to provide the melting time $t_1 \approx 1.87s$ equal to that deduced in the experiment described above and also in [56].

2.3.1 Method of separation of variables

A standard way of determining an analytic solution for a homogeneous linear heat transfer problem in a fixed domain with homogeneous boundary conditions is the use of separation of variables [18]. For the contact heat flux boundary condition, specified by (2.4), we use the transformation

$$\theta = \phi(z) + \psi(z,t), \tag{2.5}$$

since the boundary conditions are not homogeneous. This converts the heat equation (2.1) together with the boundary conditions (2.4) into a system of equations

$$\frac{d^2\phi}{dz^2} = 0, \quad \frac{d\phi}{dz}(0) = -\alpha_1, \quad \phi(H_0) = \theta_0, \tag{2.6}$$

$$\frac{\partial\psi}{\partial t} = \kappa_s \frac{\partial^2\psi}{\partial z^2}, \quad \frac{\partial\psi}{\partial z}(0,t) = \psi(H_0,t) = 0, \quad \psi(z,0) = \theta_0 - \phi(z), \tag{2.7}$$

where $\phi(z)$ and $\psi(z,t)$ represent the steady state and the transient part of the solution respectively. Equation (2.6) can easily be solved by successive integration, and (2.7) has homogeneous boundary conditions permitting the application of separation of variables. Solving (2.6) and (2.7) and substituting back into (2.5), we obtain

$$\theta(z,t) = \theta_0 + (H_0 - z)\frac{\alpha_1}{k_s} - \frac{8\alpha_1 H_0}{\kappa_s \pi^2} \sum_{n=1}^{\infty} \frac{1}{(2n-1)^2} \cos\left(\frac{2n-1}{2H_0}\pi z\right) e^{-(2n-1)^2 \kappa_s \pi^2 t/4H_0^2}. \tag{2.8}$$

In the case of the Newtonian cooling conditions (2.3), the problem is solved in a similar way yielding the solution

$$\theta(z,t) = T_a + \sum_{n=1}^{\infty} B_n e^{-\kappa_s \omega_n^2 t} \left(\cos(\omega_n z) + \frac{\alpha_2}{\omega_n} \sin(\omega_n z) \right), \tag{2.9}$$

where

$$B_n = \frac{\theta_0 - \theta_s}{\omega_n^2 \Gamma} [\alpha_2 (1 - \cos(\omega_n H_0)) + \omega_n \sin(\omega_n H_0)], \tag{2.10}$$

$$\Gamma = \frac{H_0}{2} \left(1 + \frac{\alpha_2^2}{\omega_n^2} \right) + \frac{1}{4\omega_n} \left(1 - \frac{\alpha_2^2}{\omega_n^2} \right) \sin(2\omega_n H_0) + \frac{\alpha_1}{\omega_n} \sin^2(\omega_n H_0), \tag{2.11}$$

and the eigenvalues ω_n satisfy the transcendental equation

$$\tan(\omega_n H_0) = \frac{\omega_n(\alpha_2 + \alpha_4)}{\omega_n^2 - \alpha_2 \alpha_4}, \quad n = 1, \cdots, \infty. \tag{2.12}$$

The variations of the temperature on the surface $z = 0$ are given by

$$\theta(0,t) = \theta_0 + \frac{H_0 \alpha_1}{k} - \frac{8\alpha_1 H_0}{k\pi^2} \sum_{n=1}^{\infty} \frac{1}{(2n-1)^2} e^{-(2n-1)^2 \kappa_s \pi^2 t / 4H_0^2}, \tag{2.13}$$

$$\theta(0,t) = T_a + \sum_{n=1}^{\infty} B_n e^{-\kappa_s \omega_n^2 t}, \tag{2.14}$$

corresponding to boundary conditions (2.4) and (2.3) respectively. The time when melting commences, $t = t_1$, is found by setting $\theta(0, t_1) = T_m$ in equations (2.13), (2.14) and solving for t_1.

2.3.2 The semi-infinite problem

Analytical solutions can also be obtained by noting that the boundary layers are small compared to the block thickness, as a result, we can replace the boundary conditions at δ_1, δ_2 by

$$\left. \frac{\partial \theta_1}{\partial z} \right|_{z \to \infty} = 0, \qquad \left. \frac{\partial \theta_2}{\partial z} \right|_{z \to -\infty} = 0. \tag{2.15}$$

The problem then reduces to solving a semi-infinite problem whose solution may be obtained by making use of the Laplace transform method [18, 20].

Defining $\hat{\theta}(z,s) = \int_0^\infty e^{-st}\theta(z,t)dt$ as the Laplace transform of θ with respect to the time variable, the heat equation (2.1) is transformed to

$$s\hat{\theta} - \theta_0 = \kappa_s \frac{\partial^2 \hat{\theta}}{\partial z^2}, \tag{2.16}$$

and the corresponding boundary conditions are transformed to

$$\frac{\partial \hat{\theta}}{\partial z} = -\frac{\alpha_1}{sk_s}, \quad \text{at} \quad z = 0, \tag{2.17}$$

$$\hat{\theta} = \frac{\theta_0}{s} \quad \text{as} \quad z \to \infty, \tag{2.18}$$

for the constant heat input case (2.4), and

$$\frac{\partial \hat{\theta}}{\partial z} = \alpha_2 \left(\hat{\theta} - \frac{\theta_0}{s} \right), \quad z = 0, \tag{2.19}$$

for the Newtonian cooling case (2.3).

Solving equation (2.16) subject to conditions (2.17) and (2.18) leads to

$$\hat{\theta} = \frac{\theta_0}{s} + \frac{\alpha_1}{sk_s}\sqrt{\frac{\kappa_s}{s}} e^{-\sqrt{\frac{s}{\kappa_s}}z}. \tag{2.20}$$

Transforming this solution back to the original coordinates, we obtain the temperature profile

$$\theta(z,t) = \theta_0 + \frac{\alpha_1}{\kappa_s}\left(2\sqrt{\frac{\kappa_s t}{\pi}} e^{-\frac{z^2}{4\kappa_s t}} - z\text{erfc}\left(\frac{z}{2\sqrt{\kappa_s t}} \right) \right). \tag{2.21}$$

Similarly, if condition (2.19) is used, this yields

$$\hat{\theta} = \frac{\theta_0}{s} + \frac{\alpha_2(T_s - \theta_0)}{s(\sqrt{\frac{s}{\kappa_s}} + \alpha_2)} e^{-\sqrt{\frac{s}{\kappa_s}}z} \tag{2.22}$$

whose inverse transform

$$\theta(z,t) = \theta_0 + (T_s - \theta_0)\left[\text{erfc}\left(\frac{z}{2\sqrt{\kappa_s t}} \right) - \exp(\alpha_2 z + \kappa_s t \alpha_2^2)\text{erfc}\left(\frac{z}{2\sqrt{\kappa_s t}} + \alpha_2\sqrt{\kappa_s t} \right) \right], \tag{2.23}$$

gives the solution in the interval $z \in [0, \infty]$. The solution corresponding to the interval $z \in [-\infty, H_0]$ is given by

$$\theta(z,t) = \theta_0 + (T_a - \theta_0)\left[\text{erfc}\left(\frac{H_0 - z}{2\sqrt{\kappa_s t}} \right) - \exp(\alpha_4(H_0 - z) + \kappa_s t \alpha_4^2)\text{erfc}\left(\frac{H_0 - z}{2\sqrt{\kappa_s t}} + \alpha_4\sqrt{\kappa_s t} \right) \right]. \tag{2.24}$$

Of interest is how the temperature varies on the surface $z = 0$ and the prediction of the melting time $t = t_1$. This will be used as a criteria for determining the accuracy of the approximate solutions to be derived in the subsequent sections. Using equations (2.21) and (2.23) we obtain the surface temperatures

$$\theta(0,t) = \theta_0 + 2\frac{\alpha_1}{k_s}\sqrt{\frac{\kappa_s t}{\pi}}, \tag{2.25}$$

$$\theta(0,t) = \theta_0 + (T_s - \theta_0)\left[1 - \exp(\kappa_s t\alpha_2^2)\text{erfc}\left(\alpha_2\sqrt{\kappa_s t}\right)\right]. \tag{2.26}$$

The melting time $t = t_1$ is determined by solving the equation $\theta(0, t_1) = T_m$ for t_1 using the equations (2.25) and (2.26). In the case of (2.25), this is given by

$$t_1 = \frac{\pi}{\kappa_s}\left(k_s\frac{T_m - \theta_0}{2\alpha_1}\right)^2, \tag{2.27}$$

whereas equation (2.26) can only be solved numerically.

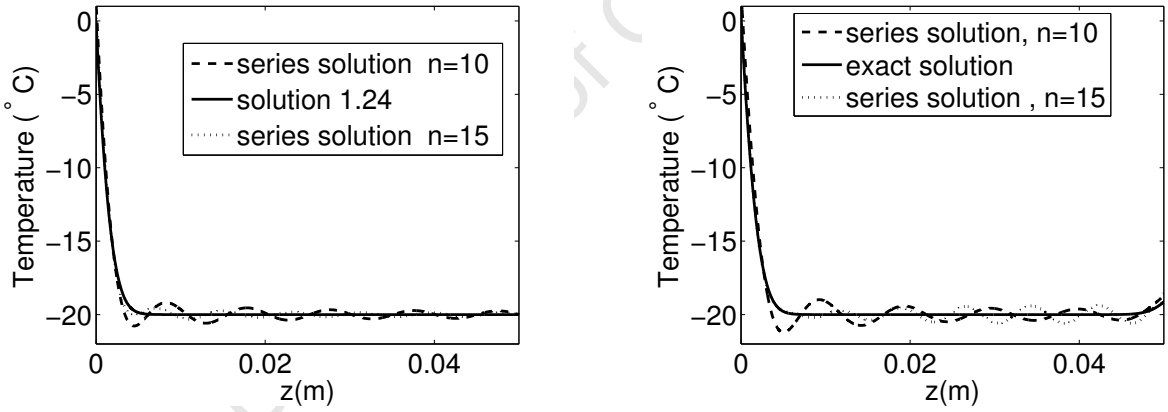

Figure 2.2: *(a) and (b) show temperature profile at the end of Phase 1 when* $t = t_1 \approx 1.87$ *s when the prescribed flux and the convective boundary conditions are used respectively. The solid line are the classical solutions (2.21) and (2.23), the dashed and the dotted lines represent the series solutions (2.8) and (2.9).*

The series solutions (2.8), (2.9) with n=10, 15 and error function solution (2.21), (2.23) derived above are represented graphically in Figure 2.2 at the time of melting $t_1 \approx 1.87s$. The oscillations decrease as n becomes large, the series solution and the exact solution are

indistinguishable by n=20. The predicted development of the thermal boundary layers is evident near the boundaries $z = 0$ for both cases, and near $z = H_0$ for the case where we have a cooling condition at the top. In these regions, both the series solutions and the error function solutions are in close agreement. This is not surprising as the small argument expansion of equations (2.8) and (2.21), near $z = 0$, gives

$$\theta = \theta_0 + a(f_1(t) - z) + \mathcal{O}(z^3), \tag{2.28}$$

$$\theta = \theta_0 + a(f_2(t) - z) + \mathcal{O}(z^2), \tag{2.29}$$

respectively, where $a = \alpha_1/k_s$, $f_1(t) = H_0 - \frac{8}{\pi^2}\sum_{n=1}^{\infty}\frac{1}{(2n-1)}\exp(-\frac{(2n-1)^2\kappa_s\pi^2 t}{4H_0^2})$ and $f_2(t) = 2\left(\frac{\kappa_s t}{\pi}\right)^{\frac{1}{2}}$. Both functions behave linearly in the space variable z and are of the same form, differing only due to the transient terms $f_1(t)$ and $f_2(t)$. Though the oscillations vanish rapidly as n increases, particularly for small values of z, they however get worse as $t \to 0$ as demonstrated in Figure 2.3. The same behaviour can be observed in the case of a cooling

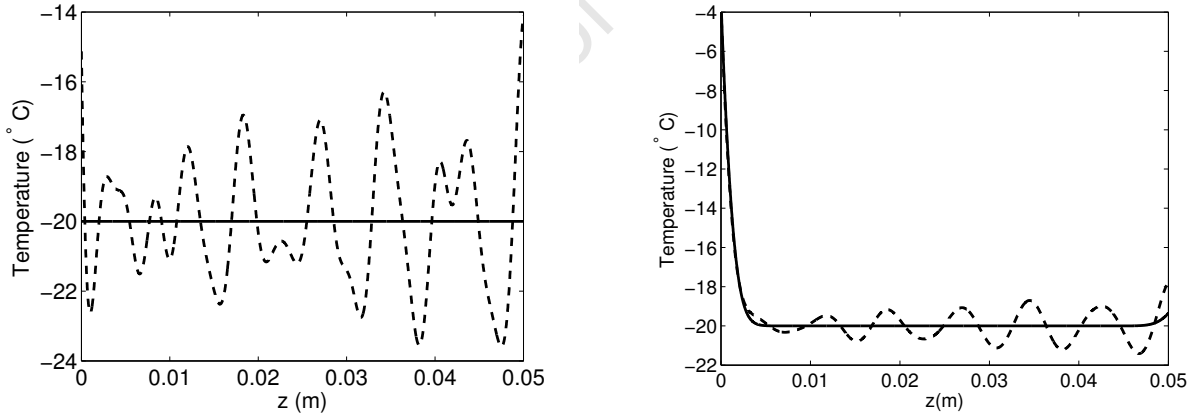

Figure 2.3: *(a) and (b) show temperature profile during Phase 1 when* $t = 0.00001s$ *and* $1.1s$ *respectively. The solid lines are the classical solutions (2.23), the dashed lines represent the series solutions (2.9).*

boundary condition. The series solution rapidly converges to the classical solution for a small number of terms. The above results illustrate that the series solutions for finite solids and in the absence of melting, can be represented by a simple, closed form solutions which are

applicable to the corresponding semi-infinite solids. This representation is valid provided the boundary layers do not meet. The temperature profile can be considered as consisting of the two semi-infinite solutions which, as shown, coincides with the series solution. A detailed discussion of the semi-infinite result can also be found in [34]. Since the semi-infinite results have no oscillations even for small time, we will use those solutions to check the accuracy of the approximate solutions to be developed in the following sections. The other reason we discard the separation of variables method is that the method is not applicable when melting commences as the problem becomes non-linear and not separable.

2.4 The heat balance integral (HBI) method

2.4.1 General theory

The HBI method presented by Goodman [22] is one of many semi-analytical techniques that is applicable to a wide range of heat transfer problems; it is based on assuming polynomial temperature profiles. This method is analogous to the general technique first introduced by Karman and Pohlhausen [64, 71] to solve hydrodynamic boundary layer problems in fluid mechanics. Since exact solutions have been found for many problems in heat transfer the HBI method has made the greatest impact on Stefan problems, where very few exact solutions exist. The method is very popular because of its simplicity and applicability to a wide range of problems giving an accuracy that is usually sufficient for most practical problems. The HBI method is applicable to one-dimensional linear and non-linear problems involving constant or temperature dependent thermal properties [23, 24, 80], non-linear boundary conditions [24, 30] and phase change problems such as freezing and melting [22, 24, 25, 30, 65]. It is with this latter class that this section and subsequent chapters are concerned. The applicability to phase change problems, which include the contact melting process, is of special importance because existing closed form solutions to these problems are highly restrictive as to allowable initial and boundary conditions.

The method is for generating approximate functional solutions to the energy equation that satisfy appropriate space boundary conditions together with an integrated form of the governing equation. This is based on the assumption that, at any finite time t, the effects of the boundary disturbances do not penetrate beyond some finite distance. These distances are the penetration depths δ_1, δ_2 that we discussed in §2.2. The HBI method converts the governing heat equation, which is a partial differential equation, to an ordinary differential equation by: (i) assuming a suitable approximating profile, (ii) satisfying the available boundary conditions, (iii) integrating the heat equation with respect to the space variable over a suitable interval to create a heat balance integral.

The method is approximate in the sense that the heat equation is satisfied only on the average, the accuracy of the solution cannot therefore be guaranteed. In the application of this method, the assumed temperature profile must be chosen with care. This sensitivity to the choice of the profile is demonstrated in the results presented by Langford [42], Myers *et al* [56], for example. In this section, we use the HBI method to solve the pre-melting problem by considering the following three types of standard profiles: (i) Quadratic polynomial, this has been applied in most melting problems by Goodman *et al* [22, 24, 25]

$$\theta(z,t) = a_0(t) + a_1(t)z + a_2(t)z^2, \tag{2.30}$$

(ii) the cubic polynomial [25, 56]

$$\theta(z,t) = a_0(t) + a_1(t)z + a_2(t)z^2 + a_3(t)z^3, \tag{2.31}$$

and (iii) the exponential profile [49, 79, 87, 88]

$$\theta(z,t) = a_0(t) + a_2(t)ze^{c(t)z^2}. \tag{2.32}$$

The accuracy of the above approximations will be checked by comparing them with the exact solutions obtained in the previous section. The comparison will be based on three criteria:

1. The accuracy with which the surface temperature is predicted.

2. The accuracy with which the overall temperature profile is predicted.

3. The accuracy with which the melting time t_1 is predicted.

2.4.2 Quadratic approximation

When the constant heat input boundary condition (2.4(a)) at the end $z = 0$ and an isothermal condition (2.4(b)) at $z = H_0$ are used, a thermal boundary layer only develops from the surface $z = 0$ where energy is absorbed. For this case, we therefore develop an approximate solution only in the region $[0, \delta_1]$. Instead of applying the quadratic profile given by (2.30), it is convenient to use the form

$$\theta(z,t) = a_0(t) + a_1(t)(\delta_1 - z) + a_2(t)(\delta_1 - z)^2, \tag{2.33}$$

where the boundary layer position δ_1, the parameters $a_0(t),\ a_1(t)$and $a_2(t)$ are to be determined. Applying the boundary conditions 2.2(b), 2.4(a) to the approximate solution (2.33), we obtain $a_0(t) = \theta_0,\ a_1(t) = 0,\ a_2(t) = \frac{\alpha_1}{2\delta_1 k_s}$. The corresponding temperature profile is given by

$$\theta(z,t) = \theta_0 + \frac{\alpha_1}{2\delta_1(t)k_s}(\delta_1 - z)^2. \tag{2.34}$$

Integrating equation (2.1) in the interval $(0, \delta_1)$, and making use of Leibniz's rule we obtain

$$\kappa_s\left[\left.\frac{\partial\theta}{\partial z}\right|_{z=\delta_1(t)} - \left.\frac{\partial\theta}{\partial z}\right|_{z=0}\right] = \frac{d}{dt}\int_0^{\delta_1}\theta(z,t)dz - \frac{d\delta_1}{dt}\theta(\delta_1,t). \tag{2.35}$$

Substituting θ from (2.34) into (2.35) leads to the initial value problem for the determination of $\delta_1(t)$

$$3\kappa_s = \delta_1\frac{d\delta_1}{dt}, \qquad \delta_1(0) = 0, \tag{2.36}$$

whose solution is

$$\delta_1(t) = \sqrt{6\kappa_s t}. \tag{2.37}$$

The temperature profile in this case is now completely determined and is given by

$$\theta(z,t) = \theta_0 + \frac{\alpha_1}{2\delta_1 k_s}(\delta_1 - z)^2, \qquad \delta_1 = \sqrt{6\kappa_s t}. \tag{2.38}$$

The corresponding depth of the thermal boundary layer when melting commences is

$$\delta_1(t_1) = \frac{2k_s(\theta_0 - T_m)}{\alpha_1}. \tag{2.39}$$

The melting time can then be obtained by using this equation together with equation (2.37) to obtain

$$t_1 = \frac{2}{3\kappa_s}\left[\frac{k_s(\theta_0 - T_m)}{\alpha_1}\right]^2 \approx 1.87s. \tag{2.40}$$

Comparing the surface temperature

$$\theta(0,t) = \theta_0 + \frac{\alpha_1}{k_s}\sqrt{\frac{3\kappa_s t}{2}}, \tag{2.41}$$

with the exact solution given in equation (2.25) shows that the results are of the same form, differing only by numerical factors $\sqrt{\frac{4}{\pi}} = 1.13$ and $\sqrt{3/2} = 1.23$. This gives an error of approximately 9% which is in accordance with the 8.6% error estimate quoted by Goodman [24] for the quadratic approximations with prescribed constant heat flux boundary condition on a semi-infinite domain.

The exact and quadratic approximations to the surface temperature are related by

$$\theta_{\text{quad}}(0,t) = \theta_0\left(\frac{4-\sqrt{6\pi}}{4}\right) + \frac{\sqrt{6\pi}}{4}\theta_{\text{exact}}(0,t). \tag{2.42}$$

showing that the difference between the two solutions, hence the error, does not depend on the size of the heat influx α_1 or any of the material constants.

Similarly, if the Newton cooling condition is applied at $z = 0$, we obtain the solution

$$\theta(z,t) = \theta_0 + \frac{\beta_0}{\delta_1(2+\alpha_2\delta_1)}(z-\delta_1)^2, \tag{2.43}$$

where $\beta_0 = \alpha_1 + \alpha_2(\theta_0 - T_s)$. Integrating equation (2.1), and using (2.43) leads to the following differential equation governing $\delta_1(t)$:

$$\frac{6\kappa_s}{2+\alpha_2\delta_1} = \frac{d}{dt}\left[\frac{\delta_1^2}{2+\alpha_2\delta_1}\right], \qquad \delta_1(0) = 0. \tag{2.44}$$

Equation (2.44) can be solved analytically to give an equation for δ_1:

$$\frac{1}{2}\alpha_2^2\delta_1^2 + 2\alpha_2\delta_1 - 4\ln[2+\alpha_2\delta_1] = 6\kappa_s\alpha_2^2 t - 4\ln 2 \tag{2.45}$$

In the region $\delta_2 < z < H_0$, the quadratic approximation becomes

$$\theta(z,t) = \theta_0 + \frac{\beta_1}{(H_0-\delta_2)[2+\alpha_4(H_0-\delta_2)]}(z-\delta_2)^2, \tag{2.46}$$

where $\beta_1 = \alpha_4(T_a - \theta_0)$. The governing equation for δ_2 is

$$\frac{6\kappa_s}{2+\alpha_4(H_0-\delta_2)} = \frac{d}{dt}\left[\frac{(H_0-\delta_2)}{2+\alpha_4(H_0-\delta_2)}\right],\ \delta_2(0) = H_0, \tag{2.47}$$

whose solution is:

$$\frac{1}{2}\alpha_4^2(H_0-\delta_2)^2 + 2\alpha_4(H_0-\delta_2) - 4\ln[2+\alpha_4(H_0-\delta_2)] = 6\kappa_s\alpha_4^2 t - 4\ln 2. \tag{2.48}$$

The temperature distribution prior to the time t_1 is therefore

$$\theta(z,t) = \begin{cases} \theta_0 + \frac{\beta_0(z-\delta_1)^2}{\delta_1(t)(2+\alpha_2\delta_1)}, & 0 \le z \le \delta_1, \\ \theta_0, & \delta_1 < z < \delta_2, \\ \theta_0 + \frac{\beta_1(z-\delta_2)^2}{(H_0-\delta_2)[2+\alpha_4(H_0-\delta_2)]}, & \delta_2 \le z \le H_0. \end{cases} \tag{2.49}$$

The temperature variation on the surface $z = 0$ is given by

$$\theta(0,t) = \theta_0 + \frac{\beta_0\delta_1}{(2+\alpha_2\delta_1)}. \tag{2.50}$$

Setting $\theta = T_m$ and $t = t_1$, in (2.50), we obtain

$$\delta_1(t_1) = \frac{2(\theta_0 - T_m)}{\alpha_2(T_m - T_s)}, \tag{2.51}$$

which can be used together with (2.45) to give an expression for the time when melting commences:

$$t_1 = \frac{1}{6\kappa_s\alpha_2^2}\left[\frac{1}{2}\alpha_2^2\delta_1^2 + 2\alpha_2\delta_1 - 4\ln[2+\alpha_2\delta_1] + 4\ln 2\right] \approx 1.67s, \tag{2.52}$$

using the values in Table 2.1. This represents approximately 11% difference from the melting time $t_1 = 1.87s$ predicted by the exact solution.

2.4.3 The cubic approximation

The standard cubic polynomial (2.31) has four time dependent parameters, determination of these parameters would require one more condition in addition to those already defined

at $z = \delta_1,\ z = 0$. This additional boundary condition is derived from the fact that the total derivative of $\theta(z,t)$ with respect to t and evaluated at $z = \delta_1(t)$ is zero (since $\theta(\delta_1(t),t) = \theta_0$), that is

$$\frac{D}{Dt}\theta(z,t) = 0 \Longrightarrow \quad \frac{\partial\theta}{\partial z}\frac{d\delta_1}{dt} + \frac{\partial\theta}{\partial t} = 0, \quad \text{at} \quad z = \delta_1. \tag{2.53}$$

Since $\frac{\partial\theta}{\partial z} = 0$ at $z = \delta_1$, and $\frac{\partial\theta}{\partial t} = \kappa_s\frac{\partial^2\theta}{\partial z^2}$, we obtain (see [22]),

$$\frac{\partial^2\theta}{\partial z^2}(\delta_1(t),0) = 0, \tag{2.54}$$

which is a smoothing condition. Using equation (2.31) and the accompanying boundary conditions for the constant heat flux case, the temperature profile is given by:

$$\theta(z,t) = \theta_0 + \frac{\alpha_1}{3\delta_1^2 k_s}(\delta_1 - z)^3. \tag{2.55}$$

Integrating the heat equation (2.1) in the interval $(0,\delta_1)$, and making use of Leibniz's theory as before yields:

$$6\kappa_s = \delta_1\frac{d\delta_1}{dt}, \qquad \delta_1(0) = 0, \tag{2.56}$$

whose solution is

$$\delta_1 = \sqrt{12\kappa_s t}. \tag{2.57}$$

The corresponding surface temperature is given by

$$\theta(0,t) = \theta_0 + \frac{2\alpha_1}{3k_s}\sqrt{3\kappa_s t}, \tag{2.58}$$

which only differs from the exact solution

$$\theta(0,t) = \theta_0 + \frac{2\alpha_1}{k_s}\sqrt{\frac{\kappa_s t}{\pi}}, \tag{2.59}$$

by numerical factors $\frac{2}{3}\sqrt{3} \approx 1.1547$ and $\sqrt{\frac{4}{\pi}} = 1.1282$, leading to the error of approximately 3% which is a significant improvement to the 9% obtained for the quadratic solution. Goodman [24] presented the error estimates for the cubic polynomial approximations with prescribed heat flux boundary conditions. Thus, subject to these boundary conditions, the cubic profile is more accurate.

The exact and the cubic surface temperatures are related by

$$\theta_{\text{cubic}}(0,t) = \theta_0\left(\frac{3-\sqrt{3\pi}}{3}\right) + \frac{\sqrt{3\pi}}{3}\theta_{\text{exact}}(0,t), \tag{2.60}$$

again showing that the difference between the exact solution and the approximate solution is constant and independent of the magnitude of the heat flux used.

For the Newton cooling condition, we obtain solutions of the form

$$\theta(z,t) = \begin{cases} \theta_0 + \frac{\alpha_2(\theta_0-T_s)}{\delta_1^2(3+\alpha_2\delta_1)}(z-\delta_1)^3 & 0 \le z \le \delta_1(t_1) \\ \theta_0 & \delta_1(t_1) < z < \delta_2(t_1), \\ \theta_0 + \frac{\alpha_4(\theta_0-T_s)}{(H_0-\delta_2)^2[3+\alpha_4(H_0-\delta_2)]}(z-\delta_2)^3 & \delta_2(t_1) \le z \le H_0 \end{cases} \tag{2.61}$$

The corresponding temperature variation on the surface $z = 0$ is then

$$\theta(0,t) = \theta_0 + \frac{\alpha_2(\theta_0 - T_s)}{(3+\alpha_2\delta_1)}\delta_1. \tag{2.62}$$

The governing equations for δ_1 and δ_2 are given respectively by

$$\frac{12\kappa_s}{3+\alpha_2\delta_1} = \frac{d}{dt}\left[\frac{\delta_1^2}{3+\alpha_2\delta_1}\right],\ \delta_1(0) = 0. \tag{2.63}$$

$$\frac{12\kappa_s}{3+\alpha_2(H_0-\delta_2)} = \frac{d}{dt}\left[\frac{(H_0-\delta_2)^2}{3+\alpha_2(H_0-\delta_2)}\right],\ \delta_2(0) = H_0. \tag{2.64}$$

Equations (2.63,2.64) have solutions of the form

$$\frac{1}{2}\alpha_2^2\delta_1^2 + 3\alpha_2\delta_1 - 9\ln[3+\alpha_2\delta_1] = 12\kappa_s\alpha_2^2 t - 9\ln 3, \tag{2.65}$$

$$\frac{1}{2}\alpha_4^2(H_0-\delta_2)^2 + 3\alpha_4(H_0-\delta_2) - 9\ln[3+\alpha_4(H_0-\delta_2)] = 12\kappa_s\alpha_4^2 t - 9\ln 3, \tag{2.66}$$

respectively, which completes the problem.

Using (2.62) together (2.65) the melting time is obtained to be $t_1 = 1.8765$s which represents a 0.3% difference from the exact solution $t_1 = 1.87$s, which is a significant increase in accuracy when compared to the 9% error obtained in the quadratic case.

2.4.4 Exponential approximation

The exponential profile proposed by Mossally *et al* [49] is motivated by the exact solution (2.21) and noting that the small z expansion of $\text{erf}z \sim \frac{2}{\sqrt{\pi}}e^{-z^2}$. Consequently they take an

approximating function of the form

$$\theta = a + \frac{bz}{\delta_1} e^{cz^2/\delta_1^2}, \tag{2.67}$$

where a, b and c are parameters to be determined. Mosally *et al* [49] also propose an alternative exponential form,

$$\theta(z,t) = a(t) + b(t)e^{c(t)z}, \tag{2.68}$$

but is never as accurate as (2.67) and is therefore not used here.

Applying the constant flux condition at $z = 0$ and the boundary conditions $\theta(\delta_1, t) = \theta_0$, $\theta_z(\delta_1, t) = 0$ to the solution (2.67), we obtain

$$a = \frac{\alpha_1 \delta_1}{k_s \sqrt{e}}, \qquad b = -\frac{\alpha_1 \delta_1}{k_s}, \qquad c = -1/2. \tag{2.69}$$

Together with the integrated form of the heat equation, this gives a governing differential equation for δ_1

$$\delta_1 \frac{d\delta_1}{dt} = \frac{\sqrt{e}}{2(2-\sqrt{e})}, \qquad \delta_1(0) = 0, \tag{2.70}$$

with solution

$$\delta_1(t) = \sqrt{\alpha^* \kappa_s t}, \qquad \alpha^* = \frac{\sqrt{e}}{2(2-\sqrt{e})}. \tag{2.71}$$

The corresponding temperature distribution is given by

$$\theta = \theta_0 + \frac{\alpha_1}{k_s}\left(\frac{\delta_1}{\sqrt{e}} - z e^{-z^2/2\delta_1^2}\right), \qquad \delta_1(t) = \sqrt{\alpha^* \kappa_s t}, \tag{2.72}$$

and the surface temperature distribution is given by

$$\theta(0,t) = \theta_0 + \frac{\alpha_1}{k_s}\sqrt{\frac{\alpha^*}{e}}\sqrt{\kappa_s t}. \tag{2.73}$$

The difference in numerical factors $\sqrt{\frac{\alpha^*}{e}}$ and $\sqrt{\frac{4}{\pi}}$ gives an error of about 16%. The corresponding linear relationship between the exact and exponential surface temperatures is

$$\theta_{\exp}(0,t) = \theta_0\left(1 - \frac{1}{2}\sqrt{\frac{\alpha^*\pi}{e}}\right) + \frac{1}{2}\sqrt{\frac{\alpha^*\pi}{e}}\theta_{\text{exact}}(0,t). \tag{2.74}$$

For the cooling boundary condition, we obtain a solution of the form:

$$\theta(z,t) = \begin{cases} \theta_0 + \frac{\beta_0}{1+\gamma_0\delta_1}(ze^{\frac{-z^2}{2\delta_1^2}} - \delta_1 e^{-1/2}), & 0 < z < \delta_1 \\ \theta_0, & \delta_1 < z < \delta_2 \\ \theta_0 + \frac{\beta_1}{1+\gamma_1(H_0-\delta_2)}[(H_0-\delta_2)e^{-1/2} - (H_0-z)e^{\frac{-(H_0-z)^2}{2(H_0-\delta_2)^2}}] & \delta_2 \leq z \leq H_0 \end{cases} \tag{2.75}$$

where $\beta_0 = \alpha_2(\theta_0 - T_s),\ \beta_1 = \alpha_4(T_a - \theta_0),\ \gamma_0 = \alpha_2/\sqrt{e},\ \gamma_1 = \alpha_4/\sqrt{e}$

The corresponding temperature variation on the surface $z = 0$ is given by

$$\theta(0,t) = \theta_0 - \frac{\beta_0}{1+\gamma_0\delta_1}\delta_1 e^{-1/2}, \tag{2.76}$$

and when melting begins on this surface at $t = t_1$, δ_1 is obtained from solving the equation

$$T_m = \theta_0 - \frac{\beta_0}{1+\gamma_0\delta_1}\delta_1 e^{-1/2}, \tag{2.77}$$

which yields

$$\delta_1(t_1) = \frac{1}{\gamma_0}\left(\left[1 - \frac{\gamma_0\sqrt{e}}{\beta_0}(\theta_0 - T_m)\right]^{-1} - 1\right). \tag{2.78}$$

The governing equations for $\delta_1(t)$ and $\delta_2(t)$ are

$$\frac{d\delta_1}{dt} = \frac{\beta_3(1+\gamma_0\delta_1)}{\delta_1[2+\gamma_0\delta_1]}, \quad \delta_1(0) = 0, \tag{2.79}$$

$$\frac{d\delta_2}{dt} = -\frac{\beta_3(1+\gamma_1(H_0-\delta_2))}{(H_0-\delta_2)[2+\gamma_1(H_0-\delta_2)]}, \quad \delta_2(0) = H_0. \tag{2.80}$$

Solving the above equations for δ_1 and δ_2 respectively, we obtain

$$\beta_3\gamma_0^2 t = \gamma_0\delta_1 - \ln(1+\gamma_0\delta_1) + \frac{1}{2}\gamma_0^2\delta_1^2, \tag{2.81}$$

$$\beta_3\gamma_0^2 t = (H_0-\delta_2)\gamma_0 - \ln(1+\gamma_0(H_0-\delta_2)) + \frac{1}{2}\gamma_0^2(H_0-\delta_2)^2, \tag{2.82}$$

where $\beta_3 = \frac{\kappa_s\sqrt{e}}{(2-\sqrt{e})}$. Using (2.78) and (2.81), the time the surface $z = 0$ starts to melt is determined to be approximately 1.38s, which represents a 26% error when compared with the melting time given by the exact solution.

2.5 Results and discussion

A comparison between the approximate surface temperature profiles (2.41), (2.73) and (2.58) with the exact solution (2.25) discloses the fact that the results are of the same form but differ

by numerical factors which represent 9%, 16% and 3% percentage errors for the quadratic, exponential and cubic respectively when the constant heat flux boundary condition is used. The established linear relationships between the surface temperature for each approximation show that these errors are independent of the size of the heat flux used or the thermal properties of the conducting material. These results together with the solutions presented in graphical form below show that, with respect to the boundary conditions used, the cubic approximation is more accurate than both the quadratic and the exponential approximations. Figure 2.4 (a) is a graphical representation of the temperature profiles (2.38), (2.55) and

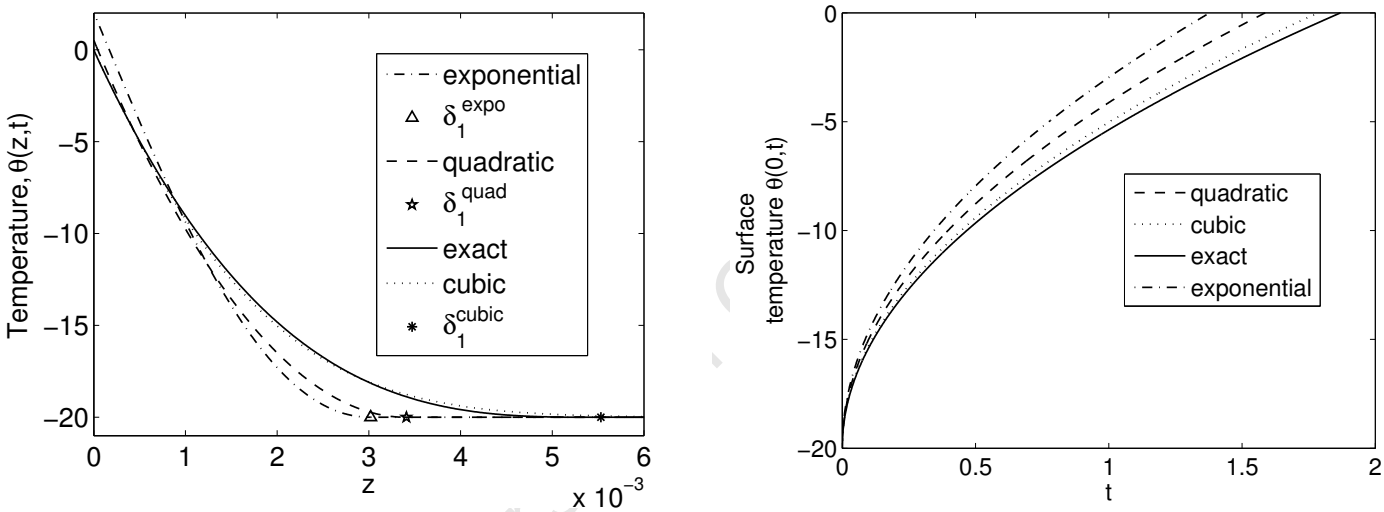

Figure 2.4: *(a) represents the quadratic, cubic, exponential and exact temperature profiles at the end of Phase 1 when* $t = t_1 \approx 1.87$ *s. The position of* δ_1 *is marked accordingly for each approximation and (b) represents the surface temperature profile.*

(2.72) together with the exact solution (2.21) in the thermal boundary layer that emanates from $z = 0$. The quadratic and exponential profiles predict a much earlier melting time than that predicted by the exact solution. When the surface $z = 0$ is at $T = 0°C$ according to the exact solution, the quadratic and the exponential profiles predict a higher temperature of approximately $1°C$ and $2°C$ respectively with the cubic prediction being indistinguishable from that of the exact solution. Figure 2.4 (b) represents the surface temperature profiles (2.41), (2.58) and (2.73) together with the exact solution (2.25). The melting times

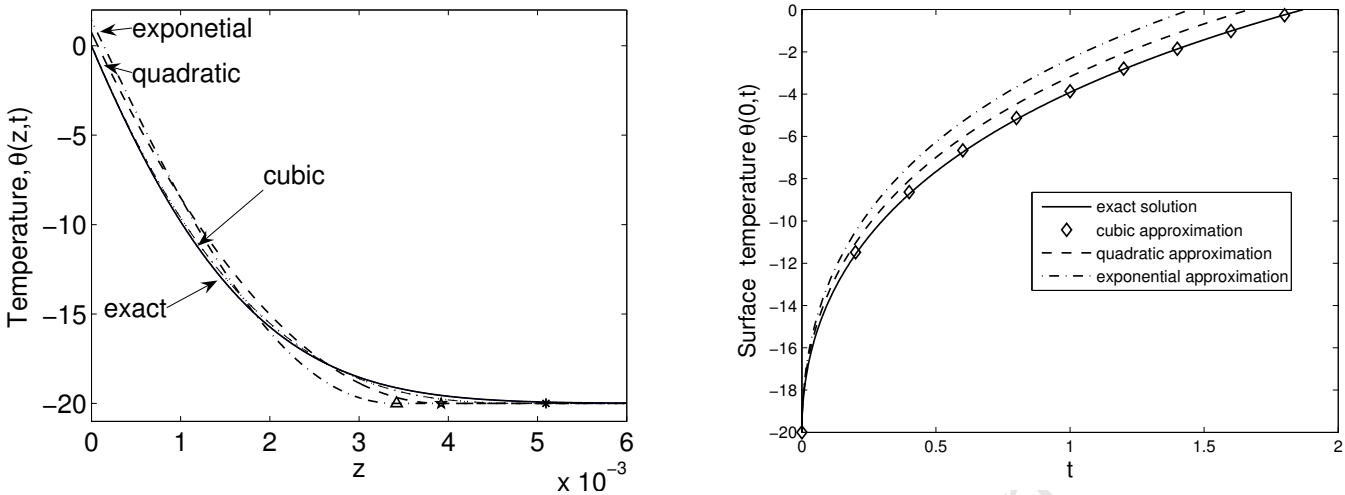

Figure 2.5: *(a) The quadratic, cubic, exponential and the exact temperature profiles near* $z = 0$ *at the end of Phase 1 when* $t = t_1 \approx 1.87$ *s in the case of cooling boundary condition. The position of* δ_1 *is denoted by '*' for each approximation. (b) represents the surface temperature profiles.*

1.67s, 1.8765s and 1.38s predicted by the quadratic, exponential and cubic approximation respectively represent errors of 10%, 0.3% and 26% respectively.

A similar trend is also observed in Figures 2.5 (a) and (b) for a cooling boundary condition. The cubic profile also gives the best approximation. Figure 2.6 shows the temperature profile at the time of melting. The cubic profile and the exact profile are in excellent agreement, being indistinguishable except in the boundary layer regions where all other profiles under predict the temperature as shown Figures 2.4 (a), 2.5 (a) in the case of the region close to $z = 0$.

2.6 Conclusions

In this chapter, we have laid the foundation for the mathematical modelling for the thermal component of the contact melting problem. Three different types of temperature profiles

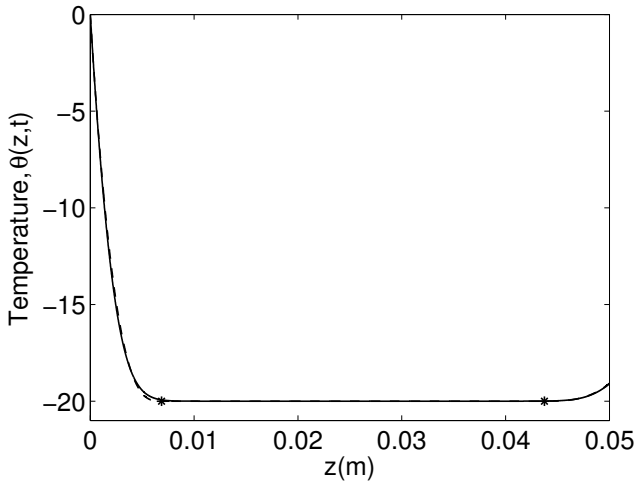

Figure 2.6: *Temperature profile at the end of Phase 1 when* $t = t_1 \approx 1.87s$. *The dashed line denotes the exact solution and the solid line denotes the cubic approximation,* $'*'$ *denote the position* δ_1 *and* δ_2.

have been considered with the view of choosing the best profile for the pre-melting problem subject to the constant heat flux and cooling boundary conditions considered. Available closed form solutions have been used to determine the accuracy of the approximations used. The results show that for short times, the series solutions obtained using the separation of variables method converges rapidly to the solution of the corresponding semi-infinite case provided the thermal boundary layers do not meet. Consequently the semi-infinite solution was used instead of the series solutions when testing the accuracy of the approximate solutions obtained by using the heat balance integral method. The HBI method, provided the cubic profile is used, proved to be capable of providing highly accurate solutions to typical problems in heat diffusion when the boundary conditions of the type considered in this work are applied. Due to the excellent agreement between the cubic approximation and the exact solutions, in the subsequent chapters we will prefer the cubic profile in predicting the temperature profile during melting. In the next chapter, the cubic approximation is confirmed to be the natural approximation by the fact that the perturbation solution performed in the liquid region also produces a cubic solution.

Chapter 3

One-dimensional melting of a finite thickness layer

3.1 Introduction

In Chapter 2, the focus was to determine the most accurate heat balance integral solution to the one-dimensional heat conduction problem in a finite slab during the pre-melting phase. The purpose of this chapter is to extend these models to carry the analysis further to allow for melting of both top and bottom of the layer. The effect of squeezing will be considered in the subsequent chapters after the thermal problem is fully analysed. Melting at the top and bottom leads to three distinct possible regions during the melting process, that is fluid-solid-fluid. The mathematical description then requires solving heat equations in the three regions and coupling the solutions with the two Stefan conditions to determine the position of the interfaces. Clearly, there is no general analytical solution to such problems and the presence of two moving boundaries coupled with three partial differential equations, makes even the numerical solution problematic. Consequently, the goal in this chapter is to determine a relatively simple approximate solution to the melting problem in a finite slab.

In the liquid region we find that an asymptotic solution, taken to first order, accurately

describes the temperature profile. In the solid region the classic boundary layer form of the temperature, particularly for small times and the presence of moving boundaries, prevents us from using a standard eigenfunction expansion. Instead the heat balance integral method is used. Once melting begins, the temperature in the solid initially has two boundary layers joined by a region of constant temperature (see Figure 1.2), two cubic profiles are used on either side to approximate the temperature profile and this is continued even after the boundary layers meet

In the following section we describe the mathematical problem. In §3.4 we deal with the classical problem of the melting of a semi-infinite block on a fixed temperature substrate. This has an analytical solution which we can then compare with our approximate solution methods. Satisfied that the approximate method is accurate, we move on to the melting of a finite block in a warm environment in §3.5. In this section the final stage involves solving the heat equations in three regions coupled with two Stefan conditions. Finally, we show how the method may be used to model a de-icing system, where an energy source at the substrate causes melting. The results of this chapter have been published in [56].

3.2 Problem description

In Chapter 2, the focus was on the initial transient when the bottom of the slab, $z = 0$, heats up to the melting temperature. This resulted in a growing thermal boundary layer, where heat diffused into the block, raising its temperature above θ_0. Similarly, if the temperature of the environment is above the melting temperature of the solid there will also be an exchange of energy between the ambient gas and the block. This results in the development of a second thermal boundary layer with heat diffusing into the block from the top; this may lead to a second melting front. We will now focus on the situation where melting takes place as well as the growth of the boundary layer. Our main interest is in the thermal problem and so we will neglect the effect of density changes. Of course there is no difficulty in introducing this to the model: for example if the solid and liquid densities are ρ_s and ρ_l and we have a

single liquid layer of thickness h, where the solid block originally has thickness H_0 and the current thickness is H, then

$$\rho_s(H_0 - H) = \rho_l h, \tag{3.1}$$

provides the appropriate relation between the heights. This will be dealt with later in Chapters 4 and 5.

The melting sequence has been discussed in Chapter 1 with all the phases depicted in Figure 1.2. It should be noted that the sequence depicted in Figure 1.2 is just one possibility; clearly other sequences are possible. For example if heat is removed at the top surface, such as in aircraft icing, melting will never occur there. Melting may occur at $z = H_0$ before $\delta_1 = \delta_2$. Also, perfect thermal contact between the block and the substrate leads to $\theta(0,t) = T_s$ and melting occurs immediately. However, these variations can all be dealt with by the methods described in the following sections. In particular we will look at the perfect thermal contact problem in §3.4, since this permits an analytical solution and some verification of our analysis.

3.3 Governing equations

The most complex version of the melting problem, occurring in Phase 4, is governed by five equations. These are three heat equations, which describe the temperature in the bottom and top liquid layers and the solid layer, and two Stefan conditions, which describe the position of the two melting boundaries. Models for the other phases are special cases of this. Figure 3.1 depicts the melting process during this stage. The full problem is described by the three heat equations

$$\frac{\partial T}{\partial t} = \kappa_l \frac{\partial^2 T}{\partial z^2}, \qquad \frac{\partial \theta}{\partial t} = \kappa_s \frac{\partial^2 \theta}{\partial z^2}, \qquad \frac{\partial \chi}{\partial t} = \kappa_l \frac{\partial^2 \chi}{\partial z^2} \tag{3.2}$$

and the two Stefan conditions

$$\rho_s L_m \frac{dh_1}{dt} = \left(k_s \frac{\partial \theta}{\partial z} - k_l \frac{\partial T}{\partial z} \right)\Bigg|_{z=h_1}, \quad \rho_s L_m \frac{dh_2}{dt} = \left(k_s \frac{\partial \theta}{\partial z} - k_l \frac{\partial \chi}{\partial z} \right)\Bigg|_{z=h_2}, \tag{3.3}$$

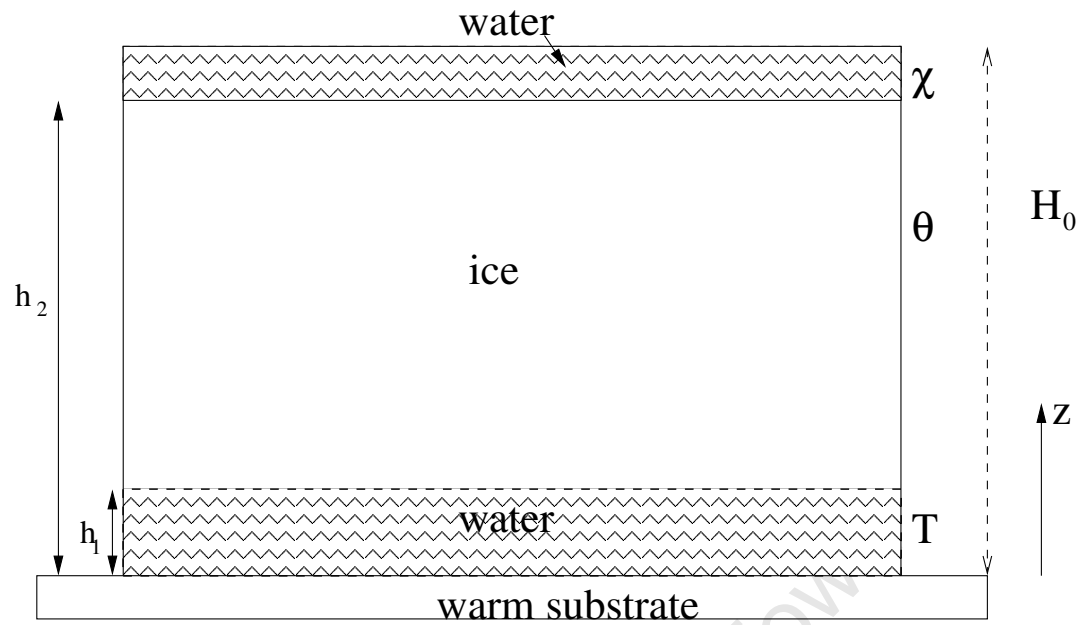

Figure 3.1: *Melting slab from the top and bottom*

where $T,\ \theta,\ \chi$ represent the temperature in the three layers, κ is the thermal diffusivity, ρ the density, L_m the latent heat of melting and k the thermal conductivity, with subscripts indicating solid or liquid.

Appropriate boundary conditions are as follows. In the case where the solid layer does not immediately melt at $z = 0$ we use the boundary condition of the form

$$\frac{\partial \theta}{\partial z} = \alpha_1 + \alpha_2(\theta - T_s). \tag{3.4}$$

A similar condition is imposed at the top surface, $z = H_0$,

$$\frac{\partial \chi}{\partial z} = \alpha_3 + \alpha_4(T_a - \chi), \tag{3.5}$$

The above conditions reduce to the Newton cooling conditions if $\alpha_1 = \alpha_3 = 0$ or a constant flux if $\alpha_2 = \alpha_4 = 0$. If $\alpha_2,\ \alpha_4 \to \infty$, then we have a fixed temperature boundary condition at each end given by $\theta(0, t) = T_s,\ \chi(H_0, t) = T_a$. Here $T_s,\ T_a$ denote the substrate and surrounding air temperatures respectively. The source terms $\alpha_1,\ \alpha_3$ can represent a number of effects, such as the energy from heating or cooling system that acts through the substrate.

In the solid accretion models described in [13, 51, 52, 53], α_3 includes the kinetic energy of incoming liquid droplets and aerodynamic heating.

When liquid appears at $z = 0$ then equation (3.4) is changed to

$$\frac{\partial T}{\partial z} = \alpha_5 + \alpha_6(T - T_s), \tag{3.6}$$

and when liquid appears at $z = H_0$ equation (3.5) is changed to

$$\frac{\partial \chi}{\partial z} = \alpha_5 + \alpha_6(T_a - \chi). \tag{3.7}$$

Any melting interfaces remain at the melting temperature T_m, and so

$$T(h_1, t) = \theta(h_1, t) = T_m, \quad \theta(h_2, t) = \chi(h_2, t) = T_m \tag{3.8}$$

Initially the solid temperature is constant. If liquid appears on $z = 0$ at $t = t_1$ and on $z = H_0$ at $t = t_3$, then

$$\theta(z, 0) = \theta_0, \quad h_1(t_1) = h_2(t_3) = 0. \tag{3.9}$$

The system of equations (3.2,3.3) and the corresponding boundary conditions cannot be solved analytically. The presence of the two moving boundaries makes the numerical solution difficult, even in the current one-dimensional problem. Hence we now seek a simplified version of the problem which is amenable to analysis. The route we will follow involves an asymptotic solution in the fluid layers, and a modified version of the heat balance integral method [25] in the solid. We will begin by demonstrating the method on a classical Stefan problem, where a semi-infinite block is placed on a surface that is maintained at constant temperature $T_s > T_m$.

3.4 A semi-infinite block on a fixed temperature substrate

We now turn to the standard problem where a semi-infinite block is in perfect thermal contact with a substrate of infinite thermal mass. This leads to a two phase problem, with

the liquid phase occupying the region $0 < z < h_1(t)$ for $t \geq 0$ and the solid phase in the region $h_1 < z$ as shown in Figure 3.2.

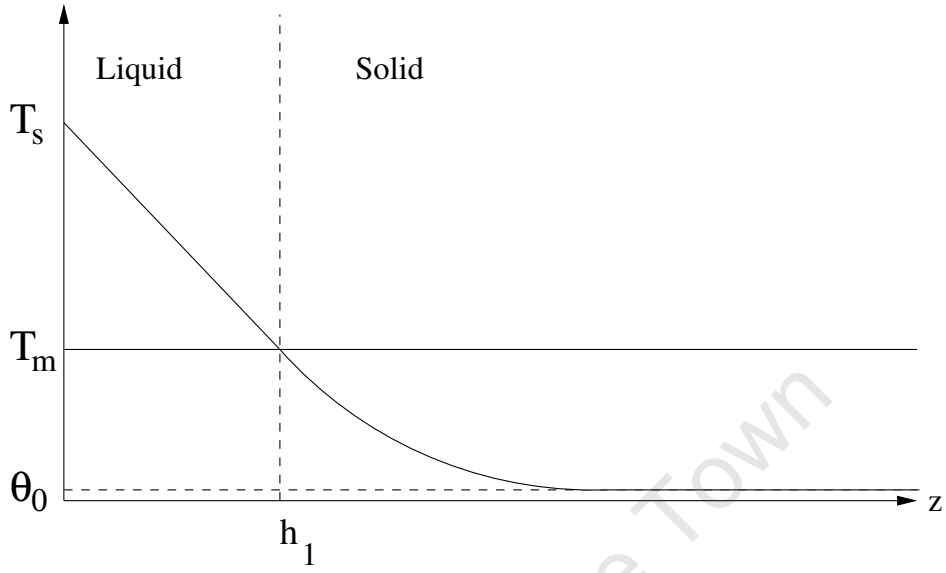

Figure 3.2: *Semi-infinite block on a warm substrate*

The problem is governed by the heat equations (3.2a, b) and the Stefan condition (3.3a) subject to the boundary conditions

$$T(0,t) = T_s, \quad T(h_1,t) = \theta(h_1,t) = T_m, \qquad \theta|_{z\to\infty} \to \theta_0, \tag{3.10}$$

and the two initial conditions

$$\theta(z,0) = \theta_0, \qquad h_1(0) = 0. \tag{3.11}$$

This corresponds to the system described in the previous section with no top liquid layer, $H_0 \to \infty$, and $\alpha_2, \alpha_4 \to \infty$ (which then requires $t_1 = 0$).

The appropriate solution has temperature profiles (see [18])

$$T = T_s + A\text{erf}\frac{z}{2\sqrt{\kappa_l t}}, \qquad \theta = \theta_0 - B\text{erfc}\frac{z}{2\sqrt{\kappa_s t}} \tag{3.12}$$

and interface height

$$h_1(t) = 2\lambda\sqrt{\kappa_l t}, \tag{3.13}$$

where

$$A = \frac{T_m - T_s}{\text{erf}\lambda}, \qquad B = \frac{\theta_0 - T_m}{\text{erfc}(\lambda\sqrt{\kappa_l/\kappa_s})}, \tag{3.14}$$

and λ is found using the Stefan condition (3.3a)

$$\rho_s L_m \sqrt{\pi\lambda} = \frac{k_s}{\sqrt{\kappa_l \kappa_s}} B \exp(-\lambda^2 \kappa_l/\kappa_s) - \frac{k_l}{\kappa_l} A \exp(-\lambda^2). \tag{3.15}$$

3.4.1 Approximate solution in the liquid layer

In this section we discuss the possible methods that can be used in determining the temperature in the liquid region depending on the size of the Stefan number. For small Stefan numbers we show that the asymptotic method is more accurate than the HBI method discussed in Chapter 2. However, for most materials, the Stefan number is quite large (that is, $St > 1$), so the perturbation method in terms of the parameter St breaks down, use is then made of the HBI method. We begin our analysis with the standard problem of the melting of a material initially at its melting temperature and with a prescribed temperature on $z = 0$. Heat is applied at $z = 0$ so that in this case melting occurs immediately. The corresponding system of equations takes the form

$$k_l \frac{\partial^2 T}{\partial z^2} = \rho_l c_l \frac{\partial T}{\partial z}, \qquad 0 < z < h, \tag{3.16}$$

$$\rho L_m \frac{dh}{dt} = -k_l \frac{\partial T}{\partial z}, \qquad \text{at } z = h, \tag{3.17}$$

$$T = 0, \qquad \text{at } z = h \tag{3.18}$$

with the initial condition

$$T(z, 0) = 0, \tag{3.19}$$

and a prescribed temperature condition

$$T = T_s, \qquad \text{at } z = 0. \tag{3.20}$$

We now express the problem in non-dimensional form by setting

$$t' = \frac{t}{\tau}, \qquad h_1' = \frac{h_1}{H_0}, \qquad z' = \frac{z}{H_0}, \qquad T' = \frac{T - T_m}{\Delta T}, \tag{3.21}$$

where τ, H_0 are time and height scales, and the temperature scale is $\Delta T = T_s - T_m$. The heat equation in the liquid becomes

$$\frac{\partial T'}{\partial t'} = \frac{\tau \kappa_l}{H_0^2} \frac{\partial^2 T'}{\partial z'^2}, \tag{3.22}$$

and the Stefan condition is now

$$\frac{\rho_s L_m H_0^2}{\tau k_l \Delta T} \frac{dh_1'}{dt'} = -\frac{\partial T'}{\partial z'}. \tag{3.23}$$

This determines the time-scale for our melting process, $\tau = \rho L_m H_0^2/(k_l \Delta T)$. Substituting this time-scale into the heat equation in the liquid leads to

$$\frac{\partial^2 T'}{\partial z'^2} = \frac{k_l \Delta T}{\rho_s L_m \kappa_l} \frac{\partial T'}{\partial t} = St \frac{\partial T'}{\partial t'}, \tag{3.24}$$

where $St = c_l \Delta T/(L_m)$, the Stefan number is independent of the choice of height scale. Using the parameter values of ice and water from Table 3.1 and $\Delta T = 20°C$ gives $St = 0.27$. Values of St for other materials may be much larger, as shown in the table, as a result a perturbation expansion of the solution in terms of this parameter will not work. The following asymptotic expansion is valid only for materials such as ice and water where typically the times taken for the solidified phase to acquire a given thickness are very much greater than the times for heat to diffuse the same distance resulting in a small St (see, [29]). We now look for a series

	L_m (J/kg)	c (J/kg° C)	T_m (°C)	St
Aluminium	3.96×10^5	900	933.4	1.45
Iron	2.67×10^5	448	1808	2.54
Copper	2.05×10^5	385	1981	3.17
Lead	0.23×10^5	130	600.75	1.73
Zinc	1.10×10^5	787	390	1.74
Ice	3.34×10^5	4186	0	0.27

Table 3.1: Stefan numbers of typical phase change materials [29].

solution for T' in the form

$$T' = T_0' + StT_1' + St^2 T_2' + \cdots \tag{3.25}$$

Substituting this into equation (3.24) produces the following set of equations

$$\mathcal{O}(1)\ :\quad \frac{\partial^2 T_0'}{\partial z'^2}=0; \qquad \mathcal{O}(St)\ :\quad \frac{\partial^2 T_1'}{\partial z'^2}=\frac{\partial T_0'}{\partial t'}; \quad \cdots; \quad \mathcal{O}(St^n):\ \frac{\partial^2 T_n'}{\partial z'^2}=\frac{\partial T_{n-1}'}{\partial t'}, \tag{3.26}$$

$n=1,2,\cdots$, with the corresponding boundary conditions

$$T_0'=1, \quad T_1'=T_2'=\cdots T_n'=0, \quad \text{at } z'=0, \tag{3.27}$$

$$T_0'=T_1'=T_2'=\cdots T_n'=0, \quad \text{at } z'=h_1'. \tag{3.28}$$

The corresponding $\mathcal{O}(1)$ and $\mathcal{O}(St)$ solutions are given by

$$T' = 1-\frac{z'}{h_1'}, \tag{3.29}$$

$$T' = 1-\frac{z}{h_1'}-St\left[\frac{z'}{6}\left(1-\frac{z'^2}{h_1'^2}\right)\right]\frac{dh_1'}{dt'}. \tag{3.30}$$

Higher order solutions include higher order derivatives of h_1, for example, the solution with terms up to $\mathcal{O}(St^2)$ is given by

$$T' = 1-\frac{z}{h_1'}-St\left[\frac{z'}{6}\left(1-\frac{z'^2}{h_1'^2}\right)\right]\frac{dh_1'}{dt'} \tag{3.31}$$

$$+St^2\left\{\frac{z'}{60}\left(\frac{dh_1'}{dt'}\right)^2\left[h_1'^3-\frac{z'^4}{h_1'^3}\right]+\frac{z'}{120}\frac{d^2h_1'}{dt'^2}\left[h_1'^2+\frac{z'^4}{h_1'^2}-2z'^2\right]\right\}. \tag{3.32}$$

Substituting this solution into the Stefan condition leads to a second order differential equation in h_1' which requires two initial conditions to solve. The current problem and the contact melting problem is only accompanied by one initial condition $h_1'(0)=0$, so including higher order terms requires prescribing additional boundary conditions. Consequently, we consider only solutions up to $\mathcal{O}(St)$ as given in (3.30).

In dimensional form, equation (3.30) is given by

$$T=T_s-(T_s-T_m)\frac{z}{h_1}-\frac{(T_s-T_m)}{6\kappa_l}z\left(1-\frac{z^2}{h_1^2}\right)\frac{dh_1}{dt}. \tag{3.33}$$

We note at this stage that this cubic solution does not have a quadratic term. This result together with the results of Chapter 2 motivates us to use a cubic polynomial in the solid layer when using the heat balance integral method.

The derivative, evaluated at $z = h_1$,

$$\left.\frac{\partial T}{\partial z}\right|_{z=h_1} = -\frac{(T_s - T_m)}{h_1} + \frac{T_s - T_m}{3\kappa_l}\frac{dh_1}{dt}, \tag{3.34}$$

will be substituted into the Stefan condition, (3.3a), once the temperature in the solid layer is determined.

As discussed above, the asymptotic expansion (3.25) is only valid for small values of St. However as shown in Table 3.1, many materials have large St (that is, $St \geq 1$). In such cases, the asymptotic method developed above breaks down, use is then made of the HBI method. Assuming a temperature profile of cubic form in $(1-z/h)$, with no quadratic terms, also expressed in non-dimensional form, we use the form

$$T' = a_0\left(1 - \frac{z}{h}\right) + a_1\left(1 - \frac{z}{h}\right)^3, \tag{3.35}$$

since this leads to coefficients a_0 and a_1 that are independent of time [82]. This formulation automatically satisfies $T(h,t) = 0$. Applying $T(0,t) = 1$ gives $a_1 = 1 - a_0$, and we are left with

$$T' = \left[a_0\left(1 - \frac{z}{h}\right) + (1 - a_0)\left(1 - \frac{z}{h}\right)^3\right]. \tag{3.36}$$

In dimensional form this is given by

$$T = T_m + (T_s - T_m)\left[a_0\left(1 - \frac{z}{h}\right) + (1 - a_0)\left(1 - \frac{z}{h}\right)^3\right]. \tag{3.37}$$

Integrating the heat equation (3.24) in the interval $[0, h]$ we obtain

$$\left.\frac{\partial T}{\partial z}\right|_{z=h} - \left.\frac{\partial T}{\partial z}\right|_{z=0} = \frac{d}{dt}\int_0^h T dz. \tag{3.38}$$

Equation (3.37) shows

$$\left.\frac{\partial T}{\partial z}\right|_{z=h} = -\frac{a_0(T_s - T_m)}{h}, \quad \left.\frac{\partial T}{\partial z}\right|_{z=0} = \frac{(a_0 - 3)(T_s - T_m)}{h}, \quad \int_0^h T dz = \frac{h(a_0 + 1)(T_s - T_m)}{4}, \tag{3.39}$$

and the Stefan condition becomes

$$\frac{a_0(T_s - T_m)}{St} = h\frac{dh}{dt}. \tag{3.40}$$

Using the Stefan condition (3.40), and results in (3.39), equation (3.38) reduces to a differential equation in terms of the two unknowns $h(t)$ and a_0 given by

$$h\frac{dh}{dt} = \frac{4(3-a_0)}{a_0+1+4St}(T_s - T_m). \tag{3.41}$$

Combining equations (3.40) and (3.41) we find that the constant satisfies a quadratic equa-

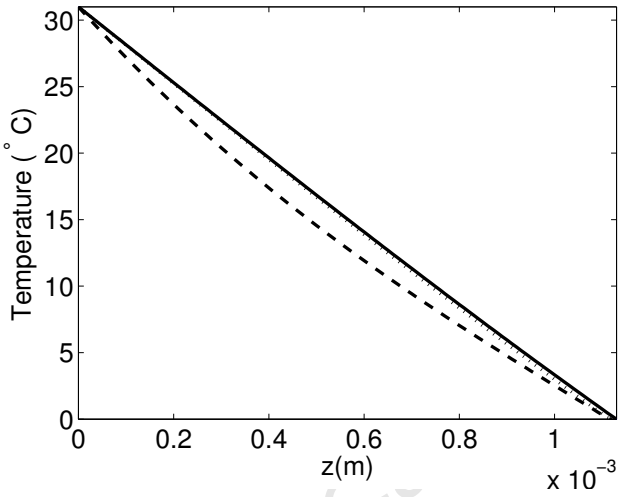

Figure 3.3: *Comparison of the HBI-solution (3.37, dash), perturbation solution (3.33, dot) and the exact solution (3.12a, solid) in the liquid region, with* $St = 0.27$.

tion and is given by

$$a_0 = (-1 - 8St + \sqrt{1 + 62St + 64St^2})/2, \tag{3.42}$$

where we have used the positive square root to ensure $T_z(h,t) < 0$. Noting that a_0 is a constant then from either (3.40) or (3.41) it is clear that

$$h = 2\alpha\sqrt{t}, \qquad \text{where } \alpha = \sqrt{a_0/2St}. \tag{3.43}$$

Now that a_0 and $h(t)$ are known we can predict the evolution of the melt front and by substituting into equation (3.37) we also know the temperature $T(z,t)$ for all time. Figure 3.3 compares the HBI solution, the perturbation solution and the exact solution obtained by using the parameters from Tables 2.1 and 3.1. Clearly the perturbation solution is more accurate as it is very close to the exact solution. This explains why we prefer the perturbation method in the later work.

3.4.2 Approximate solutions in the solid layer

In the solid layer we employ a modified version of the heat balance integral method of [25]. Once melting begins, Goodman and Shea imposed a quadratic temperature profile in the liquid layer, defined by $z \in [0, h_1]$, and another quadratic all the way across the solid layer, $z \in [h_1, H_0]$ in the case of a finite domain. We will use a similar approach but with the following differences. Firstly, the asymptotic solution in the liquid indicates that the profile is more naturally described by a cubic (with no quadratic term). This is in keeping with the small argument expansion of the error function solutions (3.12), in both the solid and liquid layer which involve only odd powers of z. Consequently we use cubic approximations rather than a quadratic (in terms of the shifted co-ordinate $\delta_1(t) - z$). Secondly, rather than stretch the single cubic across the whole solid region (which leads to a poor approximation when the liquid first appears), in Phase 2, we use two cubic profiles to define the two boundary layers in the solid. The two cubics meet when the boundary layers $\delta_1 = \delta_2$, as shown in Figure 1.2. However, for the current problem we are only interested in the semi-infinite case, hence we focus on the behaviour near $z = h_1$ to compare with the error function solution. In this case the method proceeds as follows. We choose

$$\theta(z,t) = a(t) + b(t)(\delta_1(t) - z) + c(t)(\delta_1(t) - z)^3, \tag{3.44}$$

to represent the temperature profile for $z \in [h_1, \delta_1]$. This profile matches the constant temperature region at $z = \delta_1$. There are four unknowns $a,\ b,\ c,\ \delta_1$ which are determined as follows. At the unknown position $\delta_1(t)$, the temperature smoothly approaches the initial temperature θ_0

$$\theta(\delta_1, t) = \theta_0, \qquad \left.\frac{\partial \theta}{\partial z}\right|_{z=\delta_1} = 0. \tag{3.45}$$

As discussed in Chapter 2, these two conditions lead to $a = \theta_0,\ b = 0$. The interface condition $\theta(h_1, t) = T_m$, gives

$$c(t) = \frac{T_m - \theta_0}{(\delta_1 - h_1)^3}, \tag{3.46}$$

so,

$$\theta(z,t) = \theta_0 + \frac{T_m - \theta_0}{(\delta_1 - h_1)^3}(\delta_1 - z)^3. \tag{3.47}$$

We define the integral of the temperature as

$$\tilde{\theta}(t) = \int_{h_1}^{\delta_1} \theta dz = (\delta_1 - h_1)\frac{3\theta_0 + T_m}{4}. \tag{3.48}$$

Integrating the heat equation in the solid layer from $z = h_1$ to $z = \delta_1$ gives

$$\kappa_s \left[\left.\frac{\partial\theta}{\partial z}\right|_{z=\delta_1} - \left.\frac{\partial\theta}{\partial z}\right|_{z=h_1} \right] = \int_{h_1}^{\delta_1} \frac{\partial\theta}{\partial t} dz = \frac{d\tilde{\theta}}{dt} - \theta_0 \frac{d\delta_1}{dt} + T_m \frac{dh_1}{dt}, \tag{3.49}$$

where we have interchanged the derivative with the integral. Substituting for θ_z and $\tilde{\theta}$ leads to the following equation for δ_1 and h_1:

$$\frac{12\kappa_s}{\delta_1 - h_1} = \frac{d\delta_1}{dt} + 3\frac{dh_1}{dt}. \tag{3.50}$$

The second equation comes from substituting θ_z and T_z (given in (3.34)) into the Stefan condition (3.3(a))

$$\left[\rho_s L_m - \frac{k_l(T_m - T_s)}{3\kappa_l}\right]\frac{dh_1}{dt} = -3k_s\frac{T_m - \theta_0}{\delta_1 - h_1} - k_l\frac{T_m - T_s}{h_1}. \tag{3.51}$$

The original problem, defined in terms of two PDES for the temperature and an ODE for the interface position, has now been reduced to two first order, coupled ODEs for δ_1 and h_1. These are then solved numerically using MATLAB ode45 solver package, subject to the initial conditions $h_1(0) = \delta_1(0) = 0$.

3.4.3 Comparison of results

In Figure 3.4 we compare temperature profiles, at times t=1,5,10,20s, obtained via the approximate and exact methods. The dashed line on the figures is the exact solution for the temperature in the two regions, and the solid line is the approximate solution. Within the liquid layer there is no visible difference, whereas within the solid layer there is a slight difference which is most noticeable near $z = \delta_1$ (marked with a 'dot'). However, the important

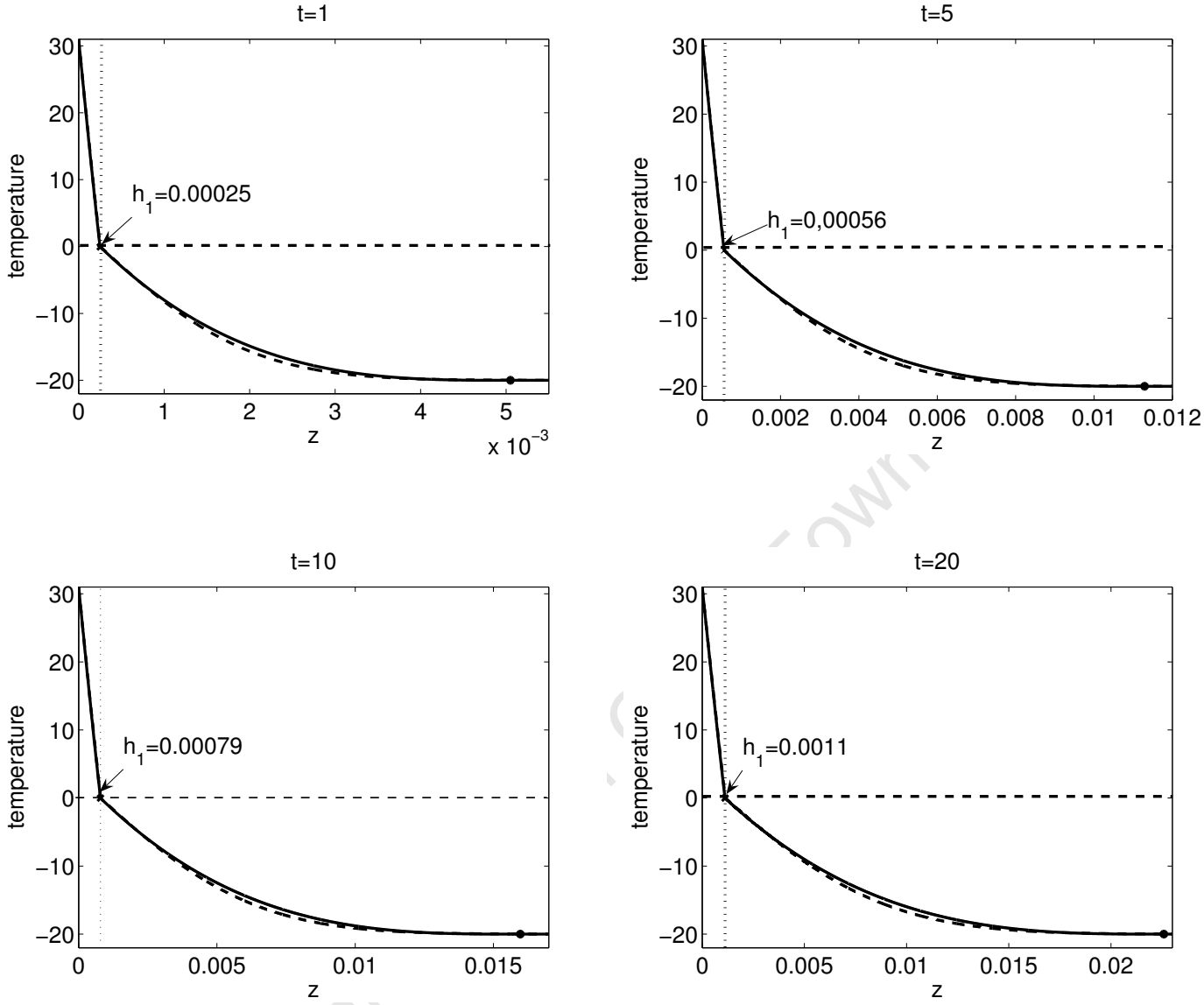

Figure 3.4: *Comparison of the exact error function solution (dashed line) with the approximate cubic solution (solid line) at* $t = 1, 5, 10, 20$ *s, '*$*$*' denotes the position of* δ_1*. Here* $St = 0.27$*.*

point is that the gradients near $z = h_1$, are similar since it is the temperature gradient that determines h_1. In this example, the error in h_1 remains constant, around 1.3%. In this chapter, we only show results using a cubic profile since: 1) it provided accurate results in all our tests that we conducted in Chapter 2; 2) it is consistent with the asymptotic approximation in the liquid and the small argument expansion of the error functions; and 3) the quadratic

solution has a discontinuity in the gradient where the temperature reaches θ_0. The quadratic gives $\theta_{zz}(\delta_1, t) = 2c(t)$, the cubic joins smoothly to the flat region, $\theta_{zz}(\delta_1, t) = 0$. In [49] a similar one-dimensional problem is investigated. They use an exponential approximating function, motivated by the fact that $\text{erf}(z) \sim ze^{-z^2}$. Using this approximation for the problem of this section gives a prediction of h_1 which is very similar to the cubic approximation. However, when applied to Phase 1 as discussed in Chapter 2, the results are significantly worse: the time at which the liquid first appears is predicted to within only 23%, rather than 0.3% for the cubic. The cubic appears to give the best results over different stages.

3.5 Melting in a warm environment

We now move on to illustrate our method on a more general problem for which there is no analytical solution, which is the melting of a finite block in a warm environment with a cooling condition. The melting progresses through the four stages depicted in Chapter 1, Figure 1.2. Phase 1 was dealt with in Chapter 2, we start our discussion with Phase 2.

Phase 2: The second phase begins when the bottom surface starts to melt and ends when the two boundary layers meet, $\delta_1 = \delta_2$, as indicated in Figure 3.5 or when the top surface begins to melt; we will only consider the former criterion. The initial values of δ_1 and δ_2 are simply those determined at the end of Phase 1. With the appearance of a liquid layer, we introduce the liquid temperature T and the interface position h_1. In this phase, there is always a region where $\theta = \theta_0$ within the block. The calculation at the top of the block remains unchanged. At $z = 0$ we now impose the cooling condition (3.6) on the liquid layer and at $z = h_1$ equation (3.8) holds.

Using the method described in §3.4.1 we find the temperature in the liquid to be

$$\begin{aligned} T(z,t) &= T_m + \frac{\beta_1}{1+\alpha_6 h_1}(z-h_1) - \frac{\beta_1}{6\kappa_l(1+\alpha_6 h_1)^2}\left[3\left(z^2 - \frac{h_1^2(1+\alpha_6 z)}{1+\alpha_6 h_1}\right)\right. \\ &\quad \left. +\alpha_6\left(z^3 - \frac{h_1^3(1+\alpha_6 z)}{1+\alpha_6 h_1}\right)\right]\frac{dh_1}{dt}, \end{aligned} \tag{3.52}$$

where, for convenience, we write $\beta_1 = \alpha_5 + \alpha_6(T_m - T_s)$. The temperature gradient at the

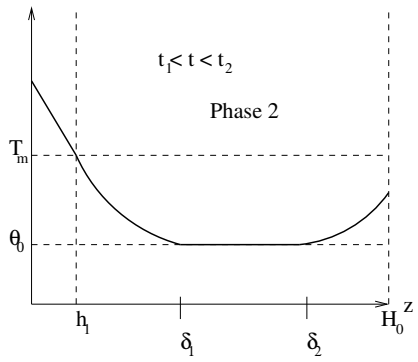

Figure 3.5: *Schematic of Phase 2 of melting when a block is placed on a surface above the melting temperature*

interface is

$$\left.\frac{\partial T}{\partial z}\right|_{z=h_1} = \frac{\beta_1}{1+\alpha_6 h_1} - \frac{\beta_1 h_1}{3\kappa_w(1+\alpha_6 h_1)^3}\left[3+3\alpha_6 h_1+\alpha_6^2 h_1^2\right]\frac{dh_1}{dt}\ . \tag{3.53}$$

In the solid boundary layer, $z \in [h_1, \delta_1]$, the temperature profile is

$$\theta_1(z,t) = \theta_0 + \frac{T_m-\theta_0}{(\delta_1-h_1)^3}(\delta_1-z)^3\ . \tag{3.54}$$

Integrating the heat equation in the solid between $[h_1, \delta_1]$ and applying (3.54) gives a first order ODE involving h_1, δ_1. The Stefan condition provides a second relation and so in the lower region the process is described by

$$\left[\rho_s L - k_w f(h_1)\right]\frac{dh_1}{dt} = \frac{3k_i(\theta_0-T_m)}{\delta_1-h_1} - \frac{k_w\beta_1}{1+\alpha_6 h_1} \tag{3.55}$$

$$3\frac{dh_1}{dt} + \frac{d\delta_1}{dt} = \frac{12\kappa_i}{\delta_1-h_1}\ , \tag{3.56}$$

where

$$f(h_1) = \frac{\beta_1 h_1}{3\kappa_w(1+\alpha_6 h_1)^3}\left[3+3\alpha_6 h_1+\alpha_6^2 h_1^2\right]\ . \tag{3.57}$$

Note that equations (3.55, 3.56) are independent of δ_2. However, we still need to calculate the temperature in the upper region to determine the end of phase 2. This could occur because either $\delta_1 = \delta_2$ or the top starts to melt, $\theta_2(H_0, t) = T_m$. We choose the first condition now and deal with the second in Phase 4. In the ice accretion model used in [51, 52, 53, 54]

it is assumed that the layers are sufficiently thin that a linear approximation holds. The contribution of the liquid layer in that model is represented by the final term in (3.55). The difference obtained by taking the cubic approximation, i.e. including the next term in the series expansion, introduces the correction factor $k_w f(h_1)\frac{dh_1}{dt}$. Since this simply moves to the left hand side, the final calculation is just as simple as in the linear approximation but there is a distinguishable gain in accuracy.

In the solid for $z \in [\delta_2, H_0]$ equation (2.61c) describes the temperature. Equation (2.64) determines δ_2 and so we solve this simultaneously with (3.55, 3.56) to find the end of Phase 2 and the initial temperature for the new phase, hence a new calculation must begin. We denote the time that Phase 2 ends as t_2.

Phase 3: This phase begins when the boundary layers meet (see Figure 3.6), $\delta_1 = \delta_2$ at $t = t_2$, it ends when the top layer reaches the melting temperature, $\theta(H_0, t) = T_m$ at $t = t_3$, and we must then start a calculation with a second liquid layer. Since there has

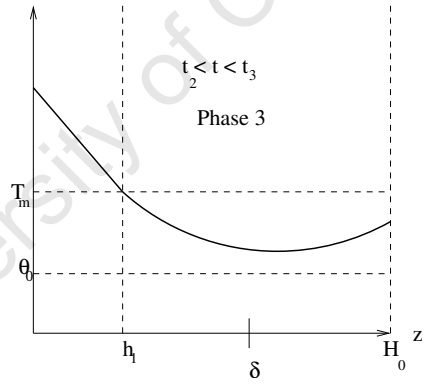

Figure 3.6: *Schematic of Phase 3 of the melting process .*

been no change to the model in the liquid layer the temperature for $z \in [0, h_1]$ is still defined by equation (3.52). During Phase 2 we approximated the temperature at either side of the block by two cubics. Obviously we would now hope to simplify the analysis by applying a single cubic across the whole layer; Goodman & Shea use a single quadratic as soon as melting starts at $z = 0$. Unfortunately, the solution profile still has a very shallow base and steep edges, so a single quadratic or cubic polynomial does not provide a good

fit. We therefore use two cubic profiles which meet at the point $z = \delta(t)$ with the initial condition $\delta(t_2) = \delta_1(t_2) = \delta_2(t_2)$. Our previous functions δ_1, δ_2 defined the points where the temperature reached θ_0 and $\theta_z = 0$. Once the boundary layers meet then the temperature will rise above θ_0 but there will still be a point where the temperature gradient is zero. This provides our definition of δ, namely

$$\theta_1(\delta) = \theta_2(\delta) \ , \qquad \left.\frac{\partial\theta_1}{\partial z}\right|_{z=\delta} = \left.\frac{\partial\theta_2}{\partial z}\right|_{z=\delta} = 0 \ .$$

The temperature for $z \in [h_1, \delta]$, $z \in [\delta, H_0]$ is now given by

$$\theta_1(z,t) = \theta_{mn}(t) + \frac{T_m - \theta_{mn}(t)}{(\delta(t) - h_1)^3}(\delta(t) - z)^3 \ , \tag{3.58}$$

$$\theta_2(z,t) = \theta_{mn}(t) - \frac{\alpha_3 + \alpha_4(T_a - \theta_{mn}(t))}{(H_0 - \delta(t))^2\big(3 + \alpha_4(H_0 - \delta(t))\big)}\big(\delta(t) - z\big)^3, \tag{3.59}$$

respectively. We no longer need to find two boundary layer thicknesses but, since we no longer know the minimum temperature in the block, we have introduced a new unknown $\theta_{mn}(t)$ which, in this case, is an increasing function of time. Substituting the temperature expressions into the heat equation and integrating over (h_1, δ) and (δ, H_0) leads to two ODEs

$$\frac{3\kappa_i(T_m - \theta_{mn})}{\delta - h_1} = \frac{\mathrm{d}}{\mathrm{d}t}\left[(\delta - h_1)\frac{(T_m + 3\theta_{mn})}{4}\right] + T_m\frac{dh_1}{dt} - \theta_{mn}\frac{d\delta}{dt} \tag{3.60}$$

$$\frac{3\kappa_i\big(\alpha_3 + \alpha_4(T_a - \theta_{mn})\big)}{3 + \alpha_4\big(H_0 - \delta\big)} = \frac{\mathrm{d}}{\mathrm{d}t}\left[\theta_{mn}(H_0 - \delta) + \frac{1}{4}\frac{\big(\alpha_3 + \alpha_4(T_a - \theta_{mn})\big)}{3 + \alpha_4\big(H_0 - \delta\big)}(H_0 - \delta)^2\right] + \theta_{mn}\frac{d\delta}{dt} \ . \tag{3.61}$$

These equations involve three unknowns, $\theta_{mn}(t), \delta(t), h_1(t)$, and the system is closed by the addition of the Stefan conditions (3.3), with θ_0 replaced by $\theta_{mn}(t)$ and the three initial conditions for $h_1(t_2)$, $\delta(t_2)$ (determined from the previous phase) and $\theta_{mn}(t_2) = \theta_0$. Hence this phase is described by three nonlinear first order ODEs. It ends at time $t = t_3$, when $\theta_2(H_0, t) = T_m$, which is found from the relation

$$T_m = \theta_{mn}(t_3) - \frac{\alpha_3 + \alpha_4(T_a - \theta_{mn}(t_3))}{3 + \alpha_4(H_0 - \delta(t_3))}\big(\delta(t_3) - H_0\big) \ . \tag{3.62}$$

Phase 4: In this final phase both surfaces of the block melt and so we have two liquid

layers and two moving fronts, denoted by h_1, h_2. This phase will continue until the block has completely melted, when $h_1 = h_2$ (see Figure 3.7). The temperature in the lower liquid

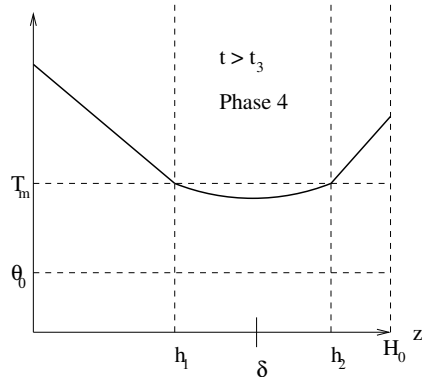

Figure 3.7: *Schematic of Phase 4 of the melting process .*

layer $\theta_1(z,t)$ is still specified by equation (3.58). In the solid the temperature between h_1, δ remains unchanged from the previous section, (3.4). In the region $z \in [\delta, h_2]$ the new boundary condition $\theta_2(h_2,t) = T_m$ results in the profile

$$\theta_2 = \theta_{mn} + \frac{T_m - \theta_{mn}}{(\delta - h_2)^3}(\delta - z)^3 \ . \tag{3.63}$$

In the new liquid layer, the temperature is governed by the heat equation (3.2c) subject to the cooling condition (3.7) and $\chi(h_2,t) = T_m$. Following the same method as for the lower liquid layer we find

$$\begin{aligned}\chi(z,t) &= T_m + \frac{\beta_2}{1+\alpha_8(H_0-h_2)}(z-h_2) \\ &\quad -\frac{\beta_2}{6\kappa_w(1+\alpha_8(H_0-h_2))^2}\Bigg[(H_0-z)^2\left(3+\alpha_8(H_0-z)\right) \\ &\quad -\frac{(H_0-h_2)^2\big(1+\alpha_8(H_0-z)\big)}{1+\alpha_8(H_0-h_2)}\left(3+\alpha_8(H_0-h_2)\right)\Bigg]\frac{dh_2}{dt} \ ,\end{aligned} \tag{3.64}$$

where $\beta_2 = \alpha_7 + \alpha_8(T_a - T_m)$. The temperature gradient required in the Stefan condition is

$$\begin{aligned}\left.\frac{\partial\chi}{\partial z}\right|_{z=h_2} &= \frac{\beta_2}{1+\alpha_8(H_0-h_2)} + \frac{\beta_2(H_0-h_2)}{3\kappa_w(1+\alpha_8(H_0-h_2))^3}\Big[3+3\alpha_8(H_0-h_2) \\ &\quad +\alpha_8^2(H_0-h_2)^2\Big]\frac{dh_2}{dt} \ .\end{aligned} \tag{3.65}$$

At this stage we can proceed as before, integrating the heat equation in the solid layer between $[h_1, \delta_1]$ and $[\delta_2, h_2]$ to find two differential equations. The Stefan conditions at the two liquid interfaces then provide another two ODEs and we are left with a system of four equations for the unknowns $\theta_{mn}, \delta, h_1, h_2$.

As the phases have progressed the complexity of the model has increased, due to the increasing number of regions and moving boundaries. In Phase 4 we have 4 unknowns, however, we can make a significant simplification by noting that the temperature in the solid is close to zero everywhere and the temperature gradient in the solid is much less than that in the liquid layers. If we neglect the contribution of the solid to the evolution of h_1, h_2 then the problem is governed by

$$\big[\rho_s L - k_w f(h_1)\big]\frac{dh_1}{dt} = -\frac{k_w\beta_1}{1+\alpha_6 h_1}\ , \qquad \big[\rho_s L + k_w g(h_2)\big]\frac{dh_2}{dt} = -\frac{k_w\beta_2}{1+\alpha_8(H_0-h_2)}\ , \tag{3.66}$$

where

$$g(h_2) = \frac{k_w\beta_2(H_0-h_2)}{3\kappa_w(1+\alpha_8(H_0-h_2))^3}\Big[3+3\alpha_8(H_0-h_2)+\alpha_8^2(H_0-h_2)^2\Big]\ , \tag{3.67}$$

and $f(h_1)$ is defined in (3.57). We therefore only have to solve two ODEs for two unknowns. As usual the initial condition on h_1 comes from the previous phase; we also impose $h_2(t_3) = H_0$.

3.5.1 Results

In all the following results we take parameter values from Table 2.1. In Figure 2.5, in Chapter 2, the temperature profile at the end of Phase 1 was shown graphically. In Figures 3.8–3.10 we show results for the subsequent stages.

Figure 3.8 shows the temperature profile at $t \approx 32.59\,\mathrm{s}$, and this marks the end of Phase 2. The two boundary layers meet at $z = \delta = 0.0285\,\mathrm{m}$, which is marked by a '$*$'. The liquid height at this time is $h_1 \approx 8.2\times10^{-4}\,\mathrm{m}$. At this stage it is still possible to obtain an analytical solution in the top region. This is shown as the dotted line, which is indistinguishable from

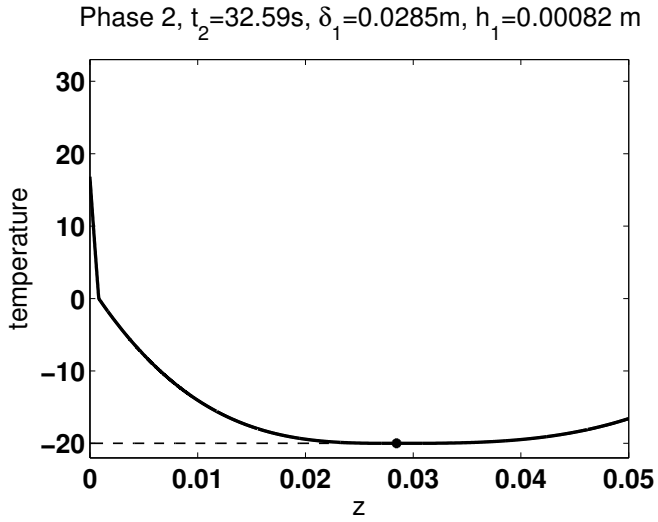

Figure 3.8: *Temperature profile at the end of Phase 2 when* $t_2 \approx 32.59\ s$ *and* $\delta_1 = \delta_2 \approx 0.0285\ m$ *(denoted here by '∗'). The dashed line denotes the error function solution near the right boundary, equation (2.24).*

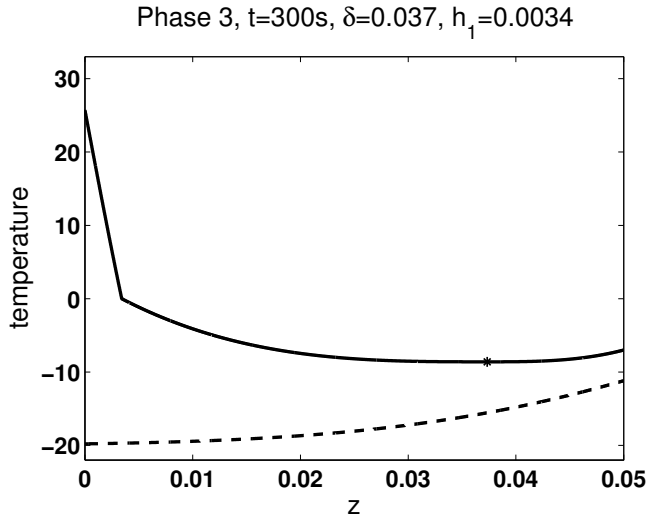

Figure 3.9: *Temperature profile during Phase 3, at* $t = 300\ s$*, where '∗' denotes the position of* $\delta \approx 0.037\ m$*. The dashed line denotes the error function solution near the right boundary, equation (2.24).*

the approximate solution for $z \in [\delta, H_0]$. After the boundary layers meet the energy from the lower layer affects the temperature in the upper region and the error function solution

becomes invalid. This may be seen in Figure 3.9, which shows a temperature profile in Phase 3, at $t = 300\,\mathrm{s}$, where the temperature is everywhere greater than that predicted by the analytical solution. The height of the liquid layer, $h_1 \approx 3.46 \times 10^{-3}\,\mathrm{m}$, is significantly greater than in Figure 3.8; also the position $z = \delta \approx 0.0373\,\mathrm{m}$, marked by a '$*$', has moved to the right. Phase 3 ends when $t = t_3 \approx 561.61\,\mathrm{s}$; this is shown in Figure 3.10(a). At this

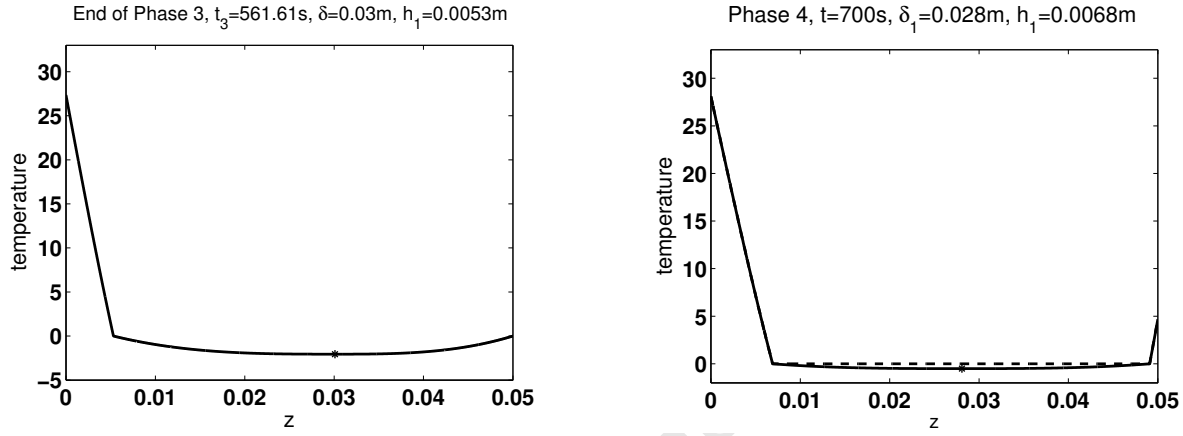

Figure 3.10: *(a) Temperature profile at the end of Phase 3 when $t_3 \approx 561.61\,s$, $\delta \approx 0.03\,m$ and $\theta(H_0, t) = T_m$.(b) Temperature profile during Phase 4, at $t = 700\,s$. The solid line includes the effect of the solid layer, and δ is marked by a '$*$', and the dashed line neglects the solid layer.*

stage $\delta \approx 0.03\,\mathrm{m}$ has moved back towards the centre and $h_1 \approx 5.4 \times 10^{-3}\,\mathrm{m}$. As mentioned at the end of the previous section, the temperature gradient in the solid is small at this time, and becomes smaller as time increases. This is the motivation for neglecting the effect of the solid layer on the evolution of the interfaces during Phase 4.

Figure 3.10(b) shows a temperature profile during Phase 4, at $t = 700\,\mathrm{s}$ (which is well into Phase 4). We have plotted two sets of profiles, the solid line is a product of the full calculation, including the solid layer temperature. For the dashed line we set $\theta = 0$ and solve (3.66) for the liquid layer thicknesses. Within the solid the temperature difference is obvious, however the temperature in the liquid is hardly effected by this approximation. For the full calculation we find $h_1 \approx 6.3 \times 10^{-3}\,\mathrm{m}$, $h_2 \approx 4.87 \times 10^{-2}\,\mathrm{m}$ at $t = 700\,\mathrm{s}$. Neglecting

the temperature in the solid layer we find $h_1 \approx 6.4 \times 10^{-3}\,\mathrm{m}$, $h_2 \approx 4.865 \times 10^{-2}\,\mathrm{m}$ (i.e. errors of 2% and 0.2% respectively). Since the boundary conditions on the solid layer are now symmetric, $\theta = T_m$ at $z = h_1, h_2$, the position of δ must move towards the centre of the solid layer and eventually remain at this point. This is confirmed in Figure 3.10(b) where the full calculation gives $\delta = 0.0276\,\mathrm{m}$ and the centre of the block is at $\frac{1}{2}(h_1 + h_2) = 0.0275\,\mathrm{m}$. This completes the solution method for one-dimensional melting with no squeeze effect.

3.6 Heat source in a cold environment

We now briefly consider a variation of the above method, where a solid layer in a cold environment is heated from below. This example is motivated by de-icing systems, see [66, 78] for example. In this case the initial temperature is linear. In a de-icing system, ice is allowed to accrete on the surface to be protected and is then removed periodically. Electrothermal de-icing systems function by rapidly applying sufficient heat to the ice-surface interface in order to melt the bonding of ice; aerodynamic or centrifugal forces then remove the bulk of ice. In general, it is not sufficient to simply calculate up to the time at which melting first occurs. The solid is typically still frozen at some other point and a liquid layer may grow for a short time until the aerodynamic forces cause the solid to break off. Consequently we may need to know, at least for a short time, the evolution after melting.

Initially we will assume that the solid is in a steady-state, determined by the ambient conditions. Energy is then applied to the lower surface; this represents switching on a de-icing device. The initial temperature of the ice is governed by the steady-state heat equation, $\theta_{zz} = 0$, subject to

$$\theta = T_s\Big|_{z=0}\,, \qquad \theta_z = \alpha_3 + \alpha_4(T_a - \theta)\Big|_{z=H_0}\,, \tag{3.68}$$

where α_3, α_4 depend on the ambient conditions. In the aircraft icing models described in [51, 52, 54] $\alpha_3 = 1.35 \times 10^5\,^\circ\mathrm{C m}^{-1}$, $\alpha_4 = 4.45 \times 10^5\,\mathrm{m}^{-1}$ and $T_s < T_a < T_m$. This gives

$$\theta = \gamma z + T_s\,, \qquad \gamma = \frac{\alpha_3 + \alpha_4(T_a - T_s)}{1 + \alpha_4 H_0}\,. \tag{3.69}$$

Note that with the current values of parameters α_3, α_4, then $\gamma > 0$ and so the temperature is greatest at $z = H_0$. Equation (3.69) provides the initial condition. At $t = 0$ a heating system is turned on such that $\theta_z = \alpha_1$ at $z = 0$, where $\alpha_1 < 0$. A typical value for α_1 is $\alpha_1 = -1428\,^{\circ}\mathrm{Cm}^{-1}$ [54]. The temperature near the lower surface starts to rise quickly but near the upper surface the temperature remains the same. Thus we assume that the solution profile is identical to the steady state solution (3.69) for some region $\delta_1(t) < z < H_0$ where $\delta_1(0) = 0$. Then, following the previously described method for melting a block in a warm environment, we assume the temperature in $0 < z < \delta_1(t)$ is of the form

$$\theta(z,t) = a(t) + b(t)\big(\delta_1(t) - z\big) + c(t)\big(\delta_1(t) - z\big)^3 . \tag{3.70}$$

At $z = \delta_1$ we require θ and θ_z to equal the steady state solution, i.e.

$$\theta(\delta_1, t) = \gamma\delta_1 + T_s \ , \qquad \theta_z(\delta_1, t) = \gamma \ . \tag{3.71}$$

These conditions, together with $\theta_z = \alpha_1$ at $z = 0$, determine the coefficients a, b, c and so (3.70) becomes

$$\theta(z,t) = \gamma\delta_1(t) + T_s - \gamma\big(\delta_1(t) - z\big) + \frac{\gamma - \alpha_1}{3\delta_1(t)^2}\big(\delta_1(t) - z\big)^3 \ . \tag{3.72}$$

To determine $\delta_1(t)$ we integrate the heat equation from $z = 0$ to $z = \delta_1$ and substitute θ from (3.72). This leads to the simple ODE

$$\delta\frac{d\delta}{dt} = 6\kappa_i \ , \tag{3.73}$$

which is independent of α_1. Applying $\delta_1(0) = 0$ gives $\delta(t) = \sqrt{12\kappa_i t}$. So the boundary layer thickness only depends on the thermal diffusivity and time. This solution is valid before melting begins, i.e. whilst $\theta(0,t) < T_m$. The boundary layer thickness when melting starts is found from (3.72) by setting $\theta(0, t_1) = T_m$. The time is then

$$t_1 = \frac{3(T_s - T_m)^2}{4\kappa_i(\alpha_1 - \gamma)^2} \ . \tag{3.74}$$

Since the external parameters, represented by T_m, T_s and γ, are fixed, this equation indicates the appropriate energy input α_1, required to cause melting within a specified time. It is

interesting to note that the ambient temperature T_a does not appear in (3.74). This is because, in this example, the boundary layer does not extend through the solid. As soon as $\delta_1 = H_0$ we have to change the boundary conditions on θ and then T_a will play a role. Figure 3.11 shows temperature profiles before melting begins. The parameter values used are

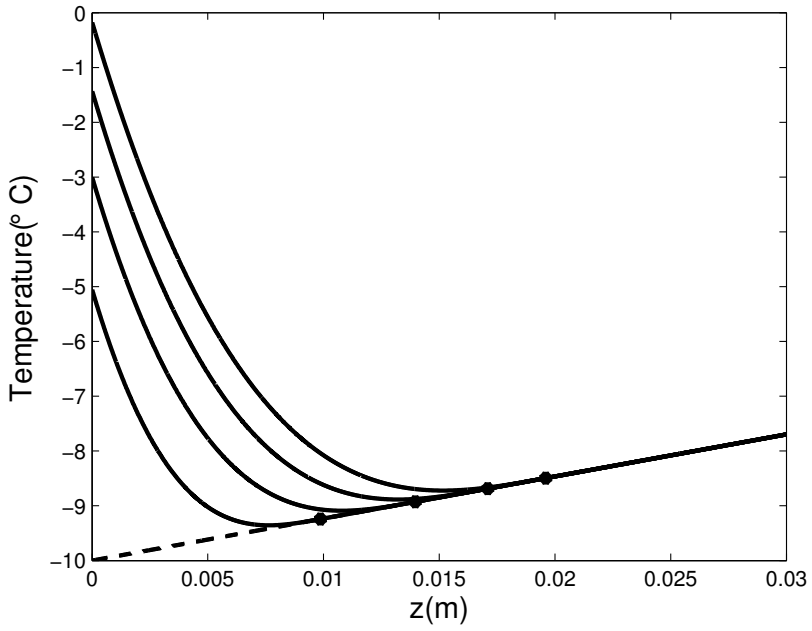

Figure 3.11: *Solution profiles of the aircraft icing example before melting begins, at* $t = 0$ *(dashed line) and* $t = 7, 14, 21, 27.6951$ *s (solid lines).*

$\alpha_1 = -1428\,\mathrm{Cm}^{-1}$, $\alpha_3 = 1.35\times10^5\,\mathrm{Cm}^{-1}$, $\alpha_4 = 4.45\times10^5\,\mathrm{m}^{-1}$, $T_s = -10\,^\circ\mathrm{C}$, $T_a = -8\,^\circ\mathrm{C}$ and $H_0 = 0.023\,\mathrm{m}$; all other parameter values are taken from Table 2.1. The dashed line denotes the initial condition (3.69) and the other lines denote the temperature at $t = 7, 14, 21, t_1\,\mathrm{s}$. The final time, $t_1 = 27.695\,\mathrm{s}$, is found using (3.74). It can be seen that this profile has $\theta(0, t_1) = 0$. The position of δ_1 is marked by a 'dot'.

In general, when considering de-icing, it is not sufficient to simply calculate up to the time at which melting first occurs. The ice is typically frozen at some other point and water may grow for a short time until aerodynamic forces cause the ice to break off. Consequently we may also need to know about the evolution after melting. We therefore introduce the

liquid temperature T and interface position $h_1(t)$, for $t \geq t_1$ and $h_1(t_1) = 0$. Using the method described in §3.4.1 we approximate the solution of the heat equation in the liquid by re-scaling using (3.21) and considering a series expansion in terms of the small parameter St. Here the boundary conditions are $T_z = \alpha_5 (= k_i \alpha_1 / k_w)$ at $z = 0$, for some $\alpha_5 < 0$, and $T = T_m$ at $z = h$. The solution up to $\mathcal{O}(St)$ is given by

$$T = T_m - \alpha_5 (h_1 - z) + \frac{\alpha_5}{2\kappa_w}(h_1^2 - z^2)\frac{dh_1}{dt} \ . \tag{3.75}$$

In the solid the temperature is given by

$$\theta = \gamma \delta_1(t) + T_s - \gamma\big(\delta_1(t) - z\big) + \frac{\gamma h_1 + T_s - T_m}{\big(h_1(t) - \delta_1(t)\big)^3}\big(\delta_1(t) - z\big)^3 \ , \tag{3.76}$$

for $h_1(t) < z < \delta_1(t)$. For $\delta_1(t) < z < H_0$ the steady state solution (3.69) holds provided $\delta_1 \leq h_1$. Using (3.75) and (3.76) in the Stefan condition we obtain

$$\left[\rho_s L_m + h_1 \frac{k_w}{\kappa_w}\alpha_5\right]\frac{dh_1}{dt} = k_s\left[\gamma - \frac{3(\gamma h_1 + T_s - T_m)}{(h_1 - \delta_1)}\right] - k_w \alpha_5, \tag{3.77}$$

and the integrated form of the heat equation in the region $[h_1, \delta_1]$ is

$$f_1(\delta_1, h_1)\frac{d\delta_1}{dt} + f_2(\delta_1, h_1)\frac{dh_1}{dt} = 12\frac{(\gamma h_1 + T_s - T_m)}{(h_1 - \delta_1)}, \tag{3.78}$$

where $f_1(\delta_1, h_1) = T_m - T_s - \gamma h_1$ and $f_2(\delta_1, h_1) = 3(T_m - T_s) - \gamma(\delta_1 + 2h_1)$. Solving (3.77) and (3.78) subject to $h_1(t_1) = 0$ and $\delta_1(t_1) = \delta_1$ enables us to follow the evolution of the film height until $\delta_1 = H_0$, at which point it would be necessary to switch to a different model. However, we stop the calculation here since the general idea is as specified in the previous section and also because it is not necessary to calculate a thick liquid film for this application.

3.7 Conclusions

In this chapter we have developed an approximate solution method to describe one-dimensional melting from an initial heating phase until completion of the melting process. In the solid

phase we employed a modification of the heat integral method of Goodman & Shea. Our approximation proved to be significantly more accurate in cases where the cooling condition is used and of a similar accuracy to the approximation of Goodman & Shea when a constant heat flux condition is applied. Furthermore, the cubic approximation is consistent with the expansions of the analytical solutions when such solutions are available. In the liquid layer an asymptotic analysis was used to determine the temperature profile; this also led to a cubic approximation.

The solution involves a number of different phases which complicate the analysis. However, the same would be true of a numerical solution, as the number of domains and moving boundaries increases. This semi-analytical method then has the advantage that the dependence of the solution on the ambient conditions may be provided explicitly.

The analysis presented here focussed on two examples. In the first a solid block was placed on a warm substrate in a warm environment and the melting followed through its various phases. This example highlighted the different stages and how they progress. Of course there are other possible scenarios but these will all follow similar lines to this example. In our second example we dealt with the problem of heating a solid layer from below. This relatively simple analysis provides an analytical formula which may be used to determine the amount of energy required to melt the base in a given time, or equivalently the time taken for melting to start with a given energy source. This has a clear application in the development of de-icing equipment.

Chapter 4

Unsteady contact melting I

4.1 Introduction

The purpose of this chapter is to develop a mathematical model describing a process of combined melting and lubrication that can occur between an isothermal phase change material (PCM) and a substrate maintained at a constant temperature $T_s > T_m$. This is depicted in Figure 4.1. This describes a simple form of the *contact melting process*, a process in which the heat transfer in both the solid and the liquid is intimately coupled with the fluid flow problem in such a way that the force that is exerted by the melting solid drives the flow of the melt. In Chapter 3 we developed an approximate solution method to describe one-dimensional melting from initial heating until completion of the melting process. That analysis will be used to deal with the thermal analysis part of the contact melting process investigated in the present chapter, although, in the isothermal case, the pre-heating stage is excluded. Consequently, we extend the previous mathematical model to incorporate fluid flow model in the melt region. In the analysis of the thermal problem, the effect of density change upon melting was ignored to be consistent with standard models. In reality there is always a change in density when melting occurs, this results in a relative movement between the solid and the liquid during the melting process. In this chapter, the effects of solid-liquid

density change will be taken into account.

A mathematical description of the contact melting problem consists of the heat and fluid flow equations in the melt layer, a Stefan condition at the melt interface and a force balance between the weight of the solid and the fluid pressure. In general we have the heat equation as well in the solid, this will be discussed in the next chapter. Since the melt layer remains thin throughout the process, we use the lubrication approximation [1, 17] to simplify the flow equations. The corresponding heat equations are simplified by making use of the fact that the heat flow in the thin fluid film is dominated by conduction across the thin film leading to a one-dimensional problem.

In §4.1.1 we will describe the contact melting process and the related results. In §4.2 we provide the problem description and discuss the governing equations, boundary conditions and the approximations that are made in deriving them. The standard squeeze film flow problem which is involved in the contact melting process is discussed in §4.3. The quasi-steady model is also discussed in §4.4 for comparison with the subsequent unsteady solutions. Finally, we show results for the melting of ice on a warm surface and discuss the differences between the present and previous models.

4.1.1 Contact melting process

Contact melting is the process whereby a PCM is placed in contact with a surface that is at a temperature above the phase change temperature. This leads to melting of the PCM, so a fluid layer forms between the two surfaces. The weight of the free solid acts to squeeze out the liquid and so the melt layer remains thin. This process is primarily studied because the heat transfer across the thin melt layer separating the heat source and the melting solid is much higher than the heat transfer by convection, which generally occurs in much thicker layers of molten material. As a consequence of higher heat fluxes, the melting time is considerably reduced, see [27, 37] for example.

In the past, mathematical models of contact melting have relied mainly on the assumption

of quasi-steady, that is, at every point in time the weight of the solid is balanced by the pressure in the liquid film. Other additional assumptions which we listed and discussed in Chapter 1, §1.1 include:

(1) The temperature of the solid remains at the melting temperature, T_m, throughout the process.

(2) Heat transfer in the liquid is dominated by conduction across the film. The film thickness is therefore uniform in the direction tangent to the heated side.

(3) The lubrication approximation holds in the liquid layer, so the flow is primarily parallel to the solid surface and driven by pressure gradient. The pressure variation across the film is negligible.

(4) The amount of melted fluid is small compared to that of the initial solid.

(5) There is perfect thermal contact between the liquid and substrate or there is a constant heat flux, see [4, 27, 37].

Recent studies show that the quasi-steady assumption is not valid for all times during the entire melting process. Yoo [84] has already noted that initially the melt height is far from constant. Their investigations show that for both perfect thermal contact and constant flux the melt thickness initially increases rapidly before reaching an almost constant height. In addition, the constant mass assumption is valid only for sufficiently small times. As the melting progresses the melted mass must at some stage be greater than that of the solid. Consequently the solid mass $M(t)$ must be a decreasing function of time (and this has an effect on the quasi-steady height). In all the investigations, the lubrication approximation is considered to be appropriate, and either assume perfect thermal contact or constant heat flux, which is an unlikely scenario, Newton cooling is more realistic.

4.2 Problem description

In this section we describe the governing equations for a finite thickness PCM placed on a substrate that is above the phase change temperature, as depicted on Figure 4.1. Energy

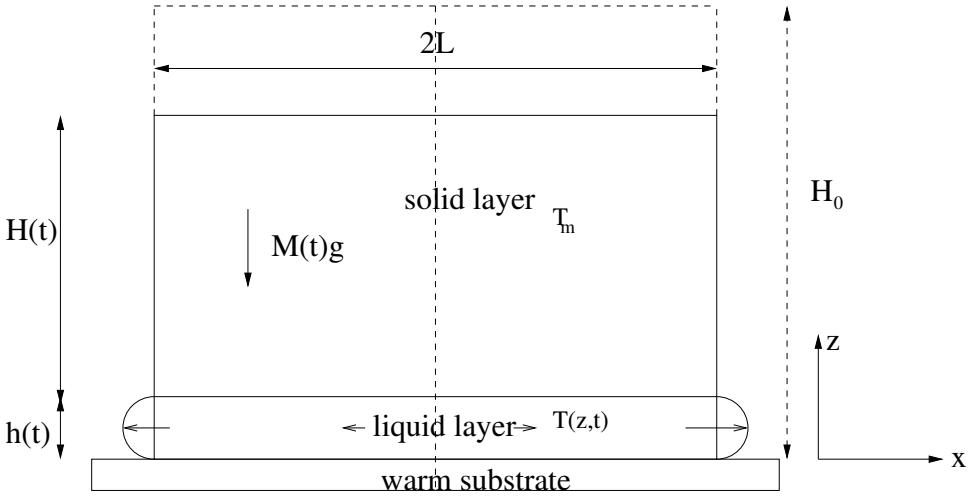

Figure 4.1: *Schematic for solid-substrate contact melting, force balance and coordinate systems.*

is supplied by the substrate and this causes the block to melt. The block has length $2L$ and height $H(t)$. If $h_m(t)$ denotes the thickness of melted solid then the height $H(t) = H_0 - h_m(t)$, where $H_0 = H(0)$ is the initial block thickness. The mass per unit width $M(t) = 2\rho_s L(H_0 - h_m(t))$. The melt layer occupies the region $z \in [0, h(t)]$. The height of the melt layer $h(t)$ differs from h_m since fluid is squeezed out at the edges $x = \pm L$. The pressure at either side of the block is ambient, without loss of generality we can set this to zero, $p(\pm L) = 0$. The block is at the melting temperature T_m. Since $T = T_m$ any rise in the temperature leads to melting, therefore the melting process happens instantly, as a result, in this case the pre-melting phase does not occur as what happens in the melting process discussed in the previous chapters 2 and 3 when the solid needed to heat up first.

4.2.1 Governing equations

The fluid and heat flow in the melt and solid may actually be three-dimensional, however, a two-dimensional model is treated in this chapter. The extension to the three-dimensional case follows easily and is discussed in Chapter 5, §5.5. Five assumptions are made regarding the behaviour of the physical model:

- The fluid is Newtonian and incompressible;
- The flow is laminar and 2-D;
- viscous dissipation is neglected;
- The effect of temperature on physical parameters such as density, specific heat capacity, thermal conductivity and viscosity of the two phases is negligible until the sudden change as melting occurs;
- The heat transfer is one-dimensional (function of z only).

The validity of these assumptions will be discussed later. Using the above assumptions, the flow in the melt induced by the squeezing effect will be modelled by the incompressible Navier-Stokes and the conservation of mass equations

$$\rho_l \left(\frac{\partial u}{\partial t} + u\frac{\partial u}{\partial x} + w\frac{\partial u}{\partial z} \right) = -\frac{\partial p}{\partial x} + \eta \left(\frac{\partial^2 u}{\partial x^2} + \frac{\partial^2 u}{\partial z^2} \right), \tag{4.1}$$

$$\rho_l \left(\frac{\partial w}{\partial t} + u\frac{\partial w}{\partial x} + w\frac{\partial w}{\partial z} \right) = -\frac{\partial p}{\partial z} + \eta \left(\frac{\partial^2 w}{\partial x^2} + \frac{\partial^2 w}{\partial z^2} \right), \tag{4.2}$$

$$\frac{\partial u}{\partial x} + \frac{\partial w}{\partial z} = 0, \tag{4.3}$$

where $\mathbf{u} = (u, w)$ is the corresponding velocity of the liquid, p the liquid pressure, ρ_l and η are the density and dynamic viscosity of the liquid.

The energy equation for the liquid film is given by

$$\frac{\partial T}{\partial t} + u\frac{\partial T}{\partial x} + w\frac{\partial T}{\partial z} = \kappa_l \left(\frac{\partial^2 T}{\partial x^2} + \frac{\partial^2 T}{\partial z^2} \right). \tag{4.4}$$

The amount of liquid in the film gap depends on the melting rate which is driven by the temperature gradient in the liquid region. The Stefan condition provides a relationship between the melting rate and the temperature gradient

$$\rho_s L_m \frac{\mathrm{d}h_m}{\mathrm{d}t} = -k_l \left. \frac{\partial T}{\partial z} \right|_{z=h}. \tag{4.5}$$

An additional equation is obtained by balancing forces at the melting interface. The pressure force in the liquid supports the weight of the solid. The equation of the downward motion

of the solid body is governed by Newton's second law,

$$Mg - \int_{-L}^{L} p dx = M \frac{dW(t)}{dt}. \tag{4.6}$$

The first term on the left hand side represents the weight of the solid, the second term is the fluid pressure acting to support this weight, and $W(t)$ is the downward velocity of the solid.

In order to render the problem mathematically tractable, in addition to the assumptions stated above, further simplifying assumptions will be made, these are:

- The aspect ratio (ϵ), and the reduced Reynolds number ($\epsilon^2 Re$) are negligible. This ensures that the inertia terms are negligible compared to the viscous and pressure terms in the momentum equation.
- The heat transfer is dominated by conduction. This is achieved by requiring that ϵ^2 and $\epsilon^2 Pe$ are negligible, where Pe is the Peclet number.

Application of the first assumption, which is the lubrication approximation [17], leads to the following system of reduced equations

$$-\frac{\partial p}{\partial x} + \eta \frac{\partial^2 u}{\partial z^2} = 0, \qquad \frac{\partial p}{\partial z} = 0, \qquad \frac{\partial u}{\partial x} + \frac{\partial w}{\partial z} = 0, \tag{4.7}$$

for the flow, and the second assumption, leads to the quasi-steady state form of the energy equation

$$\frac{\partial^2 T}{\partial z^2} = 0. \tag{4.8}$$

The Stefan condition is unchanged, the force balance equation takes the form

$$2\rho_s L[H_0 - h_m(t)]g = \int_{-L}^{L} p dx. \tag{4.9}$$

Equations (4.7a−4.7c) represent the standard lubrication approximation for the fluid flow. For realistic situations the largest term neglected in this approximation is $\mathcal{O}(\epsilon^2 Re)$ where, if U is the velocity scale and $\mathcal{H}_l$ the height-scale, the Reynolds number $Re = \rho_l U L/\eta$ and $\epsilon = \mathcal{H}_l/L$. Equation (4.8) is the heat equation in the liquid. Since the liquid layer

remains thin we assume heat transfer is conduction dominated. The largest term neglected is $\mathcal{O}(\epsilon^2 Pe)$, where the Peclet number $Pe = UL/k_l$. This is consistent with the approximations of Bejan [4]. Equation (4.9) is the reduced form of the force balance where we have neglected the acceleration term. This requires the neglect of $\mathcal{H}_l/(g\tau^2)$. We will show that the neglected terms are indeed small in §4.7

4.2.2 Boundary conditions

The boundary conditions accompanying the above system of governing equations are discussed below.

1. At both the moving and stationary boundaries, we assume a no slip boundary condition:

$$u|_{z=0} = u|_{z=h(t)} = 0. \tag{4.10}$$

and impermeable surface condition:

$$w|_{z=0}. \tag{4.11}$$

2. The vertical velocity of the fluid on the solid-liquid interface is affected by both the squeezing effect and the melting rate of the solid layer. To determine an expression of the boundary vertical velocity, we apply a mass balance across the interface. The continuity of mass flux condition is given by

$$\rho_s \mathbf{n} \cdot (\mathbf{u}_s - \mathbf{u_b}) = \rho_l \mathbf{n} \cdot (\mathbf{u} - \mathbf{u}_b), \tag{4.12}$$

where $\mathbf{u_b}$ is the velocity of the boundary, $\mathbf{u}_s$ is the velocity of the solid layer, and $\mathbf{n}$ is the vector normal to the interface. We define these quantities explicitly by:

$$\mathbf{u}_s = (0, W(t)), \qquad \mathbf{u}_b = \left(0, \frac{dh}{dt}\right), \qquad \mathbf{u} = (u, w), \qquad \mathbf{n} = \mathbf{k}. \tag{4.13}$$

Expanding (4.12) leads to

$$w|_{z=h(t)} = (1-\rho)\frac{dh}{dt} + \rho W(t), \tag{4.14}$$

where $W(t) = \frac{dh}{dt} - \frac{dh_m}{dt}$ is the difference between the liquid layer growth rate and the melting rate and $\rho = \rho_s/\rho_l$ is the non-dimensional density ratio. The first term on the right hand side of (4.14) represents the contribution of volume changes to the fluid flow on the boundary and the second term is the contribution coming from the squeezing effect. Equation (4.14) can be expressed in the form

$$w|_{z=h(t)} = \frac{dh}{dt} - \rho\frac{dh_m}{dt}. \tag{4.15}$$

In the absence of melting $w|_{z=h(t)} = \frac{dh}{dt}$ is the standard squeeze velocity.

The quasi-steady assumption [3, 69, 85] requires that $h_t = 0$, in which case (4.15) reduces

$$w|_{z=h(t)} = \rho W(t) = -\rho\frac{dh_m}{dt}. \tag{4.16}$$

3. As discussed before, the pressure must be ambient at both ends of the solid layer, that is

$$p(-L) = p(L) = 0. \tag{4.17}$$

4. The melting interface remains at the melting temperature T_m, so

$$\theta = T = T_m \quad \text{at } z = h. \tag{4.18}$$

5. No heat is lost or gained through the surfaces $z = H(t)$ and $x = \pm L$.

6. If $\theta = T_m$ liquid appears on the surface $z = 0$, a cooling condition is applied to the liquid

$$\frac{\partial T}{\partial z} = \frac{-\alpha_1 + h_{sl}(T - T_s)}{k_l}, \qquad \text{at } z = 0, \tag{4.19}$$

where α_1 represents a heat flux from the substrate. In the limit $h_{sl} \to \infty$ we retrieve the standard perfect thermal contact condition $T = T_s$ at $z = 0$. When $h_{sl} = 0$ we retrieve the constant flux condition.

4.3 The standard squeeze film problem

We now discuss briefly the standard squeeze problem which plays a major role in the contact melting process. The model under consideration is as depicted in Figure 4.1, the block in this case has a constant mass M, and in addition, for squeezing to take place, we assume initially that there is fluid thickness occupying the gape H_l between the solid and the substrate.

The standard lubrication problem as described in §4.2.1 consists of solving equations (4.7a−4.7c) subject to the no-slip boundary conditions

$$u|_{z=0,h} = 0, \quad w|_{z=h} = 0, \quad w|_{z=h} = \frac{dh}{dt}. \tag{4.20}$$

Integrating equation (4.7a) subject to (4.20a) yields the fluid velocity profiles

$$u(x,z,t) \;=\; \frac{1}{2\eta}\frac{\partial p}{\partial x}(z^2 - zh), \qquad w(x,z,t) = -\frac{1}{12\eta}\frac{\partial^2 p}{\partial x^2}z^2(2z-3h). \tag{4.21}$$

Integrating the continuity equation (4.7c) across the film leads to

$$\int_0^h \frac{\partial u}{\partial x}dz + w|_{z=h} - w|_{z=0} = 0. \tag{4.22}$$

Applying Leibniz theorem to the integral and substituting for w via (4.20c) leads to the mass balance

$$\frac{\partial Q}{\partial x} + \frac{dh}{dt} = 0, \tag{4.23}$$

which is the governing equation for the fluid flow. Here Q is the longitudinal flow rate given by

$$Q = \int_0^h u dz = -\frac{1}{12\eta}\frac{\partial p}{\partial x}h^3, \tag{4.24}$$

demonstrating that the pressure gradient is responsible for the fluid flow.

Equation (4.23) may be written as

$$\frac{\partial^2 p}{\partial x^2} = \frac{12\eta}{h^3}\frac{dh}{dt} \tag{4.25}$$

which is known as Reynolds equation.

Integrating equation (4.25) subject to the conditions $p = 0$ at $x = \pm L$ leads to

$$p = \frac{6\eta}{h^3}\frac{\partial h}{\partial t}(x - L)(x + L), \tag{4.26}$$

the corresponding horizontal and vertical velocity profiles are given by

$$u(x, z, t) = \frac{6}{h^3}\frac{dh}{dt}(z^2 - zh), \qquad w(x, z, t) = \frac{1}{h^3}\frac{dh}{dt}z^2(2z - 3h), \tag{4.27}$$

which are the typical Poiseuille flow profiles between horizontal rigid boundaries. The equation of motion (4.9) of the solid in the absence of melting (i.e $\frac{dh_m}{dt} = 0$) and with the acceleration term retained, takes the form

$$2LH_0\rho_s g - \int_{-L}^{L} p(x, t)dx = 2LH_0\rho_s \frac{d^2h}{dt^2}, \tag{4.28}$$

which together with (4.26) leads to the following initial value problem for the determination of h

$$\gamma_0 h^3 + \frac{dh}{dt} = \frac{\gamma_0}{g}h^3\frac{d^2h}{dt^2}, \qquad h(0) = \mathcal{H}_l, \qquad \left.\frac{dh}{dt}\right|_{t=0} = 0, \tag{4.29}$$

where $\gamma_0 = \rho_s g H_0/(4\eta L^2)$. In most studies , see [36, 74] for example, the moving bodies are assumed to approach each other with a constant velocity, as such, the acceleration term is ignored leading to a much simpler differential equation

$$\gamma_0 h^3 + \frac{\partial h}{\partial t} = 0, \qquad h(0) = \mathcal{H}_l, \tag{4.30}$$

whose solution is

$$h = \frac{\mathcal{H}_l}{\sqrt{1 + 2\gamma_0\mathcal{H}_l^2 t}}. \tag{4.31}$$

4.3.1 Results and discussion

Figure 4.2 shows the solution of equation (4.29) obtained numerically by using Matlab ode45 solver and the solution (4.31) corresponding to the ice-water system, the parameter values used are given in Table 2.1. It important to note that this problem has no steady-state, beyond the trivial $h = 0$. It is clear from equation (4.26) that the pressure inside the gap is proportional to $1/h^3$, hence, as the gap size decreases, the pressure increases, so that for

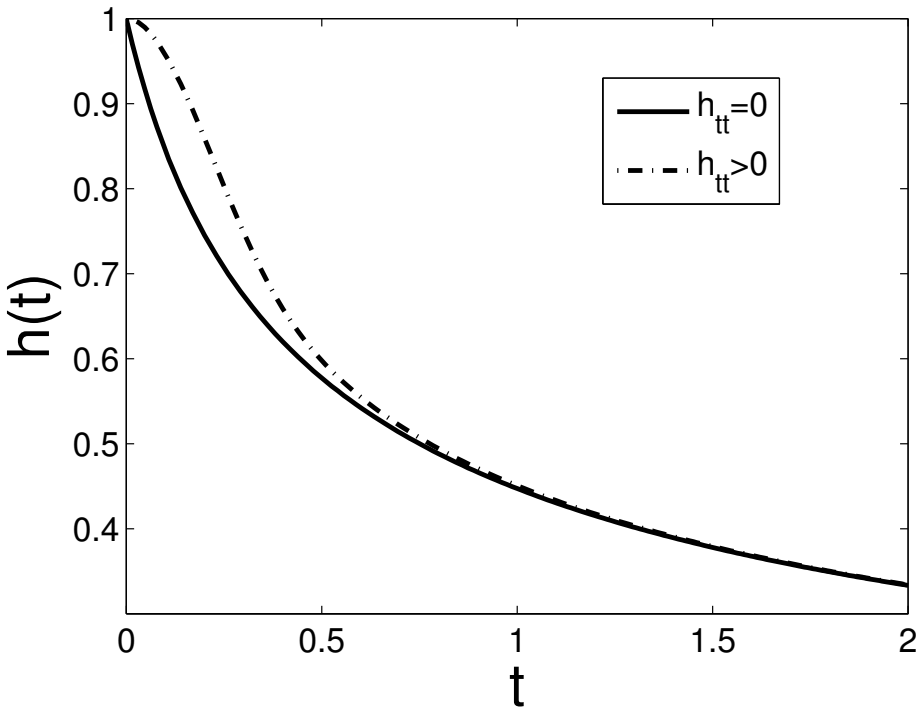

Figure 4.2: *Variation of the film thickness with time.*

sufficiently small h the solid starts to decelerate until it eventually moves with an approximately constant velocity when the force generated inside the gap balances with the weight of the solid. For such small values of h, as can be seen Figure 4.2, the solution of (4.29) coincides with the solution (4.31), this implies that the effect of the acceleration term on the right hand side of equation (4.28) is small for small h, hence it may be neglected. This justifies why the acceleration term is often neglected in contact melting problems, since in such models $h << 1$.

4.4 Standard quasi-steady analysis

Before proceeding to the full problem we first consider the standard quasi-steady solution but use the general cooling condition (4.19). The standard quasi-steady analysis requires an isothermal solid, a fixed melt layer thickness, $h_t = 0$, and a fixed solid mass, see [26, 27, 84]

for example. Assumptions 1, 2 and 5 reduce the Stefan condition and mass balance to

$$\rho_s L_m \frac{\mathrm{d}h_m}{\mathrm{d}t} = -k_l \left.\frac{\partial T}{\partial z}\right|_{z=h}, \qquad 2\rho_s L H_0 g = \frac{8\eta L^3}{h^3}\frac{\rho_s}{\rho_l}\frac{dh_m}{dt}. \tag{4.32}$$

The vertical velocity condition at $z = h$ given in equation (4.15) changes to

$$w(h,t) = -\rho\frac{dh_m}{dt} \tag{4.33}$$

and the pressure expression takes the form

$$p = -\frac{6\eta\rho}{h^3}\frac{dh_m}{dt}(x^2 - L^2). \tag{4.34}$$

Substituting for the pressure, equation (4.34) into the force balance, equation (4.32b), and integrating leads to a differential equation for h_m which integrates to

$$h_m = \frac{H_0\rho_l g h_q^3}{4\eta L^2}t\,, \tag{4.35}$$

where h_q denotes the quasi-steady melt height. Without the squeeze effect $h_m \sim \sqrt{t}$, see [18], so it is clear that the squeeze effect leads to more rapid melting. To determine h_q we must look at the thermal problem.

We solve the quasi-steady state equation

$$\frac{\partial^2 T}{\partial z^2} = 0, \tag{4.36}$$

subject to the boundary conditions

$$\left.\frac{\partial T}{\partial z}\right|_{z=0} = -\frac{q + h_{sl}(T - T_s)}{k_l}, \quad T|_{z=h} = T_m. \tag{4.37}$$

This yields the profile

$$T = T_m - \frac{\alpha_1 + h_{sl}(T_s - T_m)}{k_l + h_{sl}h}(z - h)\ . \tag{4.38}$$

Substituting into the Stefan condition gives

$$\rho_s L_m \frac{H_0\rho_l g}{4\eta L^2}h_q^3 = k_l\frac{\alpha_1 + h_{sl}(T_s - T_m)}{(k_l + h_{sl}h_q)}. \tag{4.39}$$

This provides a quartic equation for the quasi-steady height h_q, which is easily solved numerically. The melt height then follows from equation (4.35). In the limit $h_{sl}h_q \ll k_l$ we obtain

$$h_q \approx \sqrt[3]{\frac{4\eta L^2\left(\alpha_1 + h_{sl}(T_s - T_m)\right)}{\rho_s \rho_l L_m H_0 g}} \ . \tag{4.40}$$

In the limit of perfect thermal contact, $h_{sl} \to \infty$, we retrieve the standard quasi-steady result for an isothermal block, subject to $T(0,t) = T_s$

$$h_{q\infty} = \sqrt[4]{\frac{4\eta L^2 (T_s - T_m)}{\rho_s \rho_l L_m H_0 g}} \ . \tag{4.41}$$

Note there is a qualitative difference between these two expressions. If we assume perfect thermal contact then $h \sim (T_s - T_m)^{1/4}$. The more realistic condition of finite h_{sl} gives $h \sim (T_s - T_m)^{1/3}$. This same power was obtained in [84] for the case $h_{sl} = 0$ and $\alpha_1 \neq 0$. This result can be retrieved from (4.40) by setting $h_{sl} = 0$.

The melting process is complete when $h_m = H_0$, we denote this time by t_m. From equation (4.35) we find

$$t_m = \frac{4\eta L^2}{\rho_l g h_q^3} \ . \tag{4.42}$$

In Table 2.1 we present appropriate parameter values for the melting of an ice block on a substrate at 298K. The heat transfer coefficients $h_{ss} = 763 W/m^2$ and $h_{sl} = 855$ W/m^2 were obtained through simple experiments, which are described in detail in [56] and in Chapter 1. For a block with $H_0 = 0.05$m, $L = 0.1$m and $\Delta T = 25$ we find $h_q \approx 1.8 \times 10^{-4}$m and then $h_{sl}h_q \sim 0.15$, so it is reasonable to neglect this term in (4.39). For perfect thermal contact $h_{q\infty} \approx 2.70 \times 10^{-4}$m. Groulx *et al* [27] discuss the melting of a block at a constant temperature below the melting temperature, $\theta_0 < T_m$. They suggest this results in replacing L_m with $L_m + c_s(T_m - \theta_0)$ in the expression for $h_{q\infty}$. For the parameter values of Table 2.1 this reduces the height to $h_{q\infty} \approx 2.66 \times 10^{-4}$m. Results will be presented in §4.6 once the unsteady analysis is complete.

4.5 Unsteady analysis

In the quasi-steady case discussed in §4.4, both the mass of the solid and the film thickness h were assumed constant. However, in practise, due to melting, the solid mass will continuously decrease until the whole solid has completely melted. As a result the system will not reach steady state as the force generated inside the film and the weight of the solid keeps on changing.

In this section, we consider the unsteady contact melting process by dropping the constant mass assumption together with the quasi-steady state assumption $h_t = 0$. The governing equations for the fluid flow, heat transfer and the Stefan condition remain unchanged. The only changes are in the vertical velocity boundary condition and the force balance equation. The vertical velocity boundary condition now takes its full form as discussed in §4.2.2:

$$w(h,t) = \frac{dh}{dt} - \rho\frac{dh_m}{dt} \tag{4.43}$$

with the corresponding pressure distribution given by

$$p = \frac{6\eta}{h^3}\left(\frac{dh}{dt} - \rho\frac{dh_m}{dt}\right)(x^2 - L^2). \tag{4.44}$$

Using equations (4.21) in section §4.3, the corresponding velocity profiles are given by

$$u = \frac{6}{h^3}\left[\frac{dh}{dt} - \rho\frac{dh_m}{dt}\right]x(z^2 - zh), \qquad w = -\frac{1}{h^3}\left[\frac{dh}{dt} - \rho\frac{dh_m}{dt}\right]z^2(2z - 3h). \tag{4.45}$$

To incorporate variable mass, the force balance equation, equation (4.32b), takes the form

$$2\rho_s L(H_0 - h_m)g = \int_{-L}^{L} p dx. \tag{4.46}$$

The temperature profile in the liquid obtained in §4.4, equation (4.38), is still valid. Now application of the Stefan condition and the force balance equation given above leads to a system of coupled non-linear equations

$$\rho_s L_m\frac{dh_m}{dt} = \frac{k_l(\alpha_1 + h_{sl}(T_s - T_m))}{k_l + h_{sl}h}, \tag{4.47}$$

$$(H_0 - h_m)\rho_l g = -\frac{4\eta L^2}{h^3}\left(\frac{dh}{dt} - \rho\frac{dh_m}{dt}\right), \tag{4.48}$$

which we solve numerically (using MATLAB ode45 solver) subject to $h = h_m = 0$ and $t = 0$. In the case of unsteady contact melting with constant mass, equation (4.48) takes the form

$$H_0\rho_l g = -\frac{4\eta L^2}{h^3}\left(\frac{dh}{dt} - \rho\frac{dh_m}{dt}\right). \tag{4.49}$$

In the study of the unsteady contact melting conducted by Yoo [84], the relationship between the solid velocity $W(t)$ and the density ratio is derived. We give an expression of the solid velocity corresponding to the cooling condition showing similar dependence on film thickness and the density ratio. Using Equations (4.47) and (4.48), we obtain an expression for the solid velocity

$$W(t) = \frac{k_l h_{sl}(T_s - T_m)}{\rho_s L_m(k_l + h_{sl}h)}(1-\rho) - \frac{\rho_l g}{4\eta L^2}(H_0 - h_m)h^3 \tag{4.50}$$

showing its linear dependence on ρ. The only difference between this result and that in Yoo [84] is that, our results incorporates changes in mass of the melting solid and conduction of heat in the solid layer. Clearly, if the density change is ignored then the contribution of the first term on the right hand side of (4.50) which represents the effects of melting would vanish. This term has no effect as long as $H_0 - h_m$ is large, however, as $h_m \to H_0$, this term cannot be ignored, this happens towards the end of the melting process. In the current analysis, we study the melting process until completion, hence, this term should always be retained by assuming that $\rho \neq 1$. Results in §4.6 show how $W(t)$ varies with ρ, a detailed discussion is given.

4.6 Results and discussion

In all the following results we take parameter values from Table 2.1, except when we study the effect of increasing the heat transfer coefficient. In Figure 4.3 we present the evolution of the melt height h_m obtained by solving equations (4.47) and (4.48) numerically. It is clear that h_m is approximately linear with slight deviations near $t = 0$ and at the end of melting, $t = t_m \approx 960s$. The quasi-steady state solution also predicts a linear height increase with the predicted melting time $t_m \approx 225s$, which is close to a quarter of the true value. The constant

mass case (4.49) predicts a linear increase in height with melting time of approximately $883s$. There is a slight deviation between the constant mass case and the variable mass case towards

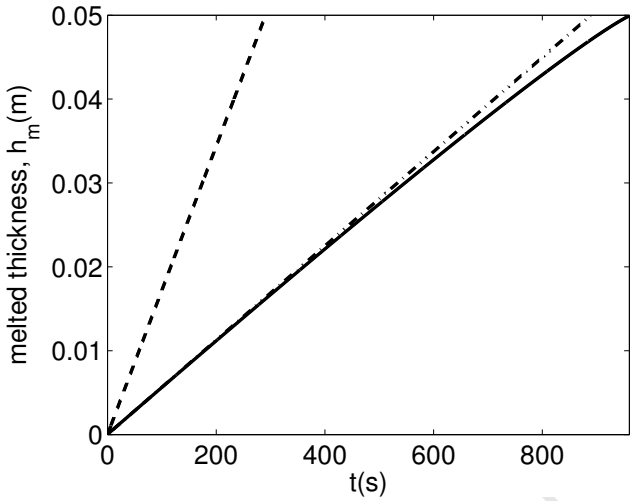

Figure 4.3: *$h_m(t)$ predicted by the current model (solid), the quasi-steady solution (dashed) and constant mass (dash-dot) when $h_{sl} = 855W/m^2$.*

the end of melting with the constant mass having a higher melting rate. Figure 4.3 shows that $h_t = 0$ has a far much bigger effect on h_m than the constant mass assumption. In Figure 4.4(a) we show the evolution of the melt height h. Also shown is the quasi-steady result with $h_q \approx 2.35 \times 10^{-4}$. The results show that as the solid mass decreases leading to an increase in fluid thickness in the melt gap, the heat reaching the interface decreases as well, as a result, the melting rate is reduced and the time for complete melting is increased. Previous studies consider $h_t = 0$ together with a constant mass. The quasi-steady and the unsteady case with constant mass give a much higher heat flux through the liquid than what our results show. Figure 4.4(b) shows the results for $t < 80$s. Initially there is a very rapid increase in film height for both the constant and variable mass model with a very high gradient. After approximately 8s the increase slows. For the next 80% of the time there is a slow increase and finally as the weight of the block becomes very small another rapid increase until the whole block is melted. These results show that if the mass varies, then the quasi-steady state is never attained. The infinity velocity observed by Yoo[84] at $t = 0$ is not present.

The evolution of the solid descending velocity is shown in Figures 4.5(a,b). In the initial

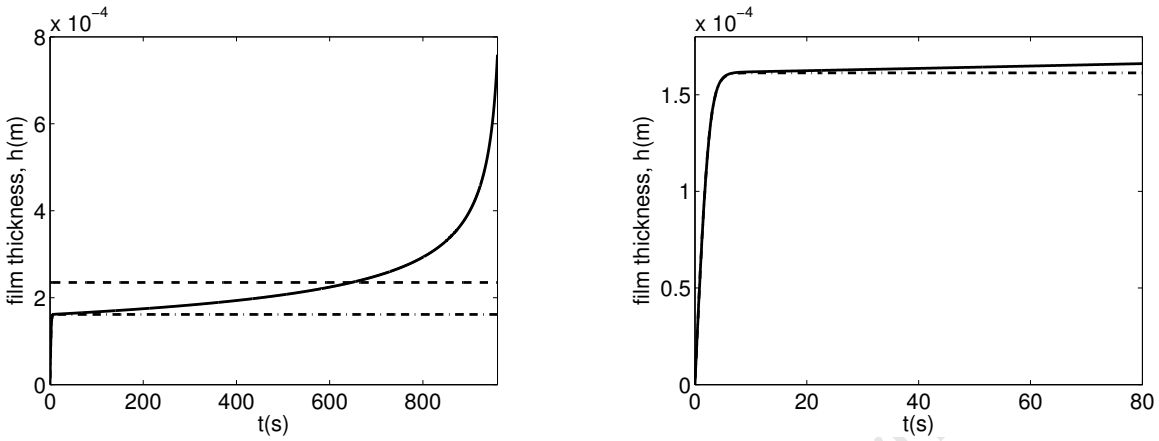

Figure 4.4: *(a) Variation of the film thickness corresponding to the steady-state (dash), variable (solid)and constant mass (dot-dash). (b) Variation of the film thickness corresponding to the variable (solid)and constant mass (dot-dash) during the initial stages of melting*

stages, approximately in the first 5 seconds of melting, the solid velocity for the constant and variable mass models rapidly approaches the steady state velocity, Figure 4.6(b). As melting proceeds the velocity corresponding to the variable mass model decreases until it becomes zero, signalling the end of melting. This is shown in Figure 4.6(a). It is evident from equation (4.50) that the transient behaviour of the solid velocity is affected by the density ratio ρ. Figure 4.5(a) illustrates the evolution corresponding to typical values of ρ during the initial stages of melting, $\rho = 0.7$ represents rime ice and $\rho = 0.917$ represents glaze ice. The initial velocity, $W(0)$, is non-zero when $\rho \neq 1$. This must occur since as soon as the liquid appears the ice must move to accommodate the fluid. When $\rho = 1$ no new space is required. This is valid for materials which occupy more volume upon melting. Figure 4.5(b) shows the dependence of the film thickness with ρ. Clearly, as the density ratio decreases, the film thickness increases, however, the melting time t_m decreases. To understand why this is so, we consider the quasi-steady case which expresses the film thickness explicitly in terms of the ρ_s (the quantity we vary to change ρ) and the melting time. Equation (4.40) shows that, keeping other parameters constant but varying ρ_s, we have that $h_q \sim \rho_s^{-\frac{1}{3}}$. Thus

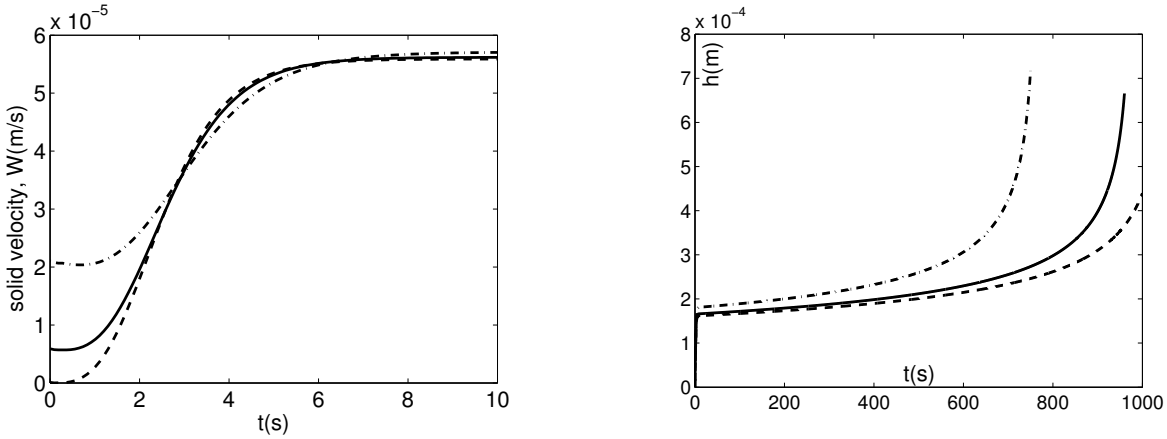

Figure 4.5: *(a)Solid velocity and (b) liquid film thickness when ρ=0.917(solid), 1 (dash), 0.7(dash-dot)*

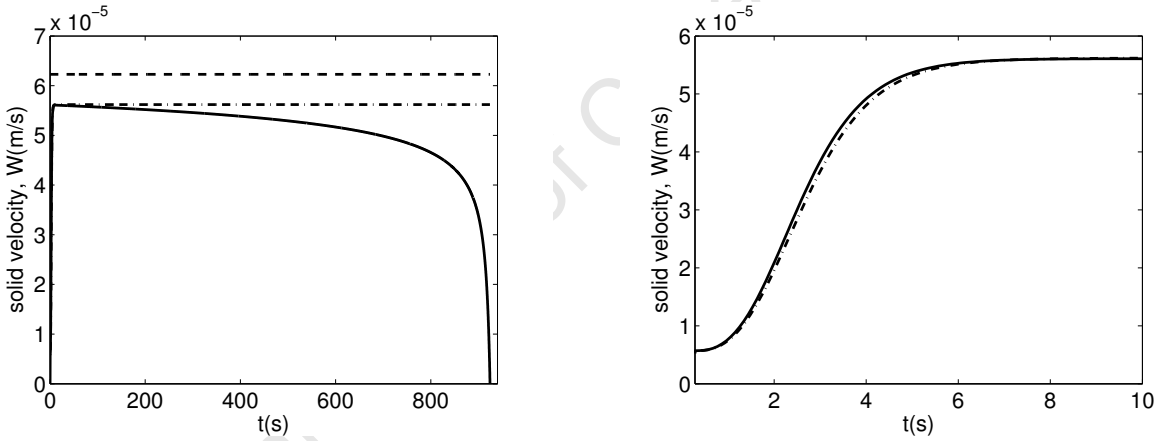

Figure 4.6: *(a) Solid velocity for the quasi-steady state and unsteady case with variable and constant mass (b) Solid velocity during the initial stages of melting*

in this case, reducing ρ by varying ρ_s results in an increase in the film thickness. However, equation (4.32)(b) shows that $dh_m/dt \sim h_q^3$. Since $h_m \sim \sqrt{t}$, it then follows that $t_m \sim \rho_s^{\frac{2}{3}}$. Consequently, reducing the solid density results in a reduction in the melting time. Figure 4.7 shows the time dependency of the mass of the solid when the heat transfer coefficient is varied. As expected, the effect of increasing the heat transfer coefficient results in a decrease in melting time. Figure 4.8 represents both the vertical and the horizontal fluid velocity

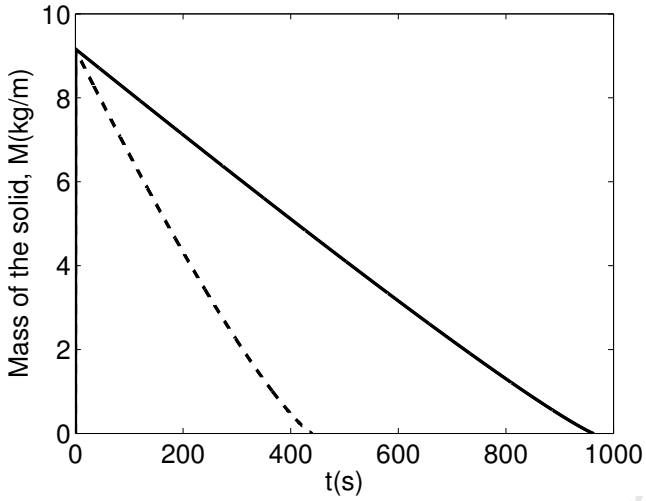

Figure 4.7: *Variation of mass with time when* $h_{sl} = 855W/m^2$ *(solid) and* $5000W/m^2$ *(dash)*

profiles of the liquid melt at different times. The horizontal velocity profiles are determined

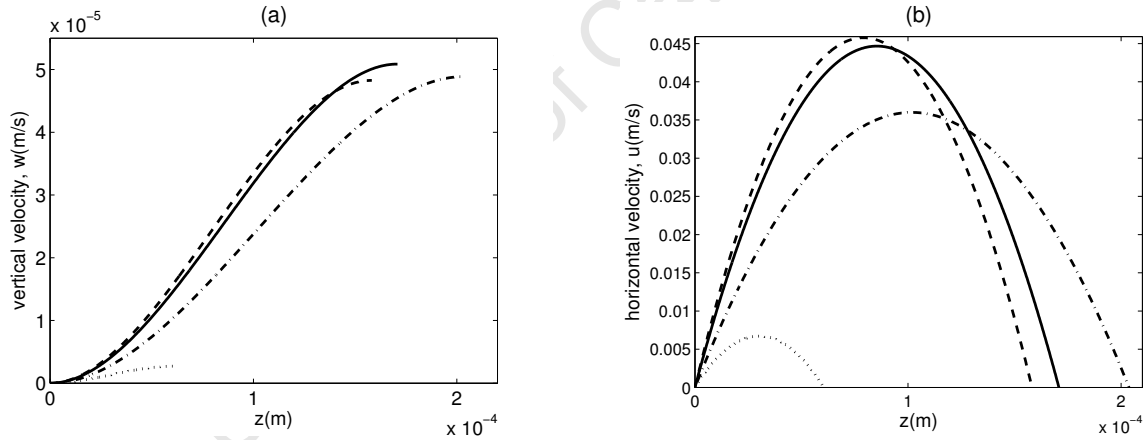

Figure 4.8: *(a)Vertical fluid velocity profiles* w *and (b) Horizontal fluid velocity profiles* u *at t=2s(dot), 10s(dash), 300s(solid), 960s(dash-dot).*

at the gap exit position $x = L$, where they both take on maximum values. As the gap size increases, both the vertical and the horizontal velocities increase rapidly as expected up to a maximum of approximately 0.045m/s for the horizontal velocity and 5.2×10^{-5}m/s for the vertical velocity then starts to decrease as time increases. This is expected since initially when the weight of the solid is large, the squeezing effect is quite high, however, due to

melting, this weight decreases as time progresses, as a result, the force pushing the fluid out of the thin gap decreases as well, resulting in both the horizontal and vertical velocities decreasing.

4.7 Justification of the approximations

The reduction of the initially complex system of the governing equations (4.1−4.4) was based on the assumption that a number of non-dimensional groupings was small. We may now check the accuracy of these assumptions. To simplify the Navier-Stokes equations we neglected terms of $\mathcal{O}(\epsilon^2 Re)$, to simplify the heat equation in the liquid we neglected terms of $\mathcal{O}(\epsilon^2 Pe)$. For our example of ice and water $\epsilon^2 Re/\epsilon^2 Pe \approx 0.135$, and so provided $\epsilon^2 Pe$ is negligible we can justify neglecting $\mathcal{O}(\epsilon^2 Re)$, consequently terms in ϵ^2 will be neglected as well since $\epsilon^2 << \epsilon^2 Re$. To calculate Pe we require an estimate for the velocity with time. In Figures 4.9 we plot the variation of the maximum horizontal fluid velocity with time. The maximum velocity occurs at $(x, t) = (\pm L, h(t)/2)$ and is obtained from equation

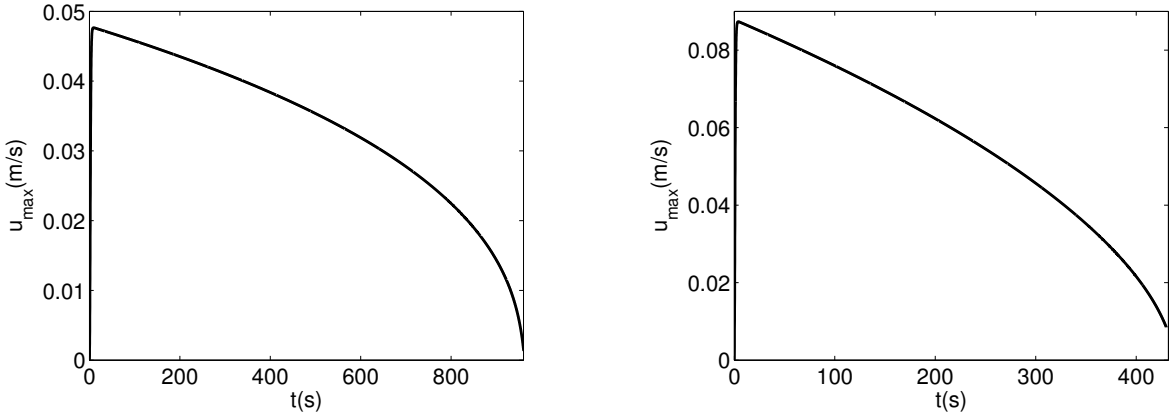

Figure 4.9: *(a) Maximum velocity in the melt region for (a)* $h_{sl} = 855W/m^2$ *(b)* $h_{sl} = 5000W/m^2$.

(4.21a), $u_{max} = p_x h^2/(8\eta)$, with $p_x = \pm\frac{3F}{2L^2}$ (from equation (4.44)). Two cases are shown with $h_{sl} = 855W/m^2$ and $5000W/m^2$. For higher heat transfer coefficient we expect more

rapid melting and consequently a thicker fluid film. This is reflected in the higher fluid velocity, with a maximum close to 9cm/s in the initial phase of melting. The decrease in velocity for larger times is related to the decrease in the mass of the solid, thus reducing the driving force. In Figure 4.10 we show the variation of

$$\epsilon^2 Pe \sim \frac{h^2}{L^2}\frac{u_{\max}L}{\kappa_l}. \tag{4.51}$$

From this we can see that for most of the time $\epsilon^2 Pe \ll 0.02$ when $h_{sl} = 855W/m^2$ and $\epsilon^2 Pe \ll 0.04$ when $h_{sl} = 5000W/m^2$. The maximum value occurring in both cases in the very final stage of melting, when h approaches a maximum. The decrease at the end reflects the drop in fluid velocity. Since we have chosen the maximum value of u at any time, our value for $\epsilon^2 Pe$ is an upper limit and consequently it is reasonable to neglect terms of $\mathcal{O}(\epsilon^2 Pe)$, however in a perturbation analysis this will usually be the term that should first be re-introduced. This is in keeping with the work of Groulx *et al* and Yoo [27, 84] who both retain the convection term wT_z. In the force balance, equation (4.9), we neglected the acceleration term which is $\mathcal{O}(\mathcal{H}_l/g\tau^2)$. Since the liquid height is always small this term is only likely to be important when there is a very rapid change. From Figure 4.3, 4.4 we see that the most rapid variations occurs near $t = 0$. If we scale the force balance, so that the

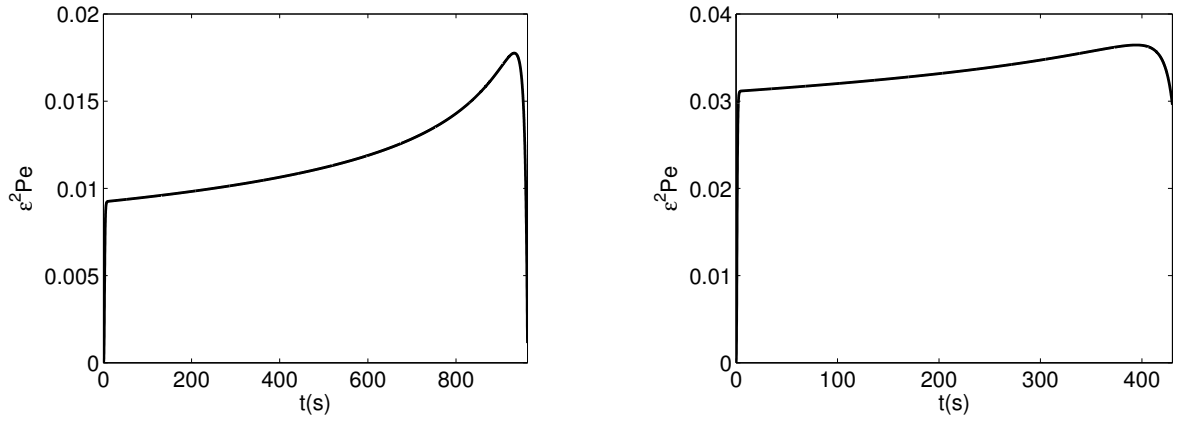

Figure 4.10: *Variation of* $\epsilon^2 Pe$ *with* t*, (a)* $h_{sl} = 855W/m^2$*, (b)*$h_{sl} = 5000W/m^2$.

acceleration term balances with the fluid pressure and set $H_0 - h_m = H_0$ then we find that

$\mathcal{H}_l \sim (2\eta L\tau/\rho_l)^{1/3}$ and the acceleration term is therefore important for time-scale $\tau \sim 0.011s$. We may infer this in a simpler manner by noting that $\mathcal{H}_l \sim 10^{-4}$ and so $\mathcal{H}_l/g\tau^2 \sim 1$ requires $\tau \sim 10^{-2}$s. It is therefore reasonable to neglect the acceleration term.

4.8 Conclusions

The work described in this chapter provides a mathematical model for the unsteady contact melting process of an isothermal solid from the initial heating phase up to complete melting. By introducing a number of standard simplifications such as the lubrication approximation, neglecting viscous heating, and convection, we have derived a set of simultaneous first-order ordinary differential equations as the model equations.

The key difference between our work and most previous models include:

1. The inclusion of a cooling condition at the interface with the substrate.
2. Modelling the varying mass of the solid.
3. The neglect of the quasi-steady assumption for the liquid height.

The cooling condition, which is obviously more realistic than perfect thermal contact, affects the temperature profile. Under the quasi-steady assumption we find that the quasi-steady height $h_q \sim (T_s - T_m)^{1/3}$ as opposed to $(T_s - T_m)^{1/4}$ which results from assuming perfect thermal contact.

Varying the mass of the solid shows that the quasi-steady state never occurs, instead the liquid height has an initial rapid increase, followed by a period of slow increase and a final rapid increase as the block mass approaches zero. The quasi-steady state approximation provides a reasonable approximation to the central period of slow increase. Since the weight of the solid provides the driving force for the squeeze flow the decreasing mass also increases the melt time. Our solution shows that the solid melting rate for the quasi-steady state model is approximately four times that of the current model. We also showed that the constant

mass assumption does not show a big difference with our model, however, the condition $h_t = 0$ causes a big difference.

The present model incorporates the effects of solid-liquid density differences that occur upon melting. The results are capable of resolving the distinctive behaviour of the solid descending velocity for non-unity density ratios during the early stage of melting in that $W(0)$ is non-zero when $\rho \neq 0$. The results also show how heat transfer coefficient affects the melting times. To validate our results, we have depended much on the published results of the corresponding quasi-steady case which acted as our limiting case. As pointed out by Yoo [84], no experiments on unsteady state melting have yet been reported to enable us to compare our results with measured data. The previously observed initial infinite velocity of the melt is not observed in our model, our results show that this is the consequence of neglecting the cooling condition.

Chapter 5

Unsteady contact melting II

5.1 Introduction

The purpose of this chapter is to extend the mathematical model of the unsteady contact melting for the isothermal PCM developed in Chapter 4 to the non-isothermal PCM. The analysis of Chapter 4 and most of the previous investigations in contact melting are based on the assumption that the temperature of the solid remains at the melting temperature, T_m, throughout the process. This simplifying assumption decouples the fluid film process in the film gap from the heat transfer process that can occur in the block. In reality the temperature in the solid is unlikely to remain constant, rather it will decrease away from the melt front. There exist papers where this assumption is relaxed. Litsek & Bejan [5] attempt to remove the constant temperature assumption by incorporating a convection term in the solid heat equation. Their expression for the temperature gradient at the melting front of the solid is then constant. This result is far from realistic. Groulx *et al* [27] assume that the solid is at a constant temperature θ_0 which is below the melt temperature, $\theta_0 < T_m$. Their final expression for the melting rate differs from previous results with the change $L_m \rightarrow L_m + c_s(T_m - \theta_0)$, where L_m is the latent heat of melting and c_s is the heat capacity of the solid.

Lacroix [39] recognises the shortcomings of current models in a study of the melting of a parallelepedic block with a varying mass and temperature within the solid (so removing assumptions 1, 2 and 5 listed in Chapter 4). Unfortunately the paper is unclear on a number of points. The force balance indicates that the PCM is floating in the melt, although there is no channel allowing the melt to move around the PCM. The linear temperature profile assumed in the bottom and top liquid layers requires a thin film approximation. This will hold in the lower layer provided the fluid removal is sufficiently rapid. In the top layer it is unlikely, particularly when the top layer is thicker than the solid. There appears to be some confusion between the melting rate and the velocity of the melt interface. Due to the squeezing effect the velocity of the interface differs from the melting rate yet these quantities appear to be identical, see their equations (4) and (15). Finally, the heat equation in the solid is solved using separation of variables. However, the solid boundaries are time dependent so the 'constant' of separation is also a function of time and the equation is not separable. Hence we will not use results from this paper for comparison purposes, although, since it is the paper where most of the standard restrictions are removed, in later sections we will point out qualitative similarities.

As in the isothermal case developed in Chapter 4, the problem is described two heat equations in the fluid layer, fluid flow in the melt, a Stefan condition at the the melt interface and a force balance between the weight of the solid and the fluid pressure. All the assumptions made in deriving the fluid flow equations and the thermal flow equations for the isothermal case discussed in Chapter 4 are applicable to the current model.

One of the reasons why only the isothermal solid layer is considered in most investigations is largely to do with the difficulties involved in estimating the temperature profile in the melting finite solid, as pointed out by Yoo [84]. The work covered in Chapters 2 and 3 focused on tackling this problem; this was done by making use of the heat balance integral (HBI) method. The results obtained in those chapters will be applied to the current problem. However, in this chapter, we will neglect melting from the top by assuming that the top of the solid is insulated. Our results can be easily extended to cover melting from the top by

incorporating the results of Chapter 3 (or Myers *et al* [56]). We will show results for the melting of ice on a warm surface and discuss the differences between the present and previous models.

5.2 Mathematical formulation

In this section we describe the governing equations for the non-isothermal contact melting process for a finite thickness block of phase change material placed on a substrate that is above the phase change temperature, as depicted in Figure 5.1. Energy is supplied by the substrate and this causes the block to melt. The substrate is maintained at a constant temperature, $T_s > T_m$. Unlike in Figure 4.1 when the temperature in the solid was maintained at T_m, in this case, we introduce a variable temperature profile denoted by θ together with the thermal boundary layer δ. The thickness of the thermal boundary layer is independent of x, as the flow of the heat into the boundary layer is independent of the longitudinal position. Initially, the block is at a constant temperature θ_0, which is below the melting temperature

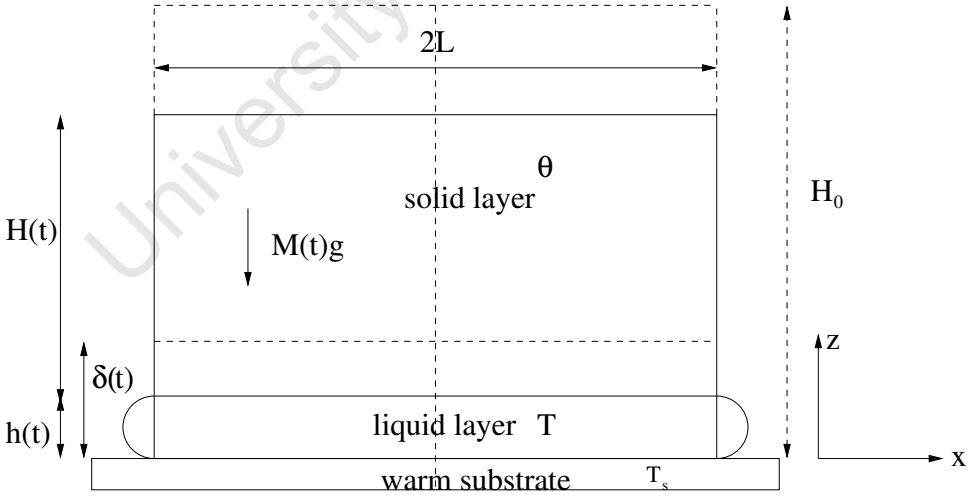

Figure 5.1: *Schematic for contact melting.*

$\theta_0 < T_m$. As was done in the previous chapters, we do not assume perfect thermal contact. As a result the melting process occurs in three distinct stages, as depicted in Figure 5.2,

where we have kept the top surface insulated. To incorporate melting at the top surface, we could follow the analysis of Chapter 3. However, in the present chapter we restrict our attention to the effect of heating from the substrate only. Melting only begins at the end of stage 1. Stage 2 defines the time when there is a region inside the block still close to the initial temperature θ_0. We define stage 3 as when the temperature inside the block is everywhere significantly above the initial temperature. To be clear we define stage 1 as occurring from $t \in [0, t_1]$ where t_1 comes from solving $\theta(0, t_1) = T_m$. Stage 2 lasts for $t \in [t_1, t_2]$ and t_2 defines when the temperature $\theta(H + h, t_2)$ first rises above θ_0. Since the heat equation has infinite speed of propagation theoretically this occurs at $t = 0$. However, the HBI method defines a heat penetration depth, $\delta(t)$, which measures where the temperature rise becomes negligible. The time t_2 is determined by $\delta(t_2) = H(t_2)$. Stage 3 continues from t_2 until the block has completely melted, $t \in [t_2, t_3]$.

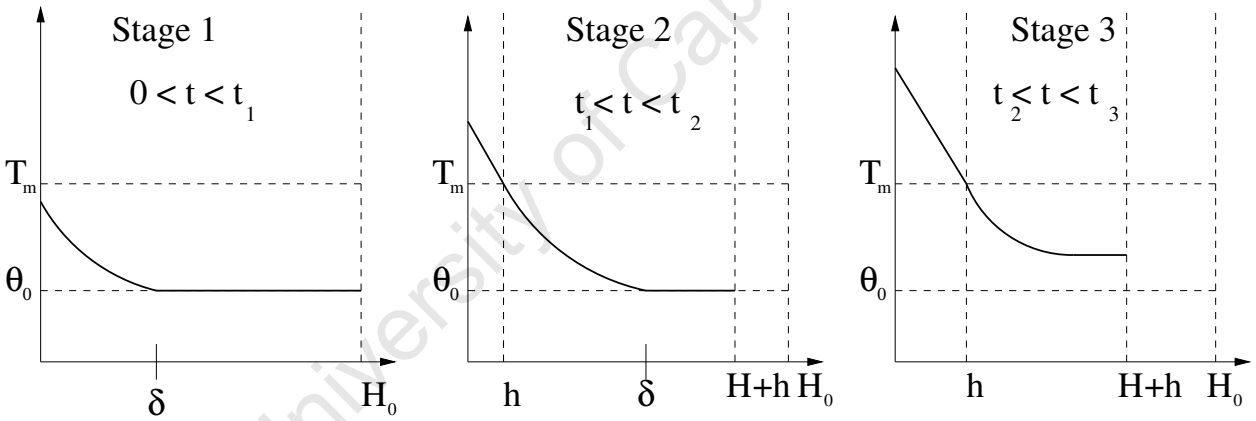

Figure 5.2: *Schematic of the 3 stages of melting when a block is placed on a surface above the melting temperature.*

5.2.1 Governing equations

The mathematical model requires the determination of the flow in the liquid layer and the temperature variations corresponding to different stages as depicted in Figure 5.2. In the end the thermal boundary layer solution inside the solid is matched to the solution for the

flow and temperature in the thin film. Following the approach in Chapter 4, a mathematical model is developed in two stages by considering a fluid flow model and a thermal flow analysis in both the solid and the liquid.

The thickness of the thermal boundary layer in the solid is independent of z, as the flow of heat into the boundary layer is independent of the longitudinal position. In the solid we neglect the diffusion in the x direction for two reasons. Firstly, in general the scaling shows it to be small and secondly there is no mechanism for temperature variation in the x-direction in the solid. This is due to the fact that the sides and top of the block are insulated and, before melting occurs, the temperature at $z = 0$ depends on the substrate temperature, which is independent of x. The assumptions $\epsilon^2 \ll 1$, $\epsilon^2 Re \ll 1$ and $\epsilon^2 Pe \ll 1$ are also valid for the current model. We will verify this again in the subsequent sections. For easy reference, we list all the equations derived in Chapter 4 without going through the derivations again, these are:

$$\eta \frac{\partial^2 u}{\partial z^2} = \frac{\partial p}{\partial x} , \qquad \frac{\partial p}{\partial z} = 0 , \qquad \frac{\partial u}{\partial x} + \frac{\partial w}{\partial z} = 0 , \tag{5.1}$$

together with the boundary conditions

$$u\big|_{z=0} = w\big|_{z=0} = 0 , \qquad u\big|_{z=h} = 0 , \qquad w\big|_{z=h} = \left(1 - \frac{\rho_s}{\rho_l}\right) \frac{\mathrm{d}h}{\mathrm{d}t} + \frac{\rho_s}{\rho_l} W(t) , \tag{5.2}$$

where

$$W(t) = \frac{\mathrm{d}h}{\mathrm{d}t} - \frac{\mathrm{d}h_m}{\mathrm{d}t}. \tag{5.3}$$

As for the thermal case, in addition to the set of governing equations and boundary conditions discussed in Chapter 4, we need to solve the heat equation in the solid,

$$\frac{\partial \theta}{\partial t} = \kappa_s \frac{\partial^2 \theta}{\partial z^2}. \tag{5.4}$$

With heat conduction in the solid, the Stefan condition then takes the form

$$\rho_s L_m \frac{\mathrm{d}h_m}{\mathrm{d}t} = k_s \frac{\partial \theta}{\partial z}\bigg|_{z=h} - k_l \frac{\partial T}{\partial z}\bigg|_{z=h}. \tag{5.5}$$

The thermal problem is subjected to different conditions in the different stages. Initially, during stage 1, no melting occurs and so a cooling condition is applied to the solid surface $z = 0$,

$$\frac{\partial \theta}{\partial z} = \frac{-\alpha_1 + h_{ss}(\theta - T_s)}{k_s}, \tag{5.6}$$

which is then replaced by another cooling condition

$$\frac{\partial T}{\partial z} = \frac{-\alpha_1 + h_{sl}(T - T_s)}{k_l}, \tag{5.7}$$

as soon as stage 2 begins. At the top $z = H(t)$ the surface is insulated and so we apply

$$\left.\frac{\partial \theta}{\partial z}\right|_{z=H(t)+h} = 0 \ , \tag{5.8}$$

noting that in stage 1, $H + h = H_0$. We do not impose a cooling condition here since this complicates the algebra and consequently obscures the main features of the melting process that we wish to highlight. The extension to a cooling condition at $z = H + h$ can easily be calculated following the work we covered in Chapter 3 or described in [56]. The melting interface remains at the melting temperature T_m, and so

$$\theta = T = T_m, \qquad \text{at } z = h. \tag{5.9}$$

The analysis is closed by considering the force balance equation

$$2\rho_s L\big[H_0 - h_m(t)\big]g = \int_{-L}^{L} p \, \mathrm{d}x \ . \tag{5.10}$$

5.3 Unsteady analysis

The crux of this problem lies in the estimation of the temperature profile in the solid. The thinness of the liquid layer ensures that the lubrication approximation is valid and that conduction in the z direction is the primary mode of heat transfer in the liquid as discussed in Chapter 4. In the solid layer we cannot use a thin layer approximation. As stated before, this is one of the reasons why it has been neglected in previous studies as pointed out by

Yoo [84] who suggested that initial subcooling of the solid may be neglected since it may not affect the fundamental nature of the melting and also because it is hard to model properly. He suggests it as a possible mechanism for the infinite velocity of the melting front that occurs with the quasi-steady model at $t = 0$. Our subsequent solutions will show that it is the perfect thermal contact assumption that leads to the infinite initial velocity.

In the solid we use the HBI method of temperature approximation developed in Chapter 3. As discussed in §5.2, the melting of the solid takes place in three distinct stages, we will work through each stage separately. Most of the details will be omitted as some of the results have been derived in the previous chapters. Reference will therefore be made to the relevant chapters.

5.3.1 Stage 1: Initial pre-melting stage, $0 \leq t \leq t_1$

During this initial phase the solid is heated at $z = 0$, until it reaches the melting temperature. The problem is governed by equation (5.4) subject to conditions (5.6,5.8). The solution to this problem was derived in Chapter 2, this is given by

$$\theta(z,t) = \theta_0 + \frac{q + h_{ss}(\theta_0 - T_s)}{h_{ss}} \left[\operatorname{erfc}\left(\frac{z}{2\sqrt{\kappa_s t}}\right) - e^{h_{ss}z/k_s + \kappa_s t (h_{ss}/k_s)^2} \operatorname{erfc}\left(\frac{z}{2\sqrt{\kappa_s t}} + h_{ss}\sqrt{\kappa_s t}/k_s\right) \right] . \quad (5.11)$$

Melting begins at time t_1 when the base reaches the melting temperature $\theta(0,t) = T_m$. However, once we move on to the melting stage we cannot find an exact solution and so, to be consistent with stage 2, we also look for a solution via the HBI method. A cubic polynomial, neglecting the quadratic term is used as the approximating function following the results of Chapter 3. This leads to the solution

$$\theta = \theta_0 + \frac{q + h_{ss}(T_s - \theta_0)}{\delta^2(3k_s + h_{ss}\delta)} (\delta - z)^3 . \quad (5.12)$$

If we integrate the heat equation (5.4) from $z = 0$ to δ, using the temperature profile of equation (5.12), we obtain the ODE

$$\frac{\mathrm{d}}{\mathrm{d}t}\left[\frac{\delta^2}{3k_s + h_{ss}\delta}\right] = \frac{12\kappa_s}{3k_s + h_{ss}\delta} \ , \qquad \delta(0) = 0 \ , \tag{5.13}$$

which has an implicit solution

$$t = \frac{k_s^2}{12\kappa_s h_{ss}^2}\left[\frac{h_{ss}\delta}{2k_s}\left(\frac{h_{ss}\delta}{k_s} + 6\right) - 9\ln\left(1 + \frac{h_{ss}\delta}{3k_s}\right)\right] \ . \tag{5.14}$$

This stage ends when melting begins at $z = 0$, $\theta(0, t_1) = T_m$. Equation (5.12) gives the appropriate value of $\delta(t_1) = \delta_1$,

$$\delta_1 = \frac{3k_s(T_m - \theta_0)}{\alpha_1 + h_{ss}(T_s - T_m)} \ , \tag{5.15}$$

and the corresponding time comes from (5.26). Note, in the limits $h_{ss} \to \infty$ or $\theta_0 = T_m$, then $\delta_1 = t_1 = 0$ and melting is immediate. For the ice-water parameter values of Table 2.1 we find $t_1 \sim 1.6$s and $\delta \sim 5.1$mm.

5.3.2 Stage 2: Initial melting stage, $t_1 \le t \le t_2$

Once melting starts the temperature in the water, as derived in Chapter 4, §4.4, is given by

$$T(z,t) \ = \ T_m - \frac{\alpha_1 + h_{sl}(T_s - T_m)}{k_l + h_{sl}h}(z - h) \ . \tag{5.16}$$

From the results in Chapter 3 and also in [56], a more accurate approximation is provided by including correction terms in the perturbation solution. However, this does not include the squeeze film effect and so allows for thicker films (where the linear approximation deteriorates). So, provided the film remains thin the approximation of (5.16) should be sufficiently accurate. In the solid the cubic approximation in the HBI method leads to the temperature

$$\theta(z,t) = \theta_0 + \frac{T_m - \theta_0}{(\delta - h)^3}(\delta - z)^3 \ , \tag{5.17}$$

where $\theta(h) = T_m$, $\theta(\delta) = 0$, $\theta_z(\delta) = 0$. Integrating the heat equation in the solid for $z \in [h, \delta]$ we find

$$3\frac{\mathrm{d}h}{\mathrm{d}t} + \frac{\mathrm{d}\delta}{\mathrm{d}t} \ = \ \frac{12\kappa_s}{\delta - h} \ . \tag{5.18}$$

The temperature expressions (5.16,5.17) allow us to calculate the temperature gradients for the Stefan condition:

$$\rho_s L_m \frac{\mathrm{d}h_m}{\mathrm{d}t} = \frac{3k_s(\theta_0 - T_m)}{\delta - h} + \frac{k_l(\alpha_1 + h_{sl}(T_s - T_m))}{k_l + h_{sl}h} \ . \tag{5.19}$$

Equations (5.18,5.19) contain three unknowns, $\delta,\ h_m,\ h$. The system is closed with the force balance equation

$$(H_0 - h_m)\rho_s g = -\frac{4\eta L^2}{h^3}\left(\frac{\mathrm{d}h}{\mathrm{d}t} - \rho\frac{\mathrm{d}h_m}{\mathrm{d}t}.\right) \tag{5.20}$$

These must be solved subject to $\delta = \delta_1,\ h = h_m = 0$ at $t = t_1$. The stage ends when the heat has penetrated all the way through the block, $\delta = H(t) + h(t) = H_0 + h(t) - h_m(t)$ at time t_2. We denote the thicknesses at this time as $\delta_2,\ h_2,\ h_{m_2}$.

If the PCM is initially at $\theta_0 = T_m$ then the temperature remains constant throughout the solid for all time. The first term on the right hand side of (5.19) is identically zero. The second term only becomes infinite at $t = t_1 = 0$ in the limit $h_{sl} \to \infty$. So if $h_{sl} \to \infty$, then $\frac{dh_m}{dt} \to \infty$, and from (5.20) it follows that $\frac{dh}{dt} \to \infty$. Consequently from equation (5.20) we see that the infinite velocity h_t, observed in previous studies is a result of the perfect thermal contact assumption, not subcooling.

5.3.3 Stage 3: Final melting stage, $t_2 \leq t \leq t_3$

Once the heat penetration depth reaches the top of the block we can no longer impose $\theta = \theta_0$ at $z = \delta$. Instead we impose $\theta_z = 0$ at $z = H + h$ and find a temperature profile

$$\theta = a_0 + (T_m - a_0)\frac{(z - H - h)^3}{H^3} \ , \tag{5.21}$$

where $a_0(t)$ replaces δ as our third unknown. We may now proceed in two ways. We can substitute θ into the heat equation and integrate as in the previous section, to obtain an ODE for a_0. This may be solved subject to $a_0(t) = \theta_0$ (which follows by continuity of temperature at $t = t_2,\ \theta(H + h, t_2) = \theta_0$). However, we choose to follow Goodman and

introduce a function ϕ where

$$\phi = \int_h^{H+h} \theta dz = \frac{H}{4}(T_m + 3a_0). \tag{5.22}$$

Goodman works with ϕ since in the case of perfect thermal contact it is not possible to determine an initial condition for a_0. In our case we retain this form since the numerical solution of the resultant differential equation appears more stable with ϕ than a_0. Integrating the heat equation across the solid leads to

$$\frac{d\phi}{dt} = \frac{3\kappa_s(T_m - a_0)}{H_0 - h_m} + a_0\left(\frac{dh}{dt} - \frac{dh_m}{dt}\right) - T_m\frac{dh}{dt}, \tag{5.23}$$

where a_0 may be expressed in terms of ϕ via equation (5.22). The temperature profile in the liquid is the same as in Stage 2 so the Stefan condition is now

$$\rho_s L_m \frac{dh_m}{dt} = \frac{3k_s(T_m - a_0)}{h - H} + \frac{k_l(\alpha_1 + h_{sl}(T_s - T_m))}{k_l + h_{sl}h}\ . \tag{5.24}$$

The system is closed with the force balance (5.20). These are solved subject to the two additional initial conditions $h_m = h_{m_2}$, $h = h_2$, $\phi = (H_0 - h_{m_2})(3\theta_0 + T_m)/4$ at $t = t_2$, which are obtained at the end of stage 2.

The systems of the governing equations obtained at all the three stages were solved numerically using Matlab ode45 solver package. The graphical solutions are presented in the next section and analysed.

5.4 Results

In all the following results we take parameter values from Table 2.1, except when we study the effect of increasing the heat transfer coefficient. Also, we will be making reference to equations and results obtained in Chapter 4 in connection with the quasi-steady case. In Figures 5.3 a, b) we present the evolution of the melt height h_m and the liquid layer height h. Figure 5.3 a) shows h_m obtained by solving the full problem and also the prediction from the quasi-steady state solution. The full solution begins at $t_1 \approx 1.6$s and shows two

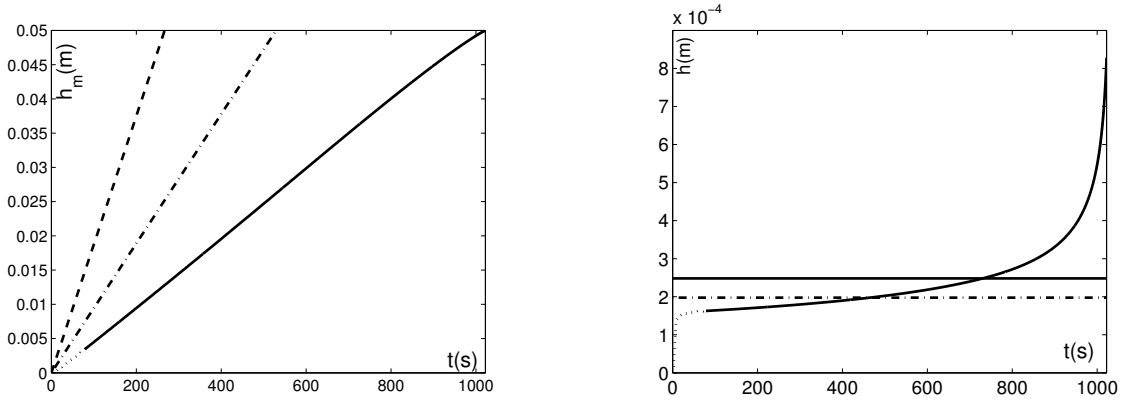

Figure 5.3: *(a) $h_m(t)$ predicted by current method ($t < t_2$ dotted, $t > t_2$ solid line) and quasi-steady solutions, $h_{q\infty}$ (dashed), h_q (dash-dot) for $h_{sl} = 855W/m^2$, (b) melt height predictions $h(t)$ ($t < t_2$ dotted, $t > t_2$ solid line), $h_{q\infty}$ (dashed), h_q (dash-dot).*

stages, for $t_1 \leq t \leq t_2$ (where $t_2 \approx 79$s) it is shown as a dotted line, subsequently for $t_2 \leq t \leq t_m$ (where $t_m \approx 1022$s), it is a solid line. It is clear that h_m is approximately linear with slight deviations near $t = 0$ and $t = t_m$. The quasi-steady solution, equation (4.35), also predicts a linear height increase. The two broken lines shown take the value of h_q (required in equation (4.35)) from either the quartic equation, (4.39), or the perfect thermal contact case, (4.41); these are shown as dash-dot and dashed lines respectively. For the perfect thermal contact case the predicted melt time of $t_m \approx 267$s is close to a quarter of the true value. For the value of h_q from the quartic equation $t_m \approx 529$s is around half the true value. The value of h_q is determined via the steady-state analysis, neglecting the temperature variation in the solid and the changing mass, so at least one of these three factors must be responsible for the discrepancy between the present theory and quasi-steady results. In Figure 5.3b) we show the evolution of the melt height h. Also shown are the quasi-steady state results, with the classical solution $h = h_{q\infty} \approx 2.48 \times 10^{-4}$m obtained from equation (4.41) and the correction for finite heat transfer, $h_q \approx 1.98 \times 10^{-4}$m predicted by equation (4.39). The full solution shows that when the block first starts to melt there is only a very thin insulating liquid layer, consequently h initially increases very rapidly. After

approximately 10s the increase slows. However, there is never a true quasi-steady state. Subsequently there is a slow increase and finally as the weight of the block becomes very small another rapid increase until the whole block has melted. The slow central increase and final rapid progression was also noted by Lacroix [39]. In Figure 5.4 we show height evolution for both the isothermal and the non-isothermal cases in which the time for complete melting are 960s and 1022s respectively. This shows clearly that heat conduction in the solid reduces considerably the total melting time. In Figure 5.5 a) we show the effect of increasing the

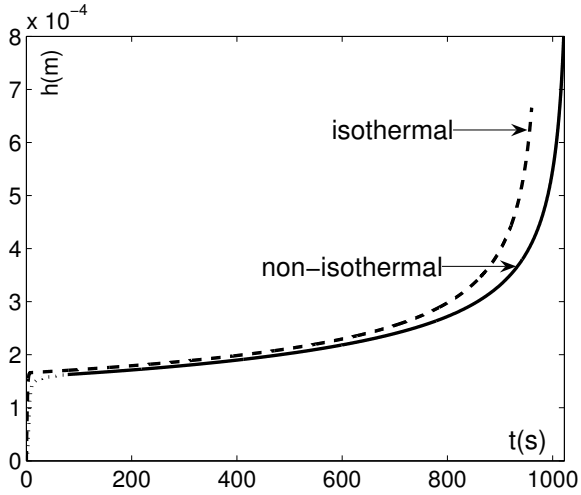

Figure 5.4: *Melt height predictions h(t) corresponding to the isothermal (dash) and non-isothermal case (solid).*

heat transfer coefficient to $h_{sl} = 5000W/m^2$ on the evolution of $h(t)$. The form of the curve is similar to the previous example, with an initial rapid increase followed by a slower change and then a final rapid increase. However, melting begins very rapidly, at $t \approx 10^{-7}$s and the initial increase occurs over a much shorter time scale than with the lower value of h_{sl} and so we see the progress towards an initial infinite velocity. Stage 2 ends at $t_2 \approx 63.8$s. As expected, as h_{sl} increases the present prediction of h_q approaches $h_{q\infty}$. In Figure 5.5 b) we show the solution for an isothermal block, with an infinite heat transfer coefficient. In this case, equation (5.24), for h_m, is singular at $t = 0$ (when $h = 0$), we avoid this by setting $h(0) = 10^{-8}$. The singularity carries through to the equation of h, (5.20), and results

in an initial infinite velocity for h. Lacroix's [39] model with heat flow in the solid has perfect thermal contact and also shows an infinite initial velocity. The melting time can be seen to decrease as the heat transfer coefficient increases, when $h_{sl} = 855W/m^2$ we find $t_m \approx 1022$s, with $h_{sl} = 5000W/m^2$ we find $t_m \approx 461$s, for $h_{sl} \to \infty$, $t_m \approx 275$s. In Figure

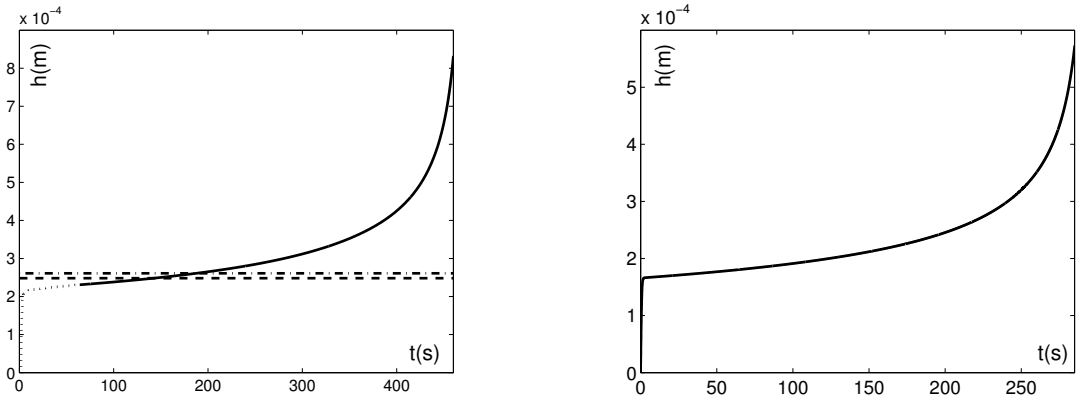

Figure 5.5: *(a) $h(t)$ when $h_{sl} = 5000W/m^2$ and quasi-steady solutions, $h_{q\infty}$ (dashed), h_q (dash-dot) $t_m \approx 450s$, (b) $h(t)$ when $h_{sl} = \infty$, $t_m \approx 275s$*

5.6 we show the temperature profiles in the melt layer and solid at the end of stage 2, when $t = t_2 \approx 79$s and mid-way through the melting process, when $t \approx 511$s. At the end of stage 2, shown as the dash-dot line, the bottom of the liquid layer is at 4.9°C (Figure 5.6b), it then decreases through a very thin layer to the melting temperature. The block has only lost a small amount of its initial mass and the total thickness of melt and block is around 0.0465m. Midway through the melting process, when the block is around half of its original thickness, shown as the solid line in Figure 5.6, the temperature in the liquid layer is similar to that at t_2 with a maximum temperature of 5.9°C (Figure 5.6b), but the solid layer is much hotter, with a minimum temperature of around -2.27°C. To ensure that the parameters used in the reduction of the governing equations remain small, we follow the approach used in Chapter 4 by considering the maximum velocity of the fluid at $(x, z) = (\pm L, h(t)/2)$. In Figure 5.7 we plot the variation of the maximum horizontal fluid velocity with time. Two cases are shown, with $h_{sl} = 855W/m^2$ and $5000W/m^2$. Again stage 2 results are shown as a dotted

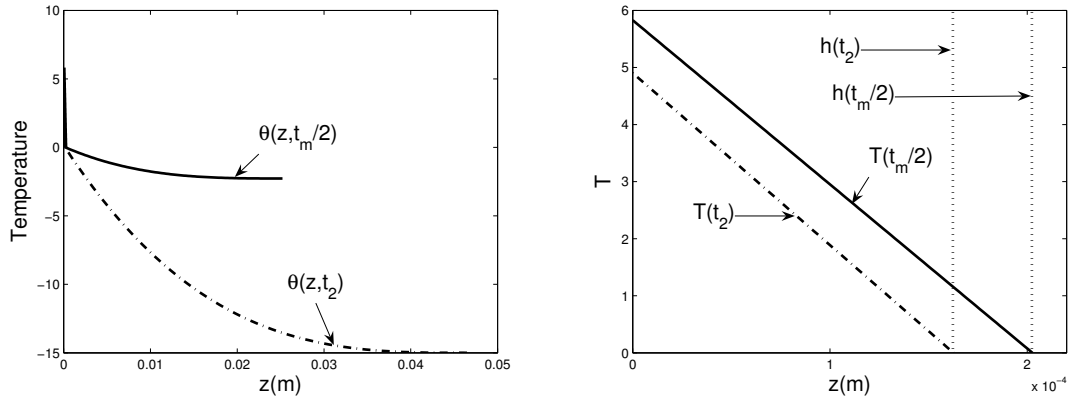

Figure 5.6: *(a) Temperature in melt and solid at $t = t_2 \approx 78.5s$ (dot-dashed line), and $t = 511s$ (solid line), (b) Temperature in melt for small values of z.*

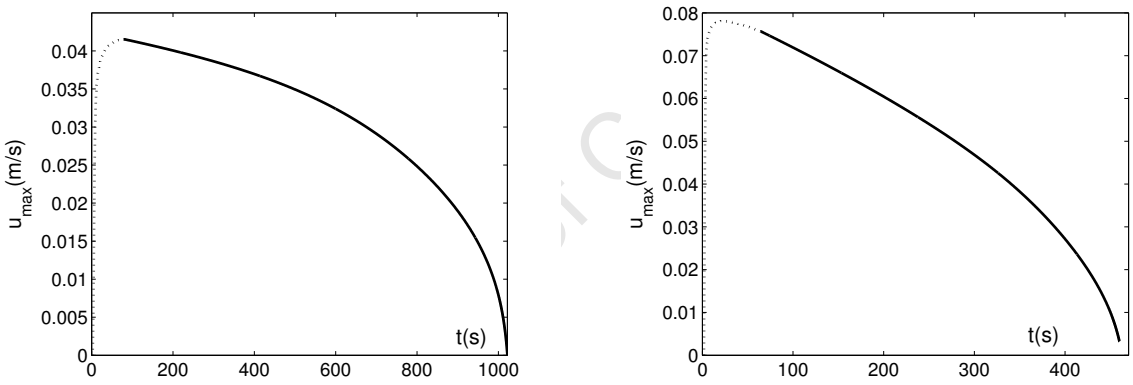

Figure 5.7: *Maximum horizontal velocity in the melt region for a) $h_{sl} = 855W/m^2$, b) $h_{sl} = 5000W/m^2$.*

line and stage 3 as a solid line. For the higher heat transfer coefficient we expect more rapid melting and consequently a thicker fluid film. This is reflected in the higher fluid velocity, with a maximum close to 8 cm/s in the initial phase of melting. The decrease in velocity for larger times is related to the decrease in the mass of solid, thus reducing the driving force. In Figure 5.9 we show the variation of

$$\epsilon^2 Pe \sim \frac{h^2}{L^2}\frac{u_{max}L}{\kappa_l} \ . \tag{5.25}$$

From this we can see that for most of the time $\epsilon^2 Pe < 0.02$ when $h_{sl} = 855W/m^2$ and $\epsilon^2 Pe < 0.045$ when $h_{sl} = 5000W/m^2$. The maximum value occurs in both cases in the very final stage of melting, when h approaches a maximum. The decrease at the end reflects the drop in fluid velocity. Since we have chosen the maximum value of u at any time, our value for $\epsilon^2 Pe$ is an upper limit and consequently it is reasonable to neglect terms of $\mathcal{O}(\epsilon^2 Pe)$, however in a perturbation analysis this will usually be the term that should first be re-introduced. This is in keeping with the work of Groulx & Lacroix and Yoo [27, 84] who both retain the convection term wT_z. In the force balance, equation (5.10), we neglected the

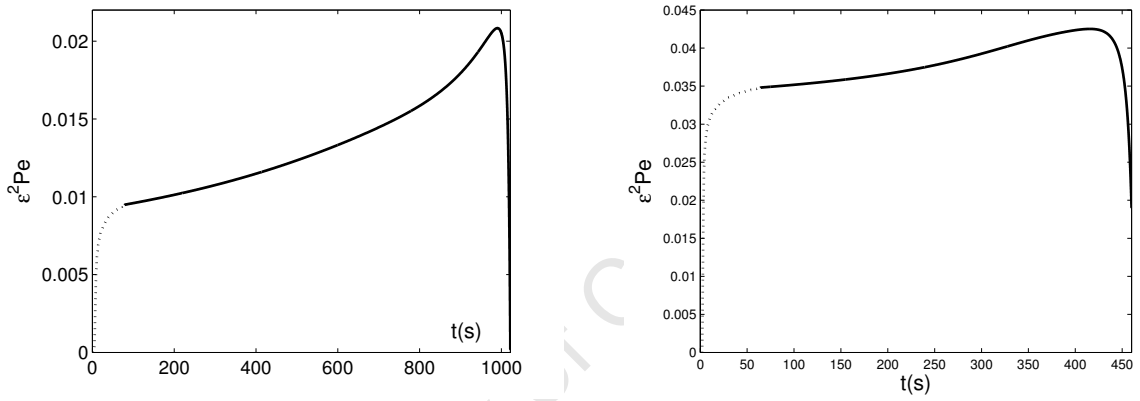

Figure 5.8: *Variation of $\epsilon^2 Pe$ with t, a) $h_{sl} = 855W/m^2$, b) $h_{sl} = 5000W/m^2$.*

acceleration term which is $\mathcal{O}(\mathcal{H}_l/(g\tau^2))$. Since the liquid height is always small this term is only likely to be important when there is a very rapid change. From Figures 5.3, 5.5 we see that the most rapid variation occurs near $t = 0$. If we scale the full force balance (given by equation (5.10) with an acceleration term added), so the acceleration term balances with the fluid pressure, and set $H_0 - h_m = H_0$ then we find $\mathcal{H}_l \sim (2\eta L\tau/\rho_l)^{1/3}$. If we take the height-scale $\mathcal{H}_l = h_q \sim 2 \times 10^{-4}$ then the acceleration term is only important for time-scales $\tau \sim 10^{-5}$s. It is therefore reasonable to neglect the acceleration term.

In Figure 5.9(a) we plot the variation of the film thickness with time for various values of the initial temperature θ_0. The melting time responds slowly to the changes in initial temperature. Changing the initial temperature from -15 °C to -30 °C results in only a

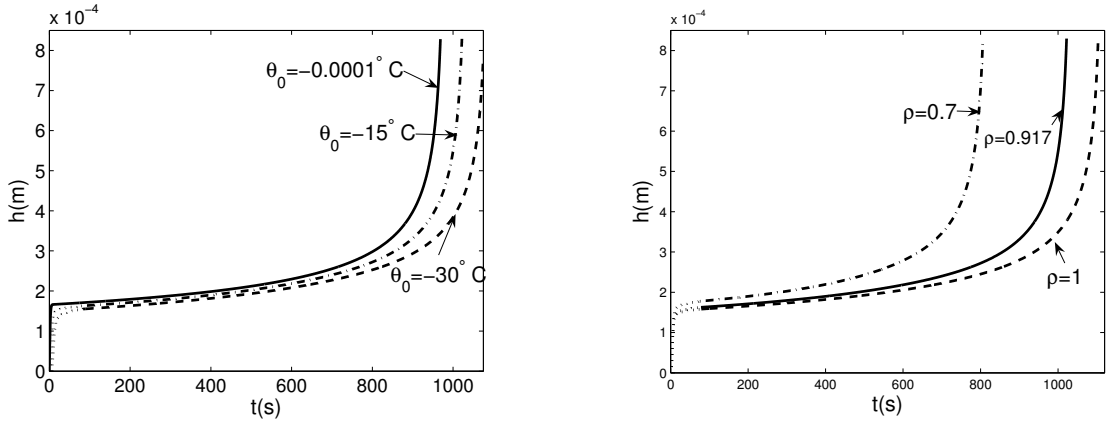

Figure 5.9: *Variation of film thickness with time when (a) varying the initial temperature θ_0, and (b) varying the density ratio ρ.*

5.3% change from t_m=1022s to t_m=1075s. Similarly, changing the initial temperature to $\theta_0 = -0.0001$°C which is close to the melting temperature of ice results in only another 5.3% change in melting time from t_m=1022s to $t_m = 968$s. This shows that the temperature gradient in the solid only has a small effect on the melting rate of the solid. What drives the interface motion is the high temperature gradient in the fluid. Figure 5.6(a) shows the relative magnitudes between the temperature gradients in both the solid and the liquid. Figure 5.6(b) is the corresponding blow up of the melt region. Also the film thickness at the time of complete melting slowly increases linearly as $\theta_0 \to T_m$. In Figure 5.9(b) we fix the initial temperature and vary the density ratio ρ. We notice that although the final film thickness remains almost constant, the melting time t_m changes from $t_m = 805.5s$ to $t_m = 1022s$ when we move from rime ice $\rho = 0.7$ to glace ice $\rho = 0.917$ which represents a significant change of about 27%, this increases to 33% when $\rho = 1$. This demonstrates that ignoring liquid-solid density changes can result in large errors in predicting the melting time.

5.4.1 Time to complete melting and approximate solutions

The melting process is complete when $h_m = H_0$, and we denote this time by t_m. For the quasi-steady model described in Chapter 4,§4.4, this is determined by substituting for h_m in

equation (4.35) to give

$$t_m = \frac{4\eta L^2}{\rho_l g h_q^3} \ , \tag{5.26}$$

where h_q can be determined by solving the quartic, equation (4.39), or using the approximations given by equations (4.40) or (4.41). For the current problem we do not have a simple expression for h_m, however, from Figure 5.3 a) it is clear that $h_m \propto t$ throughout the melting period. To identify the constant of proportionality we consider the early part of Stage 3, where $t \approx t_2$ and so $a_0 \approx \theta_0$. From Figure 5.3 a) we see that $h \ll H$, and at the start of stage 3 $H \approx H_0$ and $a_0 = \theta_0$ consequently, from equation (4.38) we find

$$\frac{dh_m}{dt} \approx \frac{1}{\rho_s L_m}\left[\frac{3k_s(\theta_0 - T_m)}{H_0} + \frac{k_l(\alpha_1 + h_{sl}(T_s - T_m))}{k_l + h_{sl}h_q}\right] = \alpha \ . \tag{5.27}$$

Since $t_1 \ll t_m$ we may impose the initial condition $h_m(0) = 0$ and so integrate this equation to give $h_m \approx \alpha t$. The time to melting predicted by this method is therefore

$$t_m = \frac{H_0}{\alpha} \ , \tag{5.28}$$

where α is defined in (5.27). When $h_{sl} = 855W/m^2$ the numerical solution predicts $t_m \approx$ 1022s, using the quartic solution for h_q to determine α we find $t_m \approx 1054$s (a 3% error). The quasi-steady approximation gives $t_m \approx 529$ (a 48% error). Note, if we neglect the first term on the right hand side of equation (5.27) then we will obtain the appropriate prediction for a PCM at the phase change temperature, $\theta_0 = T_m$. In this case we find $t_m \approx 929$s, or an error of 9%, so it appears that at least for the melting time prediction the quasi-steady assumption is worse than neglecting the temperature variation in the solid.

Equation (5.27) allows us to calculate the relative magnitude of the conduction terms through the solid and liquid. Using the values in Table 2.1 we find that the solid conduction term is a factor 10 less than the liquid conduction term. This indicates that the subcooling, θ_0, has a relatively small effect on the process. This could also be inferred from Figure 5.6, where it is clear the temperature gradient in the liquid is much greater than in the solid. Simulations carried out with changing the initial temperature θ_0 showed that the melting time shows a slow linear increase with decreasing θ_0, in the range [-30, 0]°C (where $t_m = 1140$s for

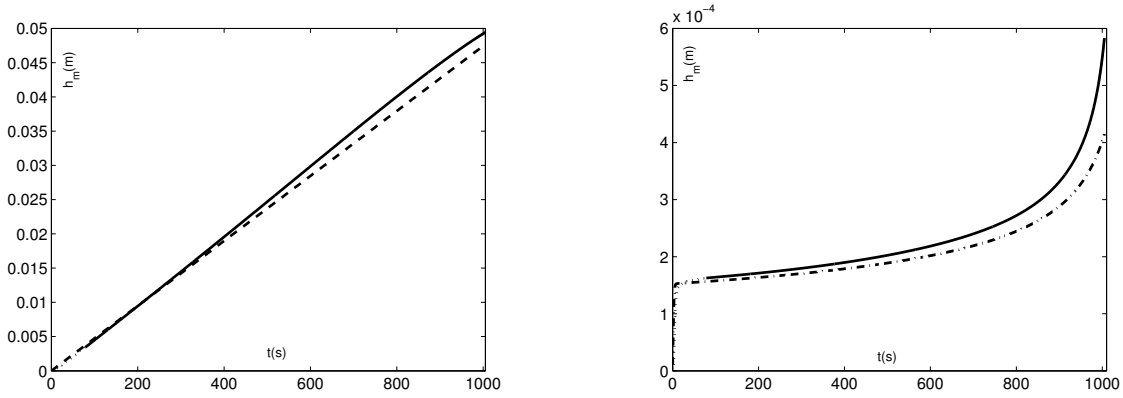

Figure 5.10: *Comparison of solutions for a) $h_m(t)$, b) $h(t)$. Solid lines represent the exact solution, dashed lines are the linear approximation.*

$\theta_0 = -30°\text{C}$). Note, the fact that the process is driven by the temperature gradient in the liquid also explains why, although the solid temperature is calculated incorrectly in [39] our results show similar features. Neglect of the mass variation, so $H = H_0$ for all time, leads to $t_m \approx 940\text{s}$. Consequently, we may deduce that the large differences in melting times between the present work and previous results may be attributed to the use of a cooling condition, rather than perfect thermal contact.

Finally, given that we have a simple expression for h_m that holds (approximately) for all $t > t_1$, we are able to substitute this into equation (4.48) to find a single first order differential equation for $h(t)$

$$\frac{dh}{dt} = \frac{\rho_s}{\rho_l}\alpha - \frac{(H_0 - \alpha t)\rho_l g}{4\eta L^2}h^3 \ , \qquad h(0) = 0 \ . \tag{5.29}$$

The problem of contact melting can therefore be reduced to solving this equation. In Figure 5.10a) we compare the full solution for h_m with the linear approximation for $h_{sl} = 855W/m^2$. In Figure 5.10b) we compare the full solution for h with the numerical solution of the equation (5.29). Obviously both comparisons indicate that the simple solution provides a good approximation to the solution of the full system.

5.5 Extension to three dimensions with sliding

Many recent studies have dealt with contact melting in three dimensions, see [3, 84] for example. Having established the basic formulation for the two-dimensional problem we now briefly outline the extension to three dimensions; in addition we describe the inclusion of sliding, which is also discussed in [3, 84].

For the three-dimensional problem, provided the heat flow is dominated by conduction in the z direction, the only differences in the formulation are to the flow equations and the force balance:

$$\eta\frac{\partial^2 u}{\partial z^2} = \frac{\partial p}{\partial x} , \qquad \eta\frac{\partial^2 v}{\partial y^2} = \frac{\partial p}{\partial y} , \qquad \frac{\partial p}{\partial z} = 0 \tag{5.30}$$

$$\frac{\partial u}{\partial x} + \frac{\partial v}{\partial y} + \frac{\partial w}{\partial z} = 0 , \qquad 4\rho_s LW[H_0 - h_m(t)]g = \int_{-L}^{L}\int_{-W}^{W} p\; dydx , \tag{5.31}$$

where the width of the block is $2W$. If we allow the top surface to move in the x direction with velocity U then

$$u = \frac{p_x}{2\eta}z(z-h) + U\frac{z}{h} , \qquad v = \frac{p_y}{2\eta}z(z-h) . \tag{5.32}$$

Integrating the incompressibility condition from $z = 0$ to h we find

$$w(h) - w(0) = \frac{\partial h}{\partial t} - \frac{\rho_s}{\rho_l}\frac{\partial h_m}{\partial t} = -\frac{\partial}{\partial x}\int_0^h u\; dz - \frac{\partial}{\partial y}\int_0^h v\; dz \tag{5.33}$$

$$= \frac{h^3}{12\eta}\nabla^2 p - \frac{Uh}{2} . \tag{5.34}$$

So we see the main difference between the two and three-dimensional models: the pressure satisfies Poisson's equation

$$\nabla^2 p = \frac{12\eta}{h^3}\left(\frac{\partial h}{\partial t} - \frac{\rho_s}{\rho_l}\frac{\partial h_m}{\partial t} + \frac{Uh}{2}\right) = f(t) , \tag{5.35}$$

subject to $p(\pm L, y) = p(x, \pm W) = 0$. To determine the pressure we employ an eigenfunction expansion of the form

$$p = \sum_{n=1}^{\infty} b_n(s)\sin(\omega_n r) , \tag{5.36}$$

where for convenience we set $r = (x + L)/2$, $s = (y + W)/2$ and the eigenvalue $\omega_n = n\pi/L$. Substituting this back into (5.35) gives

$$\sum_{n=1}^{\infty} \left(\frac{d^2 b_n}{ds^2} - \omega_n^2 b_n \right) \sin \omega_n s = 4f(t) \ . \tag{5.37}$$

By orthogonality

$$\frac{d^2 b_n}{ds^2} - \omega_n^2 b_n = \frac{8f}{L} \int_0^L \sin \omega_n s \ ds = q_n(t) \ , \tag{5.38}$$

where $q_n(t) = 8f(t)(1 - (-1)^n)/(n\pi)$. Applying the conditions $b_n(0) = b_n(W) = 0$, we determine the eigenfunctions

$$b_n(s) = \frac{q_n(t)}{\omega_n^2} \left[\cosh(\omega_n s) - 1 + \frac{1 - \cosh(\omega_n W)}{\sinh(\omega_n W)} \sinh(\omega_n s) \right] \ . \tag{5.39}$$

The load carried by the fluid is then

$$F = 4 \int_0^W \int_0^L p(r, s) dr ds = 4 \sum_{n=1}^{\infty} \frac{q_n(t)}{\omega_n^3} \left[\frac{\sinh(\omega_n W)}{\omega_n} - W + \frac{(1 - \cosh(\omega_n W)^2)}{\omega_n \sinh(\omega_n W)} \right] (1 - (-1)^n) \tag{5.40}$$

The analysis now proceeds in a similar manner to the two-dimensional formulation with the only difference coming through the expression for the force. We replace the force balance, equation (5.20), with

$$4\rho_s LW[H_0 - h_m(t)]g = 32 f(t) \sum_{n=1}^{\infty} \frac{(1 - (-1)^n)^2}{n\pi\omega_n^3} \left[\frac{\sinh(\omega_n W)}{\omega_n} - W + \frac{(1 - \cosh(\omega_n W))^2}{\omega_n \sinh(\omega_n W)} \right] \tag{5.41}$$

where $f(t)$ is given by equation (5.35).

5.6 Conclusion

A model has been developed to describe unsteady contact melting of a non-isothermal solid from the initial heating up phase to complete melting. In our examples we used data for ice and water since this is the easiest to obtain, however the governing equations should be valid for other melting systems provided the small parameters remain negligible.

The key differences between our work and most previous models include:

1. The modelling of the temperature profile in the solid.

2. The inclusion of a cooling condition at the interface with the substrate.

3. Modelling the varying mass of the solid.

4. The neglect of the quasi-steady assumption for the liquid height.

Modelling the temperature in the solid allowed us to include the solid temperature gradient in the Stefan condition. This term acted to slow down the melting. The time to complete melting slowly increased linearly with a decrease in subcooling, $\theta_0 - T_m$. Since the weight of the solid provides the driving force for the squeeze flow the decreasing mass also leads to an increase in the melt time. Further, the mass variation prevented the quasi-steady state from occurring, instead the liquid height has an initial rapid increase, followed by a period of slow increase and a final rapid increase as the block mass approaches zero. The quasi-steady approximation provides a reasonable approximation to the central period of slow increase. However, it is the cooling condition and the introduction of a heat transfer coefficient that has the greatest effect on the melting. Increasing the heat transfer coefficient from 855 to 5000 W/m^2 halved the melting time. Further, with a cooling condition melting does not occur immediately, so we must examine a pre-melting stage, which then determines the time for melting to start and also the temperature profile in the solid when this occurs. The initial infinite velocity observed in previous studies did not show up in our simulations and was shown to be due to the perfect thermal contact assumption.

For our main example the combined effects of modelling the temperature in the solid, using a heat transfer coefficient and a decreasing mass, led to a fourfold increase in the melting time from the classical solution of Bejan. Yoo points out that there are no adequate experiments to compare with the theory: it has therefore only been tested against numerical solutions, where the physical set-up has been chosen to match the idealised conditions assumed in the theoretical model. Consequently the importance of the effects discussed in this chapter appear not to have been recognised. Also shown in our results is the significant effect of the

density ratio on the time for complete melting, ignoring the change in density upon melting results in approximately 27% error in the prediction of the melting time for the rime and glaze ice parameters used in our calculations.

Our results showed that the melting rate is approximately constant, so $h_m \approx \alpha t$. A similar result is true for the quasi-steady approximation but the constant of proportionality is significantly different. This observation allowed us to determine the constant of proportionality from the Stefan condition so the time for melting may be estimated via a simple analytical expression. The evolution of the melt layer thickness reduced to solving a single first order differential equation for the liquid layer height. This is clearly a simpler prospect than the three coupled differential equations that result from our full analysis.

Chapter 6

Conclusions and further work

In this thesis, we have investigated the combined phenomenon of squeeze film flow and heat transfer which describes unsteady contact melting. The main objective was to develop mathematical models of unsteady contact melting that take into account: (a) modelling of the temperature profile in the solid (PCM), (b) the inclusion of a cooling condition at the interface with the substrate, (c) modelling the varying mass of the PCM , (d) the neglect of the quasi-steady assumption for the liquid height, and (e) the effect of the solid-liquid density ratio on the solid descending velocity. The aim was to investigate what effect if any, these have on the time for complete melting and the evolution of the film height.

In Chapter 2 we focused mainly on the determination of the best approximate solution to the heat conduction problem in a finite slab prior to melting. Semi-analytical solutions were obtained using the heat balance integral method based on the quadratic, cubic and the exponential approximating functions. The approximate solutions were derived subject to two types of boundary conditions: a prescribed heat flux and a cooling condition which are common in most contact melting problems. The exact solutions admitted by the pre-melting problems, which were determined using separation of variables and the Laplace transform were then used to ascertain the accuracy of the approximate solutions. The results showed that, based on the prediction of the time melting commences and the surface temperature

profiles, the cubic temperature approximation provides a more accurate solution compared to the exponential and quadratic approximations.

In Chapter 3, a mathematical model to describe the one-dimensional heat conduction problem for the melting of a finite block from an initial heating phase until completion of the melting process was developed. The focus was exclusively on the thermal analysis of the contact melting problem. In the melt region, an asymptotic series expansion in terms of the Stefan number St was used to describe the temperature solution for materials such as ice and water whose $St \ll 1$. For phase change materials with $1 < St$, a discussion on the use of the HBI method was given together with the model equations that may be used. In the melt region, solutions were then developed to first order, yielding a cubic polynomial. This together with the results of Chapter 2 motivated the use of the cubic polynomial in the solid to approximate the thermal boundary layers. Furthermore, the cubic approximation is consistent with the expansions of the analytical solutions when such solutions are available. Comparison of the results of our model with exact solutions for a semi-infinite solid showed a good agreement (to within less than 1%). Our approximation proved to be more accurate than the quadratic approximation used by Goodman and Shea [25]. The method involved determining the temperature profile in three different phases. Each phase requires solving the heat equation in three regions and then coupling them with Stefan conditions to determine positions of the interfaces which complicates the method of solution. However, the same would be true of a numerical solution as the number of the domains and moving boundaries increases. In our analysis we presented an example which dealt with the problem of heating an ice layer from below. This relatively simple analysis provided an analytical formula which may be used to determine the amount of energy required to melt the base in a given time, or equivalently the time taken for melting to start with a given energy source. This has applications in the development of de-icing equipment.

In Chapters 4 and 5 we developed models to describe unsteady contact melting of an isothermal and non-isothermal solid respectively, from the initial heating up to complete melting. Modelling the temperature in the solid allowed us to include the solid temperature gradient

to the Stefan condition this significantly reduced the melting rate. Incorporating the variation of solid mass in our model prevented the quasi-steady state observed in most previous investigations from occurring, instead the liquid height has an initial rapid increase, followed by a period of slow increase and a final rapid increase as the block mass approaches zero. Our results show that the quasi-steady approximation provides a reasonable approximation to the central period of slow increase. However, it is the cooling condition and the introduction of a heat transfer coefficient that has the greatest effect on the melting. The cooling condition, which is obviously more realistic than perfect thermal contact, affects the temperature profile in the liquid. Under the quasi-steady assumption we found that the quasi-steady height $h_q \sim (T_s - T_m)^{1/3}$ as opposed to $(T_s - T_m)^{1/4}$ which results from assuming perfect thermal contact. The initial infinite velocity observed in previous studies did not show up in our simulations, this we proved to be due to the perfect thermal contact assumption. Our results have also shown that neglecting the density change upon melting may result in close to 27% error in the prediction of the time for complete melting.

The combined effects of modelling the temperature in the solid, using a heat transfer coefficient and a decreasing mass led to a fourfold increase in the melting time from the classical solution of Bejan. Due to the absence of adequate experimental results, previously the theory has been tested against numerical solutions where the physical set-up has been chosen to match the idealised conditions of the theory. Consequently the importance of the effects discussed in this thesis appears not to have been recognised.

Our results showed that the melting rate is approximately constant, so $h_m \approx \alpha t$. A similar result is true for the quasi-steady approximation but the constant of proportionality is significantly different. This observation allowed us to determine the constant of proportionality from the Stefan condition so the time for melting may be estimated via a simple analytical expression. The evolution of the melt layer thickness reduced to solving a single first order differential equation for the liquid layer height. This is clearly a simpler prospect than the three coupled differential equations that result from our full analysis. A brief extension to the three dimensional case with sliding was discussed and the model equations derived. We

intend to extend these results in our future work on this area.

The models developed in this thesis have provided insight into the unsteady contact melting process. However, several features of this study could be further investigated:

- In this study, the heat transfer and fluid flow problems were solved provided the reduced Reynolds $\epsilon^2 Re$ and Peclet ($\epsilon^2 Pe$) parameters remained small during the entire melting process. A more general study is required to generalize the method used in this thesis to cover cases where convective terms play a significant role in the contact melting process. This will involve using numerical methods or perturbation methods in terms of the largest small parameter $\epsilon^2 Pe$.

- We have established the basic formulation for the two-dimensional unsteady contact melting problem. In recent studies [3, 84], research in this area has been extended to contact melting in three dimensions with the inclusion of sliding. However, these studies have exclusively relied on quasi-steady contact melting processes and neglected heat conduction in the solid and the effect of variation of mass. We have briefly outlined the extension to three dimensions with sliding. Further work to cover applications of these results would significantly increase the applicability of this work.

- Comparison with experimental data. It would be extremely useful to combine this work with an experimental investigation to verify the results presented for practical purpose.

- Our results can be applied to problems in conduction controlled re-wetting processes. Most of the investigations carried out so far consider only a quasi-steady state analysis, see [70, 83] for example. However, only a few investigations [68, 83] have been reported on the use of the heat balance integral method on the rewetting analysis. The analysis employed in this work can be extended to investigate such processes.

- The results of this thesis can also be used to study the phenomenon of floating drops (Leidenfrost [8, 10]). In this case a vapour film separates a drop of a liquid from a hot

substrate. Our models could be adapted to describe the characteristics of the vapour layer on which the drop floats, its relationship to the drop size and how both vary with time as evaporation takes place.

****

Bibliography

[1] D. J. Acheson. *Elementary Fluid Dynamics*. Clarendon Press: Oxford, 1990.

[2] M. Bareiss and H. Beer. An analytical solution of the heat transfer process during of an unfixed solid phase change material inside a horizontal tube. *Int. J. Heat and Mass Trans.*, 27:739–745, 1984.

[3] A. Bejan. The fundamentals of sliding contact melting and friction. *J. Heat Trans.*, 111:13–20, 1989.

[4] A. Bejan. *Contact Melting Heat Transfer*, volume 24. Academic Press, 1994.

[5] A. Bejan and P. A. Litsek. Sliding contact melting: The effect of heat transfer in the solid parts. *J. Heat Trans.*, 112:809–812, 1990.

[6] G. E. Bell. A refinement of the heat balance integral method applied to a melting problem. *Int. J. Heat and Mass Trans.*, 21:1357–1362, 1978.

[7] G. E. Bell. Solidification of a liquid about a cylindrical pipe. *Int. J. Heat and Mass Trans.*, 22:1681–1686, 1979.

[8] A. L. Biance, C. Clanet, and D. G. Quere. Leidenfrost drops. *Phys. Fluids*, 15(6):1632–1637, 2003.

[9] M. A. Biot. New methods in heat flow analysis with application to flight structures. *J. aeronaut. Sci*, 24:857–873, 1957.

[10] G. Bleiker and E. Specht. Film evaporation of drops of different shape above a horizontal plate. *Int. J. Thermal Sci.*, 46:635–841, 2007.

[11] G. Bleiker and E. H. Specht. Film evaporation of drops of different shape above a horizontal plate. *Int. J. Thermal Sciences*, 46(9):835–841, 2007.

[12] B. A. Boley. A method of heat conduction analysis of melting and solidification problems. *J. Math. Phy.*, 40:300–313, 1961.

[13] T. W. Brakel, J. P. F. Charpin, and T. G. Myers. One-dimensional ice growth due to incoming supercooled droplets impacting on a thin conducting substrate. *Int. J. Heat and Mass Trans.*, 50:1694–1705, 2007.

[14] J. Caldwell and C.C. Chan. Numerical solution of Stefan problems in annuli by enthalpy method and heat integral method. *Comm. Numer. Methods Eng.*, 16:569–583, 2001.

[15] J. Caldwell and C.K. Chiu. Numerical solution of one-phase Stefan problems by heat integral method, Part I-Cylindrical and spherical geometries. *Comm. Numer. Methods Eng.*, 16:569–583, 2000.

[16] J. Caldwell and Y.Y. Kwan. Perturbation methods for the Stefan problem with time-dependent boundary conditions. *Int. J. Heat and Mass Trans.*, 46:1497–1501, 2003.

[17] A. Cameron. *Basic Lubrication Theory*. Longman, 1970.

[18] H. S. Carslaw and J. C. Jaeger. *Conduction of heat in solids*. Clarendon Press, Oxford, 1947.

[19] S. J. Citron. Heat conduction in a melting slab. *J. Aeros. Sci.*, 27:219–228, 1960.

[20] J. Crank. *Mathematics of Diffusion*. Clarendon Press, Oxford, 1975.

[21] R. W. Gent, N. P. Dart, and J. T . Cansdale. Aircraft icing,. *Philos. Trans. R. Soc. Lond.*, A 358:2873–2911, 2000.

[22] T. R. Goodman. The heat-balance integral and its application to problems involving a change of phase. *Trans. ASME*, 80:335–342, 1958.

[23] T. R. Goodman. The heat balance integral-further considerations and refinements. *J. Heat Trans.*, 83C:83–86, 1961.

[24] T. R. Goodman. Application of integral methods to transient nonlinear heat transfer. *Adv. Heat Trans.*, 1:51–122, 1964.

[25] T. R. Goodman and J. J. Shea. The melting of finite slabs. *J. Appl. Mech.*, 27:16–27, 1960.

[26] D. Groulx and M. Lacroix. Effects of convection and inertia on close contact melting. *Int. J. Heat and Mass Trans.*, 42:1073–1080, 2003.

[27] D. Groulx and M. Lacroix. Study of close contact melting of ice from a sliding heated flat plate. *Int. J. Heat and Mass Trans.*, 49:4407–4416, 2006.

[28] A. G. Herrmann. *Radioactive Abfalle.* 148-152, 1961.

[29] J. M. Hill. *One-Dimensional Stefan Problems: An Introduction.* Longman Scientific Technical, Harlow, 1987.

[30] A. W. D. Hills. A generalized integral-profile method for analysis of unidirectional heat flow during solidification. *Trans. Metall. Soc . A.I.M.E*, 245:1471–1479, 1969.

[31] C. Huang. Perturbation solutions of planar diffusion-controlled moving-boundary problems. *Int. J. Heat and Mass Transfer*, 18:689–695, 1975.

[32] F. Jackson. Moving heat sources with change of phase. *J. Heat Trans.*, 87:329–332, 1965.

[33] J. D. Jackson. A Study of Squeeze Flow. *App. Sci. Research*, 11:148–152, 1961.

[34] A. Jain. Simple solutions of the partial differential equation for diffusion(or heat conduction). *Proc.Roy. Soc. Lond. Series A, Mathematical and Physocal Sciences*, 243:359–374, 1958.

[35] E. Javierre, C. Vuik, F. J. Vermolen, and S. Van der Zwaag. A comparison of numerical models for one-dimensional Stefan problems. *J. Comput. Appl. Math*, 192:445–459, 2006.

[36] Z. Ke-Oinu, R. Ling, and L. Yi. Linear stability of flows in a squeeze film. *China Physical Letters*, 22:1460–1463, 2005.

[37] H. Kumano, A. Saito, S. Okawa, K. Takeda, and A. Okuda. Study of direct contact melting with hydrocarbon mixtures as the pcm. *Int. J. Heat Mass Transfer*, 48(15):3212–3220, 2005.

[38] H. Kumano, A. Saito, S. Okawa, and Y. Yamada. Direct contact melting with asymmetric load. *Int. J. Heat Mass Transfer*, 48(15):3221–3230, 2005.

[39] M. Lacroix. Contact melting of a phase change material inside a heated parallelepipedic capsule. *Energy Cons. and Management*, 42:35–47, 2001.

[40] J. L. Laforte, M. A. Allaire, and J. Laflamme. State of the art on power line de-icing. *Atmos. Res.*, 46:143–158, 1998.

[41] H. G. Landau. Heat conduction in a melting solid. *Quart. Appl. Math*, 8:81–94, 1950.

[42] D. Langford. The heat balance integral method. *Int.J. Heat. Mass. Trans.*, 16:2424–2428, 1973.

[43] G. S. H. Lock. On the perturbation solution of the ice-water layer problem. *Int. J. Heat and Mass Trans.*, 14:642–644, 1871.

[44] B. D. Marsh. On the cooling of ascending andesitic magma. *Philos. Trans. Roy. Soc.*, A288:611–625, 1978.

[45] S. L. Mitchel and T. G. Myers. A heat balance integral method for one-dimensional ablation of a finite block, *to appear. J. Thermophysics. Heat Trans.*, 2008.

[46] S. L. Mitchel and T. G. Myers. Approximate solution methods for one-dimensional solidification from an incoming fluid, *to appear. J. Comp. App. Math Trans.*, 2008.

[47] M. K. Moallemi and R. Viskanta. Analysis of close contact melting and heat transfer. *Int. J. Heat and Mass Trans.*, 29:855–867, 1986.

[48] M. K. Moallemi, B. W. Webb, and R. Viskanta. An experimental and analytical study of close-contact melting. *Int. J. Heat and Mass Trans.*, 108:894–899, 1986.

[49] F. Mosally, A. S. Wood, and A. Al-Fhaid. An exponential heat balance integral method. *App. Math. Comp.*, 130:87–100, 2002.

[50] T. G. Myers. Extension to the messinger model for aircraft icing. *AIAA*, 39:211–218, 2001.

[51] T. G. Myers and J. P. F. Charpin. A mathematical model for atmospheric ice accretion and water flow on a cold surface. *Heat and Mass Transfer*, 47:5483–5500, 2004.

[52] T. G. Myers, J. P. F. Charpin, and S. J. Chapman. The flow and solidification of a thin fluid film on an arbitrary three-dimensional surface. *Phys. Fluids*, 14:2788–2803, 2002.

[53] T. G. Myers, J. P. F. Charpin, and C. P. Thompson. Slowly accreting ice due to supercooled water impacting on a cold surface. *Phys. Fluids*, 14:240–256, 2002.

[54] T. G. Myers and D. W. Hammond. Ice and water film growth from incoming supercooled water droplets. *Int. J. Heat and Mass Trans.*, 42:240–256, 1999.

[55] T. G. Myers, S. L. Mitchell, and G. Muchatibaya. Unsteady contact melting of a rectangular cross-section phase change material, to appear. *Phys. Fluids.*

[56] T. G. Myers, S. L. Mitchell, G. Muchatibaya, and M. Y. Myers. A cubic heat balance integral method for one-dimensional melting of a finite thickness layer. *Int. J. Heat Mass Trans*, 50:5305–5317, 2007.

[57] F. Neumann. Die Paruellen Differentialgleichungen der Mathematischen Physik. *Riemann-Weber*, 2:121, 1912.

[58] D. Nicholas and Y. Bayazitoglu. Thermal storage of a phase-change material in a horizontal cylinder. *Alt. Energy Sources III*, 1:351–367, 1983.

[59] B. Noble. Heat balance methods in melting problems. *Moving boundary problems in heat flow and diffusion*, 245:208–209, 1974.

[60] H. Ockendon and J. R. Ockendon. *Viscous Flow*. Cambridge University Press, 1995.

[61] D. R. Oliver, R. C. Ashton, and G. D. Wadelin. The load bearing capacity of a continuous-flow squeeze liquid. *App. Sci. Res.*, 34:25–47, 1978.

[62] M. N. Ozisik. *Heat Conduction*. Wiley, New York, 1980.

[63] P. I. Pedroso and G. A. Domoto. Exact solution by a perturbation method for planar solidification of a saturated liquid with convection at the wall. *Int. J. Heat and Mass Trans.*, 16:1816–1819, 1973.

[64] K. Pohlhausen. Zur naherungsweisen Integration der Differentialgleichunger der laminaren Grenzschicht. *Zeitschrift fur Angewandte Mathematik und Mechanik*, 1:252–258, 1921.

[65] G. Poots. On the application of integral methods to the solution of problems involving the solidification liquids initially at fusion temperature. *Int. J. Heat and Mass Trans.*, 5:525–531, 1962.

[66] G. Poots. *Ice and snow accretion on structures*. Research Studies Press, UK, 1996.

[67] W. C. Reynolds and T. A. Dolton. Use of integral methods in transient heat transfer analysis. *American Society of Mchanical Engineers*, 1:248, 1958.

[68] S. K. Sahu, P. K. Das, and S. Bhattacharyya. A comprehensive analysis of conduction controlled rewetting by the Heat Balance Integral Method. *Int. J. Heat Mass Transfer*, 49:4978–4986, 2006.

[69] A. Saito, H. K. Hong, and O. Hirokane. Heat transfer enhancement in the direct contact melting process. *Int. J. Heat and Mass Trans.*, 35:295–305, 1992.

[70] A. K. Satapathy and P. K. Kar. Rewetting of an infinite slab with boundary heat flux. *Numer. Heat Transfer*, 37:87–99, 2000.

[71] H. Schlichting. *Boundary layer theory.* McGraw-Hill Book Company, Inc., New York,N.Y, 1955.

[72] T. J. Sheer. Pneumatic conveying of ice particles through mine-shaft pipelines. *Powder Tech.*, 85:203–219, 1995.

[73] E. M. Sparrow and G. T. Geiger. Melting in a horrizontal tube with the solid either constrained or free to fall under gravity. *Int. J. Heat Mass Transfer*, 29:1007–1019, 1986.

[74] J. T. Stuart, R. C. DiPrima, P. M. Eagles, and A. Davey. On the instability of the flow in a squeeze lubrication film. *Proc. Math. and Phys. Sci.*, 430:347–375, 1990.

[75] L. C. Tao. Generalized numerical solutions of freezing a saturated liquid in cylinders and spheres. *A.I.Ch.E*, 13:165–169, 1967.

[76] L. C. Tao. Generalized solution of freezing a saturated liquid in a convex container. *A.I.Ch.E*, 14:720, 1968.

[77] L. N. Tao. The Stefan problem with arbitrary initial and boundary conditions. *Quart. App. Math*, 36:223–233, 1978.

[78] S. K. Thomas, R. P. Cassoni, and C. D. MacArther. Aircraft anti-icing and de-icing techniques and modelling. *J. Aircraft 33*, 5:841–854, 1996.

[79] E. Vallerani. Integral technique solution to a class of simple ablation problems. *AIAA*, 14(3):404–406, 1976.

[80] V. N. Volkov and V. K. Li Orlov. A refinement of the integral method in solving the heat conduction equation. *J. Heat Trans.*, 2:41–47, 1970.

[81] S. K. Wong and A. Walton. Numerical solution of single-phase stefan problem using a fictitious material. *Numer. Heat Transfer*, 8:211–213, 1999.

[82] A. S. Wood. A new look at the heat balance integral method. *App. Math. Modelling*, 25:815–824, 2001.

[83] L. S. Yao. Rewetting of a vertical surface with internal heat generation. *AIChe Symp. Ser: Solar Nucl. Heat Transfer*, 73:46–50, 1976.

[84] H. Yoo. Analytical solutions to the unsteady close-contact melting on a flat plate. *Int. J. Heat Fluid Flow*, 43:1457–1467, 2000.

[85] H. Yoo, H. Hong, and C. J. Kim. Effects of transverse convection and solid-liquid density difference on the steady close-contact melting. *Int. J. Heat Fluid Flow*, 19(4):368–373, 1998.

[86] M. Zerroukat and C. R. Chatwin. An explicit unconditionally stable variable time-step method for one-dimensional Stefan problems. *Int. J. Numer. Methods Eng*, 35:1503–1520, 1992.

[87] T. F. Zien. Approximate calculation of transient heat conduction. *AIAA, Aero. Sci. Meeting*, 14, 1976.

[88] T. F. Zien. Integral solutions of ablation problems with time dependent heat flux. *AIAA, Aero. Sci. Meeting*, 16, 1978.